UNIVERSITY OF CALIFORNIA, SAN DIEGO

The Role of Post-translational Modifications in Genome Maintenance

A dissertation submitted in partial satisfaction

of the requirements for the degree

Doctor of Philosophy

in

Chemistry

by

Jason Liang

Committee in charge:

Professor Huilin Zhou, Chair
Professor Daniel J. Donoghue, Co-Chair
Professor Thomas Hermann
Professor Richard D. Kolodner
Professor Susan S. Taylor

2016

The dissertation of Jason Liang is approved, and it is acceptable in quality and form for publication on microfilm and electronically:

_____

_____

_____

_____

Co-Chair

_____

Chair

University of California, San Diego

2016

Dedication

In memoriam

S.M.

We don’t always get to choose our family, but I’m glad we chose you.

Epigraph

If your experiment needs statistics,

you ought to have done a better experiment.

Ernest Rutherford

Huilin Zhou

Table of Contents

List of Abbreviations

DSB – Double stranded break

DSBR – Double stranded break repair

HR – Homologous recombination

NHEJ – Non-homologous end joining

GCR – Gross chromosomal rearrangement

ssDNA – Single stranded DNA

rDNA – Ribosomal DNA

NTS1 – Non-transcribed spacer region 1

NTS2 – Non-transcribed spacer region 2

FHA – Fork-head associated

SUMO – Small ubiquitin-like modifier

SIM – SUMO Interacting Motif

STUbL – Sumo Targeted Ubiquitin Ligase

RENT – Regulator of nucleolar silencing and telophase (Net1-Sir2-Cdc14)

MCM – Mini-chromosome maintenance (Mcm2-7 hexamer)

NPC – Nuclear pore complex

CPT – Camptothecin

MMS – Methyl methanesulfonate

HU – Hydroxyurea

YPD – Yeast peptone dextrose

GST – Glutathione S-transferase

TAF – 6xHis-FLAG-TEV-ProteinA epitope

MS – Mass spectrometry

LC-MS/MS – Liquid chromatography tandem mass spectrometry

SILAC – Stable Isotope Labeling via Amino acid in Culture

List of Figures

List of Tables

Acknowledgements

First I would like to acknowledge and thank my advisor, Huilin Zhou, for his support and guidance through these years as I developed my skills as a scientist. I am grateful for the opportunity to work with him and the freedom he gave to allow me to explore and pursue my interests. Even through tough times he has taught me that success is achieved only after all other failures have been exhausted. I have learned a great deal here and I know the training I have received here will be impactful when I move on to my next endeavors.

I am so thankful to my family for their unwavering support all these years as I continued my education beyond their expectations. I am grateful to my parents Charles and Chi-lng for their love and encouragement that I follow my passions. I wish to also acknowledge my sister Amy and nephew Kadin for always taking the time to spend with Julia and me whenever we would make our annual trip back home. I also want to thank my second family, my friends from UCSD (Jerry, James, Le, Fong, Mike, Josh, Edith), for all the great adventures and memories we made. In particular, I want to thank Steven Mi for his tremendous friendship. He left us too soon and we all miss him dearly.

I would also like to thank the members of the lab past and present for our heated discussions, helpful criticisms, and support as I went through this journey. From each and every one of you I have learned something valuable that I will take with me. I would like to acknowledge Claudio for being the older-little brother I never had, and for being the initial one that nurtured my interest

for learning the mass spec. I thank Sheng-hong for always being an available friend that I could go talk to for advice even after he graduated and left the lab. I thank Ray for being my friend, who I can count on to support my experiments and ideas, as well as the pleasure to collaborate with on several projects both here and when he left for Stony Brook. I thank Christie for joining us and being a fresh mind to stimulate discussion and pointing out valuable tips for my professional life. I thank Chris for his help working with me on my project and his willingness to do what it takes no matter the time to finish the work we need. I thank Nathan for always being a team player and helping to take care of the lab. I would also like to thank the students who came through the lab that have showed me how much I enjoy teaching and mentoring, including Eyan, Nancy, and Alex.

I am grateful for the opportunity to work at the Ludwig Institute with some of the best colleagues. They have always been very generous with their time and open to my plethora of questions about science, careers, and life. Even though many are now gone I am grateful for the time we shared together. In particular I would like to acknowledge Kevin Corbett and Namit Singh for their help in our collaboration on the study in Chapter 4.

Lastly, I wish to thank my wife Julia for her unconditional love and support through these long years. She has always been my biggest supporter and my best friend. I am grateful for her willingness to put up with my long and crazy schedules and constant returns to the lab both late at night and on the

weekends. Her understanding and patience has been central to my accomplishments and successes moving forward.

Chapter 2, in full, is a reprint of the material as it appears in Phosphorylation of Sae2 Mediates Forkhead-associated (FHA) Domain-specific Interaction and Regulates Its DNA Repair Function. *J Biol Chem*. 2015 Apr 24;290(17):10751-63, Liang J, Suhandynata RT, Zhou H. The dissertation author is the primary author for this paper.

Chapters 3, in full, is a reprint of the material as it appears in Molecular Circuitry of the SUMO (Small Ubiquitin-like Modifier) Pathway in Controlling Sumoylation Homeostasis and Suppressing Genome Rearrangements. *J Biol Chem*. 2016 Apr 15;291(16):8825-35, de Albuquerque CP, Liang J, Gaut NJ, Zhou H. The dissertation author is primary co-author for this paper.

Chapter 4, in part is in preparation for publication of the material and will appear as Monopolin stabilizes rDNA silencing complexes through direct recruitment of the SUMO isopeptidase Ulp2. Liang J, Singh N, Carlson CR, Albuquerque CP, Corbett KD, Zhou H. The dissertation author is primary co-author for this paper.

Vita

2007 BS, Biochemistry/Chemistry, University of California, San Diego

2009 MS, Chemistry, University of California, San Diego

2016 PhD, Chemistry, University of California, San Diego

2015 Micro-MBA Certificate, Rady Center for Executive Development

2016 ADMET Process Certificate, UC San Diego Extension

Publications

Liang J, Singh N, Carlson CR, Albuquerque CP, Corbett KD, Zhou H. *Monopolin stabilizes rDNA silencing complexes through direct recruitment of the SUMO isopeptidase Ulp2.* In preparation.

de Albuquerque CP, Liang J, Gaut NJ, Zhou H. *Molecular circuitry of the SUMO (Small Ubiquitin-like Modifier) pathway in controlling sumoylation homeostasis and suppressing genome rearrangements*. J Biol Chem, 2016 291(16):8825-35.

Chen X, Suhandynata RT, Sandhu R, Rockmill B, Mohibullah N, Niu H, Liang J, Lo HC, Miller DE, Zhou H, Börner GV, Hollingsworth NM. *Phosphorylation of the Synaptonemal Complex Protein Zip1 Regulates the Crossover/Noncrossover Decision during Yeast Meiosis.* Plos Biol, 2015 13(12).

Israelson A, Ditsworth D, Sun S, Song S, Liang J, Hruska-Plochan M, McAlonis-Downes M, Abu-Hamad S, Zoltsman G, Shani T, Maldonado M, Bui A, Navarro M, Zhou H, Marsala M, Kaspar BK, Da Cruz S, Cleveland DW. *Macrophage*

migration inhibitory factor as a chaperone inhibiting accumulation of misfolded SOD1. Neuron, 2015 86(1):218-32.

Liang J, Suhandynata RT, Zhou H. *Phosphorylation of Sae2 Mediates Forkhead-associated (FHA) Domain-specific Interaction and Regulates Its DNA Repair Function.* J Biol Chem, 2015 290(17):10751-63.

Suhandynata R, Liang J, Albuquerque CP, Zhou H, Hollingsworth NM.
A method for sporulating budding yeast cells that allows for unbiased identification of kinase substrates using stable isotope labeling by amino acids in cell culture. G3, 2014 4(11):2125-35.

Baldo V, Liang J, Wang G, Zhou H. *Preserving Yeast Genetic Heritage through DNA Damage Checkpoint Regulation and Telomere Maintenance.*
Biomolecules, 2012 2(4):505-23.

Zhou H, Albuquerque CP, Liang J, Suhandynata RT, Weng S. *Quantitative phosphoproteomics: New technologies and applications in the DNA damage response.* Cell Cycle, 2010 9(17):3479-84.

Chen SH, Albuquerque CP, Liang J, Suhandynata RT, Zhou H. *A proteome-wide analysis of kinase-substrate network in the DNA damage response.* J Biol Chem, 2010 285(17):12803-12.

ABSTRACT OF THE DISSERTATION

The Role of Post-translation Modifications in Genome Maintenance

by

Jason Liang

Doctor of Philosophy in Chemistry

University of California, San Diego, 2016

Professor Huilin Zhou, Chair
Professor Daniel J. Donoghue, Co-Chair

Maintaining genome stability is essential for cell viability and growth. Post-translational modifications such as phosphorylation have been implicated in regulating the cellular processes that maintain genome integrity. Under genotoxic stress, cells initiate a DNA damage response that includes the activation of a phosphorylation-mediated pathway known as the DNA damage checkpoint. Several processes are regulated by the DNA damage checkpoint including cell cycle arrest, DNA repair, transcription, and cell apoptosis. In *Saccharomyces cerevisiae*, Mec1 and Tel1 are key protein kinases that initiate the activation of the DNA damage checkpoint. Several studies have identified substrates of Mec1/Tel1 including Sae2, a DNA double-strand break repair protein involved in DNA end resection and processing of hairpin structures. In this study we identify Mec1/Tel1 consensus sites on Sae2, T90 and T279, which when mutated to non-phosphorylatable alanine causes genome instability and hyper-activation of the downstream checkpoint kinase Rad53, similar to a *sae2*Δ mutant. We find that phosphorylation of T90 and T279 on Sae2 mediates protein-protein interaction with several Forkhead associated-domain containing proteins including checkpoint kinases Rad53 and Dun1. Taken together, this suggests that the interaction of phosphorylated Sae2 with Rad53 and Dun1 is important for its role in DNA repair and genome maintenance.

Pathways that regulate other post-translational modifications have also been implicated in genome stability, including the small ubiquitin-like modifier (SUMO). Recently, SUMO E3 ligases have been shown to be suppressors of

gross chromosomal rearrangements, but not much is known of the enzymes that deconjugate SUMO. In this study, we discover a role for SUMO isopeptidases, Ulp1 and Ulp2, in preventing gross chromosomal rearrangements. We identify targets of Ulp1 and Ulp2 and find that Ulp2 distinctly regulates sumoylation at three chromosomal regions: rDNA, centromeres, and origins of replication. In contrast, Ulp1 globally targets most sumoylated proteins and mutating *ULP1* leads to an unexpected decrease in sumoylation of Ulp2 substrates. Moreover, we find that Ulp2 is able to target its substrates at the rDNA and centromeres through interaction with a kinetochore-associated complex Csm1-Lrs4. Structural and biochemical analysis demonstrates that the C-terminus of Ulp2 binds to the globular domain of the Csm1 homodimer. Mutations to the residues on Ulp2 that interact with Csm1 elevate sumoylation of the nucleolar protein Tof2 and reduce its protein abundance, resulting in a loss of transcriptional silencing at the rDNA. Lastly, we show that the loss of Tof2 protein levels in *ulp2* mutants are triggered by the ubiquitin E3 ligase complex, Slx5-Slx8.

CHAPTER 1

Introduction to the DNA damage checkpoint and sumoylation

Signaling pathways that regulate genome maintenance are necessary to ensure the faithful replication and transmission of genetic information in cells. During DNA replication, spontaneous mutations can occur from errors caused by the DNA replication machinery, such as intrinsic errors by DNA polymerases or the replication of short repetitive sequences. Genotoxic stress caused by endogenous or exogenous sources such as exposure to UV or ionizing radiation can also cause DNA damage leading to stalled replication forks and even deleterious DNA double-stranded breaks (DSBs). Cells have developed a DNA damage response that utilizes several pathways to deal with such genotoxic stresses, including repair of DNA through several mechanisms including nucleotide excision repair (NER), base excision repair (BER), mismatch repair (MMR), homologous recombination (HR), and non-homologous end joining (NHEJ) [1]. Moreover, cells activate the DNA damage checkpoint to couple DNA repair with cell cycle control to prevent further progression until the repair is completed. Thus, mutation to genes in these pathways leads to genome instability and can result in oncogenesis [2, 3]. In the budding yeast *Saccharomyces cerevisiae*, mutations to genes involved in the DNA damage checkpoint have been shown to cause a spectrum of gross chromosomal rearrangements, including deletions, interstitial deletions, inverted duplications, and translocations [4-7]. In humans, mutations to these same genes cause cancers or cancer-prone diseases [8-10].

1.1 DNA damage checkpoint

Faithful replication of the genome is essential for proliferating cells to survive and avoid the accumulation of mutations. Cell cycle checkpoints are in place to ensure that each stage of the cell cycle is completed in an orderly manner [11]. When DNA lesions are detected in the genome, cells respond with the activation of the DNA damage checkpoint, which consists of a protein kinase cascade leading to a multitude of responses including gene transcriptional changes, DNA repair, cell cycle arrest and apoptosis, among others [12-14]. In *S. cerevisiae*, Mec1 and Tel1, two PIKK family protein kinases, act at the top of the kinase cascade in the DNA damage checkpoint and are orthologs of the mammalian ATR and ATM kinases, respectively (Figure1.1 [15, 16]). Mec1 and Tel1 are among the first proteins to be recruited to the sites of DNA damage [17]. Once recruited, Mec1 and Tel1 activate downstream effector kinases Chk1 and Rad53, the ortholog of mammalian Chk2, via several adaptor proteins including Rad9 and Mrc1 among others [18-22]. Activation of Rad53, through Mec1 and Tel1 phosphorylation, leads to further propagation of the DNA damage checkpoint and subsequent cell cycle arrest, DNA repair, maintenance of DNA replication forks, block of late origin firing, and up-regulation of dNTP levels in cells [23-26].

1.1.1 Regulation of DNA damage checkpoint in DSBR

Two major pathways are known to be involved in DNA DSB repair, including NHEJ and HR [27]. A critical step in the choice of these DNA DSB

repair pathways is the nucleolytic processing of DSBs. Several enzymes have been identified to catalyze this nucleolytic processing in *S. cerevisiae*. The Mre11-Rad50-Xrs2 (MRX) complex and Sae2 act at the initial steps of DSB recognition and processing, followed by an extensive resection by the nucleases Dna2 and Exo1 together with the Sgs1-Top3-Rmi1 complex [28, 29]. DNA DSB processing is tightly coupled to the DNA damage checkpoint, which becomes activated to halt the cell cycle thus allowing time for DNA repair. Tel1 binds to Xrs2 of the MRX complex and is thus recruited to DNA DSBs [30]. Following the processing of DSBs into ssDNA, Replication Protein-A (RPA) binds to ssDNA and recruits Mec1 [31], which plays a major role in the activation of the DNA damage checkpoint. Once recruited to the site of DNA damage, Mec1 and Tel1 phosphorylate many proteins at the sites of DNA damage, including RPA, MRX and Sae2 [32-34]. Mutations of *MEC1* and *TEL1* are known to cause substantial increases in gross chromosomal rearrangements (GCRs) [4, 6, 35]. Although telomere fusion is thought to contribute to chromosomal rearrangements, as observed in the *mec1Δ tel1Δ* mutant, loss of telomerase alone does not cause similar chromosomal rearrangements [4, 6], indicating that defective DNA repair might also be involved. Many substrates of Mec1 and Tel1 have been identified; however, a major challenge has been to identify and characterize Mec1/Tel1 substrates whose phosphorylation specifically regulates DNA repair and genome maintenance.

Following the completion of DNA repair, cells must inactivate the DNA damage checkpoint, which is accompanied by the dephosphorylation and inactivation of Rad53, in order to resume cell growth and division [36]. Thus, the activity of Rad53 is intimately coupled to the status of DNA damage repair and must be tightly regulated. While much is known about the mechanisms of Rad53 activation and the nature of damaged DNA structures involved, such as the recruitment of Mec1, Tel1 and others [31, 37-39], relatively little is known about how Rad53 is inactivated following the completion of DNA repair. Moreover, the molecular basis for the coordination between DNA damage repair and the activity of Rad53 remains poorly understood. It remains unclear whether there exists an intrinsic signal for the completion of DNA repair or if it is merely a passive process following the removal of damaged DNA structures.

1.2 SUMO a ubiquitin-like modifier

Small ubiquitin-like modifier (SUMO) is a conserved eukaryotic post-translational modification that is essential for cellular function. In mammals there are three paralogs of SUMO, SUMO1 and the near identical SUMO2/3, while only a single gene encodes SUMO in yeast. In *S. cerevisiae* SUMO is initially synthesized as an inactive precursor that requires the cleavage of its C-terminal tail by the SUMO protease Ulp1. This reveals a diglycine motif that is the mature form of SUMO, which is competent in conjugation. Similar to the ubiquitin conjugation process [40], SUMO is initially activated by an E1 activating

heterodimer (Aos1/Uba2), which in an ATP-dependent-manner forms a thioester bond with a maturated SUMO. SUMO can then be transferred to the catalytic cysteine on the E2 conjugating enzyme Ubc9. In budding yeast there are three mitotic E3 ligases [17, 18, 41], Siz1, Siz2, and Mms21, and a meiotic-specific ligase Zip3 [42]. These E3 ligases contain SP-RING domains and catalyze the transfer of SUMO from Ubc9 onto the lysines of targeted substrates. The SUMO modification is dynamic and attachment on substrates is removed by two SUMO proteases Ulp1 and Ulp2 that are primarily localized to the nucleus [43-46].

SUMO was initially discovered as a modification on RanGAP1 that localized it from the cell cytosol to the NPC [47] and since then SUMO has been found to mediate many cellular processes. Other such processes regulated by SUMO include the transcriptional status of chromatin [48, 49], the state of protein confirmation [50], and protein-protein interactions through a short hydrophobic rich sequence typically consisting of a variant of (V/I-X-V/I-V/I) known as a Sumo-Interacting Motif (SIM) [51]. Cells also undergo extensive sumoylation upon induction of cellular stress or DNA damage [52-56], although the molecular basis for sumoylation of these proteins in response to these perturbations is not well understood.

1.2.1 Sumoylation in genome maintenance

Studies on DNA damage-induced sumoylation have found that not only does SUMO accumulate at the sites of DNA lesions, but the same proteins

which undergo sumoylation are also involved in the DNA damage response. In human cells, ionizing radiation triggers accumulation of SUMO1 and SUMO2/3 to the site of breaks and is conjugated to DNA damage checkpoint factors 53BP1 and BRCA1, respectively [54]. While in yeast, exposure of the DNA alkylating agent MMS results in Siz2-dependent sumoylation of proteins involved in HR and the DNA damage checkpoint [53]. Although many sumoylated proteins have been identified, only a few targets have been well characterized. In BER, SUMO attachment to thymine DNA glycosylase (TDG) [50] leads to a conformational change that drives release of the abasic site generated after hydrolysis to continue repair. Sumoylation of the DNA polymerase processivity factor PCNA (proliferating cell nuclear antigen) also plays a role in post-replicative repair. SUMO conjugation to K164 or K127 on PCNA [57, 58], primarily by Siz1, prevents unscheduled recombination during replication through the recruitment of the anti-recombinase Srs2 [59].

While Siz1 and Siz2 control the majority of the sumoylation in the cell [60], single deletion of either E3 ligase does not cause severe sensitivity to DNA damaging agents. Even genome instability assays that measure GCRs do not show strong effects for loss of Siz1 or Siz2 [60], but rather *siz1Δ* mutation suppresses mutants that cause HR-dependent GCRs [61, 62]. In contrast, removal of the SP-RING in Mms21 markedly increases the rate of accumulating GCRs in strains that predominantly detect for translocations, caused by

segmental duplications [60]. Thus, it is intriguing to see whether other enzymes involved in SUMO attachment and removal play a role in genome stability.

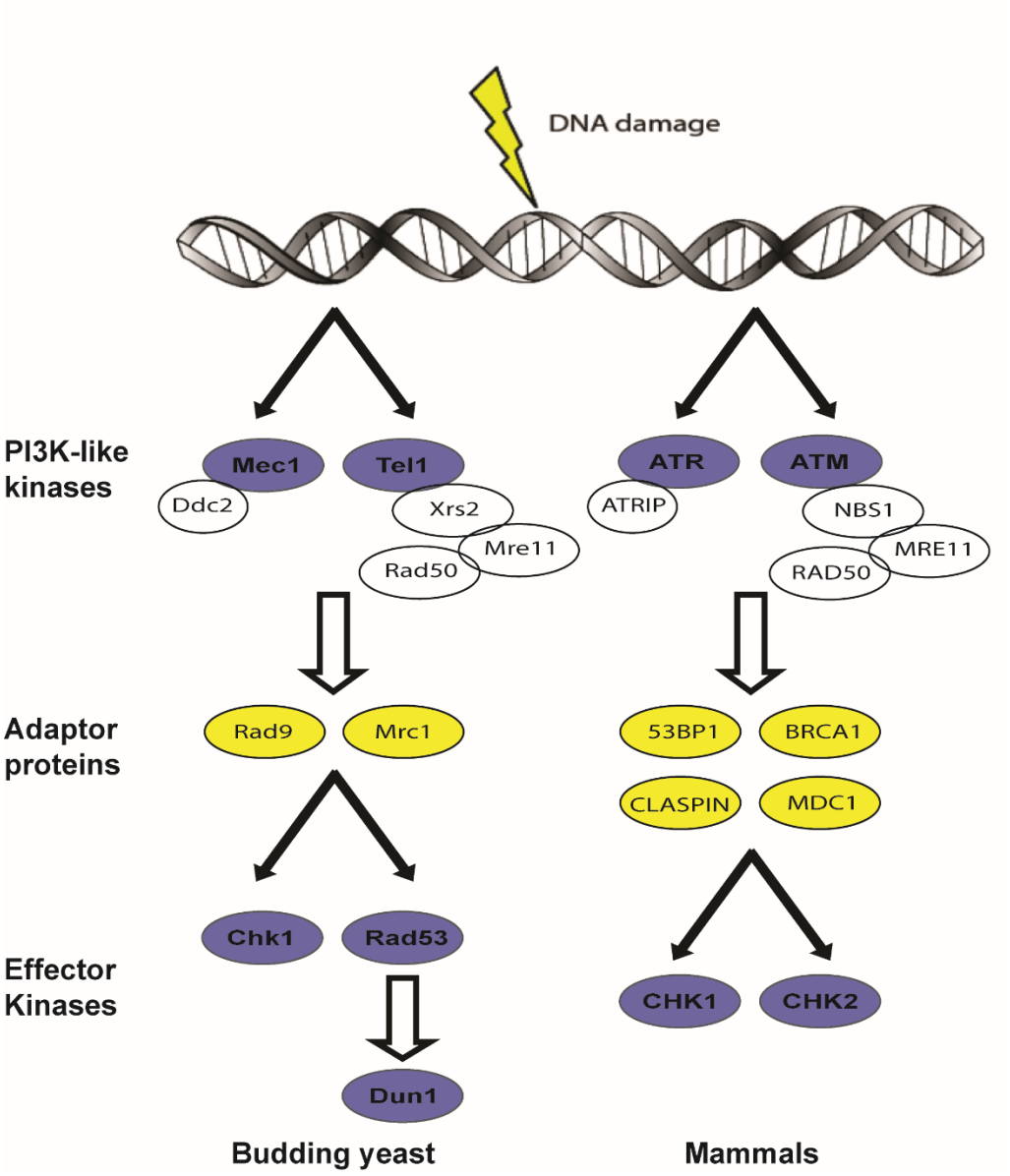

Figure 1.1 The DNA damage checkpoint is conserved from yeast to humans

Illustration depicting the main factors involved in the DNA damage checkpoint pathway in *S. cerevisiae* and *H. sapiens*.

CHAPTER 2

Phosphorylation of Sae2 mediates FHA-specific interaction

2.1 Summary

Saccharomyces cerevisiae Sae2 and its ortholog CtIP in higher eukaryotes have a conserved role in the initial processing of DNA lesions and influencing their subsequent repair pathways. Sae2 is phosphorylated by the ATR/ATM family kinases Mec1 and Tel1 in response to DNA damage. Among the Mec1/Tel1 consensus phosphorylation sites of Sae2, we found that mutations of T90 and T279 of Sae2 into alanine caused a persistent Rad53 activation in response to a transient DNA damage, similar to the loss of Sae2. To gain insight into the function of this phosphorylation of Sae2, we performed a quantitative proteomics analysis to identify its associated proteins. We found that phosphorylation of T90 of Sae2 mediates its interaction with Rad53, Dun1, Xrs2, Dma1 and Dma2, whereas Rad53 and Dun1 additionally interact with phosphorylated T279 of Sae2. Mutations of the ligand-binding residues of FHA domains of Rad53, Dun1, Xrs2, Dma1 and Dma2 abolished their interactions with Sae2, revealing the involvement of FHA-specific interactions. Mutations of T90 and T279 of Sae2 caused a synergistic defect when combined with ***sgs1Δ*** and ***exo1Δ***, and elevated gross chromosomal rearrangements (GCRs). Likewise, mutations of *RAD53* and *DUN1* caused a synthetic growth defect with ***sgs1Δ*** and elevated GCRs. These findings suggest that threonine-specific phosphorylation of Sae2 by Mec1 and Tel1 contributes to DNA repair and genome maintenance via its interactions with Rad53 and Dun1.

2.2 Introduction

DNA double stranded breaks (DSBs) are one of the most deleterious forms of DNA damage. If left unrepaired, DSBs can lead to aberrant chromosomal rearrangements and cell death [13]. Two major pathways are known to be involved in DNA DSB repair, including nonhomologous end-joining (NHEJ) and homologous recombination (HR) [27]. A critical step in the choice of these DNA DSB repair pathways is the nucleolytic processing of DSBs. Several enzymes have been identified to catalyze this nucleolytic processing in *Saccharomyces cerevisiae*. The Mre11-Rad50-Xrs2 (MRX) complex and Sae2 act at the initial steps of DSB recognition and processing, followed by an extensive resection by the nucleases Dna2 and Exo1 together with the Sgs1-Top3-Rmi1 complex [28, 29]. DNA DSB processing is tightly coupled to the DNA damage checkpoint, which becomes activated to halt the cell cycle thus allowing time for DNA repair. Tel1 binds to Xrs2 of the MRX complex and is thus recruited to DNA DSBs [30]. Following the processing of DSBs into ssDNA, Replication Protein-A (RPA) binds to ssDNA and recruits Mec1 [31], which has a major role in DNA damage checkpoint activation. Once recruited to the site of DNA damage, Mec1 and Tel1 phosphorylate many proteins at the sites of DNA damage, including RPA, MRX and Sae2 [32-34]. Mutations of *MEC1* and *TEL1* are known to cause substantial increases in gross chromosomal rearrangements (GCRs) [4, 6, 35]. Although telomere fusion is thought to contribute to chromosomal rearrangements observed in *mec1Δ tel1Δ* mutant,

loss of telomerase alone does not cause similar chromosomal rearrangements [4, 6], indicating that defective DNA repair might also be involved. Despite many substrates of Mec1 and Tel1 have been identified; a major challenge has been to identify and characterize those Mec1/Tel1 substrates whose phosphorylation specifically regulates DNA repair and genome maintenance.

Of particular interest here is Sae2, which is phosphorylated by Mec1 and Tel1 in response to DNA damage [34, 63]. Mutation of five SQ/TQ sites of Sae2, *sae2*^{2,5,6,8,9}, which conform to the consensus phosphorylation motif of Mec1 and Tel1, eliminated the bulk of its DNA damage induced phosphorylation and caused persistent Rad53 activation in response to transient DNA damage treatment similar to the deletion of *SAE2* [34, 63]. Furthermore, these *sae2* mutations caused a defect in suppression of chromosomal translocation mediated by NHEJ [64]. Interestingly, mammalian CtIP, ortholog of Sae2, is phosphorylated by ATR and ATM [65-67], which are orthologs of Mec1 and Tel1, respectively. In particular, phosphorylation of T859 on human CtIP by ATR/ATM was shown to have a role in HR [67]. Moreover, T859A mutation of CtIP caused a reduced RPA-foci formation and loss of viability following camptothecin (CPT) treatment. T859 of human CtIP is conserved in Xenopus, and a corresponding phosphorylation of T818 on Xenopus CtIP was shown to regulate CtIP association to chromatin [66]. Finally, T279 of Sae2, which conforms to a Mec1/Tel1 consensus phosphorylation site, corresponds to T859 of human CtIP and T818 of Xenopus CtIP. These findings suggested that

phosphorylation of this conserved threonine of Sae2/CtIP by ATR/ATM family kinases likely has an important function in DNA repair, although the specific function of T279 of Sae2 has not yet been determined.

Sae2 is also phosphorylated by cyclin-dependent kinase (CDK) [68]. It was shown that phosphorylation of Sae2 on S267 is required for cells to confer resistance to DNA damaging agents and S267A mutation impaired resection of an irreparable DSB induced by HO endonuclease. A recent study showed that phosphorylation of Sae2 by CDK and Mec1/Tel1 appeared to alter its oligomeric state by converting Sae2 into a monomeric and active state [69]. However, Ctp1, the ortholog of Sae2 in *S. pombe*, lacks such CDK phosphorylation. Instead, Ctp1 is phosphorylated by casein kinase [70], which was shown to mediate an interaction between Ctp1 and FHA domain of Nbs1, the *S. pombe* ortholog of *S. cerevisiae* Xrs2. On the other hand, several putative CDK sites on human CtIP were shown to facilitate the interaction between CtIP and Nbs1 [67], suggesting that different kinases phosphorylate Ctp1 and CtIP to promote their association with Nbs1 in different organisms. A possible interaction between Sae2 and Xrs2 in *S. cerevisiae* has not been identified. It is also unclear whether phosphorylation of Sae2 by CDK, casein kinase or possibly other kinases, helps to regulate the interaction between Sae2 and Xrs2.

Here we characterized phosphorylation of Sae2 further. Through mutagenesis analysis of Mec1 and Tel1 phosphorylation sites of Sae2, we identified two conserved threonine residues T90 and T279 of Sae2 to have a

redundant role for its function in the DNA damage response. We further applied quantitative mass spectrometry (MS) to identify Sae2-associated proteins, which are mediated by phosphorylation of T90 and T279, and then examined the role of this phosphorylation of Sae2 in DNA repair and maintaining genome integrity.

2.3 Results

2.3.1 Mutation of both T90 and T279 of Sae2 cause an elevated sensitivity to genotoxic agents

Sae2 has five serine and threonine residues that follow the consensus phosphorylation motif, SQ/TQ, of Mec1 and Tel1 [34]. To identify the specific SQ/TQ sites of Sae2 important for its function, we performed a sequence alignment of Sae2 orthologs in fungi and human and found that T90 and T279 of Sae2 are conserved among fungi (Figure 2.1A). In particular, T279 is located in a conserved C-terminal region of Sae2, which is also present in CtIP. To study their functions, we changed T90, S249 and T279 of Sae2 into alanine and integrated these mutations in the *SAE2* chromosomal locus. First, we analyzed the effect of these *sae2* mutations on the electrophoretic mobility shift of Sae2 using Sae2-3HA strain. Treatment of Sae2-3HA strain by either phleomycin or camptothecin (CPT) caused an accumulation of slower migrating bands, representing phosphorylated species of Sae2. As shown in Figure 2.1B, *sae2-T90A* mutation partially reduced the slowest migrating species of Sae2 caused

by phleomycin treatment, whereas *sae2-T279*A mutation caused an accumulation of more slower-migrating species of Sae2. The *sae2-2AQ* mutation, containing both *T90A* and *T279A*, caused an intermediate effect on the electrophoretic mobility shift of Sae2. On the other hand, *sae2-S249A* mutation caused a reduction of slower migrating species of Sae2, indicating that S249 is a major DNA damage induced phosphorylation site. The *sae2-3AQ* mutation, containing *S249A*, *T90A* and *T279A*, eliminated the bulk of slower migrating bands of Sae2. Thus, S249, T90 and T279 are the major phleomycin-induced phosphorylation sites of Sae2 (Figure 2.1B, bottom panel, lane 7). CPT-induced Sae2 electrophoretic shift (Figure 2.1B, top panel) appears to be somewhat less pronounced compared with phleomycin treatment, but the overall changes are similar.

We next examined growth of these *sae2* mutants on plates containing methyl methane sulfonate (MMS), CPT, and phleomycin. Compared to a wild-type strain, *sae2-T90A*, *sae2-S249A* and *sae2-T279A* mutants did not show appreciable elevated sensitivity to these drugs (Figure 2.1C). Interestingly, *sae2-T90A, T279A (sae2-2AQ)* mutant showed a significantly elevated sensitivity to MMS, CPT, and to a lesser extent phleomycin (Figure 2.1C), albeit not to the same extent as ***sae2Δ*** mutant. Although *sae2-S249A* mutation removes the majority of Sae2 electrophoretic shift (Figure 2.1B), it does not alter MMS, CPT or phleomycin sensitivity of *sae2-T90A,* sae2-*T279A* or *sae2-2AQ* mutant. Thus, T90 and T279 of Sae2 redundantly confer resistance to chronic

treatments of MMS and CPT, while phosphorylation of S249 of Sae2 does not contribute to this function of Sae2. To further examine CPT sensitivity of *sae2-2AQ* and ***sae2Δ*** mutants, we examined their growth in liquid culture in the presence of varying concentrations of CPT using a previously published method [71]. We found that *sae2-2AQ* mutant is less sensitive than the ***sae2Δ*** mutant at lower CPT concentrations (Figure 2.1D). However, at a higher concentration such as 20 μM CPT, *sae2-2AQ* mutant grew similarly to ***sae2Δ*** mutant (Figure 2.1D). The elevated sensitivity of *sae2-2AQ* mutant to chronic MMS and CPT treatments could be due to a cell cycle arrest, loss of viability, or both. To test for a loss of viability, wild-type strain, *sae2-2AQ* and ***sae2Δ*** mutants were treated with increasing amounts of MMS for 1 hour and quantified for surviving colonies. MMS treatment caused a dosage dependent and increased loss of viability of *sae2-2AQ* mutant, although not to the same extent as ***sae2Δ*** mutant (Figure 2.1E).

2.3.2 MMS treatment caused persistent Rad53 activation in *sae2-2AQ* mutant

Previous studies showed that mutations of all five Mec1/Tel1 consensus phosphorylation sites of Sae2 caused persistent Rad53 phosphorylation in response to DNA damage [34, 63]. Here we investigated whether T90 and T279 of Sae2 are specifically involved. Following MMS treatment, Rad53 became hyperphosphorylated as evident by its slower electrophoretic mobility (Figure 2.2A). Rapid Rad53 dephosphorylation ensued within 30 minutes after wild-type

cells were released into fresh media and it was essentially complete within 2 hours. As expected, Rad53 in ***sae2Δ*** mutant remained phosphorylated for up to 2 hours following its release into fresh media (Figure 2.2A). Interestingly, Rad53 remained phosphorylated for up to 2 hours after being released in fresh media in *sae2-2AQ* mutant, while *sae2-T90A* and *sae2-T279A* mutations did not appreciably alter the kinetics of Rad53 dephosphorylation compared to wild-type strain (Figure 2.2A). Thus, T90 and T279 of Sae2 have a redundant role in allowing Rad53 dephosphorylation to occur during recovery from a transient MMS treatment.

Activation of Rad53 requires two adaptor proteins Rad9 and Mrc1, which are phosphorylated by Mec1 and Tel1 and control Rad53 activation in both redundant and distinct manners, depending on the types of genotoxic stresses [20, 72, 73]. In particular, Rad9 has a more important role for Rad53 activation in response to DNA damage. Like Rad53, Rad9 remains hyperphosphorylated in *sae2-2AQ* and ***sae2Δ*** mutants following a transient MMS treatment (Figure 2.2B), indicating the defect of Rad53 dephosphorylation in *sae2-2AQ* mutant occurs at an earlier step. One possibility is that *sae2-2AQ* mutant suffers from a DNA repair defect. To examine this further, we examined the effect of deleting *RAD9* and *MRC1* on the growth of *sae2-2AQ* mutant in the presence of CPT, which causes covalent DNA-protein adducts. Deleting *RAD9* modestly improves growth of *sae2-2AQ* mutant at a lower concentration of CPT (10 μM), but not at a higher concentration of CPT (20 μM) (Figure 2.2C). This finding suggests that

the accumulation of CPT-induced DNA lesion may require the function of Sae2 in DNA repair via its phosphorylation at T90 and T279, and cell growth cannot be fully rescued by the loss of Rad9 to reduce Rad53 activity. On the other hand, deleting *MRC1* does not have an appreciable effect on growth of *sae2-2AQ* mutant (Figure 2.2D), indicating that Mrc1 does not contribute to the CPT sensitivity of *sae2-2AQ* mutant.

Deletion of *MRC1* is known to cause defects in DNA replication and compromise Rad53 activation in response to hydroxyurea (HU) treatment [20, 22]. Interestingly, *sae2-2AQ mrc1Δ* double mutant showed a significantly improved growth compared to *mrc1Δ* mutant in the presence of HU (Figure 2.2E), while deleting *RAD9* has little effect on HU sensitivity of *sae2-2AQ* mutant. Considering that *sae2-2AQ* mutant has an elevated Rad53 activity, while *mrc1Δ* mutant has a defect in Rad53 activation in response to HU treatment [20, 22], we reason that *sae2-2AQ* mutation would elevate Rad53 activation in *sae2-2AQ mrc1Δ* double mutant, thus allowing it to better cope with HU treatment than *mrc1Δ* mutant (Figure 2.2E). Taken together, these findings suggest that *sae2-2AQ* mutant may suffer from both DNA repair and hyper-activated Rad53 defects, which cause different outcomes in combination with the loss of Rad9 and Mrc1, depending on the types of genotoxic agents used.

2.3.3 Genetic interactions between *SAE2, SGS1,* and *EXO1*

Sgs1 and Exo1 are known to function in DNA DSB processing [28]. To explore the role of Sae2 phosphorylation in DNA resection, we first examined

effect of combining various *sae2* mutations with ***sgs1Δ*** and ***exo1Δ*** mutations. Interestingly, we found that *sae2-2AQ* ***sgs1Δ exo1Δ*** triple mutant is lethal (Figure 2.3A), while *sae2-T90A* ***sgs1Δ exo1Δ*** and *sae2-T279A* ***sgs1Δ exo1Δ*** triple mutants are viable (Figure 2.3A). This finding again supports a redundant role of T90 and T279 of Sae2 for its DNA repair function. Although ***sae2Δ sgs1Δ*** double mutant is known to be lethal [74, 75], *sae2-2AQ* ***sgs1Δ*** double mutant is viable and lacks any obvious growth defect. However, *sae2-2AQ* ***sgs1Δ*** double mutant did show a significantly elevated sensitivity to CPT compared to *sae2-2AQ* and ***sgs1Δ*** single mutants (Figure 2.3B). To further study the role of Sae2 phosphorylation in genome maintenance, we used the *yel072w::CAN1/URA3* assay, which measures GCRs formed by both segmental duplication and single-copy sequences [76]. Compared to wild-type strain, there is a 4-fold increase in the rate of accumulating GCRs in *sae2-2AQ* mutant (Figure 2.3C, Table 2), similar to that in ***sae2Δ*** mutant and a phosphorylation-defective allele where all five putative Mec1/Tel1 phosphorylation sites of *SAE2* are mutated [77]. The rate of accumulating GCRs in *sae2-2AQ* ***sgs1Δ*** double mutant is modestly higher than that in ***sgs1Δ*** mutant.

Next, we examined possible genetic interactions between Sae2 and Exo1. The *sae2-2AQ* ***exo1Δ*** double mutant has a comparable CPT sensitivity like *sae2-2AQ* mutant (Figure 2.3D). The rate of accumulating GCRs in *sae2-2AQ* ***exo1Δ*** double mutant is comparable to that in *sae2-2AQ* and ***exo1Δ*** mutants (Figure 2.3E). These findings indicate either a lack of genetic

interaction between these mutations or an epistasis relationship between them. Taken together, these findings reveal an essential role of Sae2 phosphorylation in cells lacking both Sgs1 and Exo1 for cell survival, and Sae2 phosphorylation is important in coping with CPT-induced DNA legions in cells lacking Sgs1, but not Exo1.

2.3.4 Quantitative MS identified the proteins associated with phosphorylated Sae2

A possible function of phosphorylated T90 and T279 of Sae2 is to mediate specific protein-protein interactions. To test this, we used biotinylated phosphopeptides of Sae2 containing either phosphorylated T90 (pT90) or T279 (pT279) that were immobilized on streptavidin resins to purify their associated proteins, and then identified them using quantitative MS (Figure 2.4A). Two separate experiments were performed to identify the associated proteins of Sae2 using pT90-containing peptide. As shown in Figure 2.4B, those proteins whose abundance were significantly enriched using pT90-containing peptide than mock-purified sample are Xrs2, Rad53, Dun1, Dma1 and Dma2. The same approach was used to identify pT279-associated proteins. Interestingly, only Rad53 and Dun1 were enriched by both pT90 and pT279 containing peptides of Sae2 (Figure 2.4C), while Xrs2, Dma1 and Dma2 were only enriched by pT90-containing peptide of Sae2. These MS findings are summarized in Figure 2.4D.

A common feature of Xrs2, Rad53, Dun1, Dma1 and Dma2 is that they contain a Forkhead-associated (FHA) domain, which is known to specifically interact with phosphothreonine ligands [78, 79]. To examine the involvement of FHA domain in binding to Sae2, each FHA domain of Dma1, Dma2, Xrs2, Rad53 and Dun1 was expressed in bacteria and cell extract was used to incubate with pT90- or pT279- containing peptide of Sae2. We found that Rad53 FHA1 domain is strongly enriched by pT90 and pT279 containing phosphopeptides, but not when these phosphopeptides were dephosphorylated by Lambda phosphatase (Figure 2.5A, top panel), indicating that these bindings require phosphorylated T90 and T279 of Sae2. The R70A mutation removes a conserved arginine residue in the FHA1 domain that is directly involved in binding to phosphorylated ligand [78]. This mutation largely eliminates binding between Rad53 FHA1 domain and pT90- and pT279- containing phosphopeptides of Sae2 (Figure 2.5A, bottom panels), further supporting a phosphorylation-mediated interaction between Sae2 and Rad53 FHA1 domain. In contrast, Rad53 FHA2 domain does not show detectable binding to either pT90 or pT279 phosphopeptides (Figure 2.5B). Thus, binding between Rad53 and Sae2 is specific to Rad53 FHA1 domain and it involves both phosphorylated T90 and T279 of Sae2.

We next examined the binding between Sae2 phosphopeptides and Dun1 FHA domain. Dun1 FHA domain was enriched by both pT90- and pT279-containing phosphopeptides of Sae2 and these binding were eliminated by a

prior treatment of Lambda phosphatase to dephosphorylate these Sae2 phosphopeptides (Figure 2.5C, top panel). Once again, R60A mutation of the conserved arginine in Dun1 FHA domain involved in ligand binding eliminated binding between Dun1 FHA domain and either pT90 and pT279 phosphopeptides (Figure 2.5C, lower panels), suggesting that this binding between Dun1 and Sae2 is phosphorylation-specific. Consistent with the above MS finding that Xrs2 was identified using pT90 but not pT279 containing phosphopeptide (Figure 2.4), we found Xrs2 FHA domain was enriched by pT90 and not pT279 containing phosphopeptides (Figure 2.5D). This binding was eliminated by both Lambda phosphatase treatment and the R32G and S47A mutations in Xrs2 FHA domain, indicating a phosphorylation-specific interaction. Similarly, both Dma1 and Dma2 FHA domains were enriched by pT90 and not pT279 phosphopeptides in agreement with the above MS findings (Figure 2.5E). Collectively, these findings showed that Sae2 interacts directly with FHA domains of Rad53, Dun1, Xrs2, Dma1 and Dma2 via its phosphorylated T90 and T279, in agreement with the above MS findings.

2.3.5 FHA domains of Rad53, Dun1 and Xrs2 exhibit phosphorylation-specific interaction with Sae2

To further characterize the interactions between Sae2 and Rad53, Dun1 and Xrs2, which are known to have important functions in the DNA damage response, we performed pull-down experiments by incubating FHA domains of Rad53, Dun1 and Xrs2 with cell extracts derived from Sae2-3HA strain and its

variants. We found that Rad53 FHA1, Dun1 and Xrs2 FHA domains specifically enriched Sae2 and this enrichment was eliminated when Sae2-3HA cell extract was pre-treated by Lambda phosphatase (Figure 2.6A), indicating phosphorylation of Sae2 is required for its binding to these FHA domains. Next, we examined mutations of various phosphorylation sites of *SAE2* and their effects on binding to various FHA domains. We found that *sae2-T90A* mutation partially reduced the amount of Sae2 bound to Rad53 FHA1 domain (Figure 2.6B, lane 6), while *sae2-T279A* mutation caused a further enrichment of Sae2 by Rad53 FHA1 domain (Figure 2.6B, lane 7), which was completely eliminated by *sae2-2AQ* mutation and *R70A* mutation in Rad53 FHA1 domain (Figure 2.6B, lane 8 and 9). Thus, both pT90 and pT279 of Sae2 are involved in binding to Rad53 FHA1 domain, in agreement with the above findings (Figures 2.4 and 2.5A). The *sae2-T279A* mutation might enhance this interaction by increasing the amount of Sae2 that is phosphorylated at T90 (Figure 2.1B). Like Rad53 FHA1 domain, Dun1 FHA domain also specifically enriched Sae2 (Figure 2.6C), which are partially reduced by *sae2-T90A* and *sae2-T279A* mutations. The binding between Dun1 FHA domain and Sae2 is completely eliminated by *sae2-2AQ* mutation and *R60A* mutation of Dun1 (Figure 2.6C). Thus, binding between Sae2 and Dun1 involves both phosphorylated T90 and T279 of Sae2 and FHA domain of Dun1. Consistent with the binding between Xrs2 FHA domain and Sae2 pT90-containing phosphopeptide (Figure 2.5D), Xrs2 FHA domain specifically enriched Sae2 (Figure 2.6D), which was largely eliminated by *T90A*,

but not *T279A* mutation of Sae2. Again, mutations of the conserved residues R32 and S47 in Xrs2 FHA domain, which are expected to interact with phosphothreonine ligands, abolished the interaction between Xrs2 FHA domain and Sae2 (Figure 2.6D), indicating the binding specificity.

Due to inherent differences in the experiments in Figures 2.5 and 2.6, it is difficult to compare the relative binding efficiency between them. It is further possible that phosphopeptides of Sae2 may not behave the same as phosphorylated Sae2 protein, which is phosphorylated at T90 and T279 at unknown levels. Moreover, the binding affinity between full length Rad53, Dun1 and Xrs2 (together with Mre11 and Rad50) with Sae2 remain to be investigated. Nevertheless, these findings here show that phosphorylation of T90 and T279 of Sae2 specifically mediate its interactions with FHA domains of Rad53, Dun1 and Xrs2 via the known phosphorylation-dependent FHA recognition mechanism. These findings also provided indirect evidence for phosphorylation of T90 and T279 of Sae2.

2.3.6 Genetic relationships between *RAD53* and *DUN1 with SGS1 and EXO1*

Considering the lethality of *sae2-2AQ sgs1Δ exo1Δ* triple mutant and that Rad53 and Dun1 interact with Sae2 via T90 and T279 (Figures 2.4, 2.5 and 2.6), we reasoned that *rad53* and *dun1* mutants might share similar genetic interaction profiles like *sae2-2AQ* mutant. To test this, we examined the effect of mutating *RAD53* and *DUN1* in *sgs1Δ* and *exo1Δ* mutants. We found that

dun1Δ rad53-R70A,N107A sgs1Δ triple mutant is dead (Figure 2.7A), while *dun1Δ exo1Δ sgs1Δ* and *rad53-R70A,N107A exo1Δ sgs1Δ* triple mutants are viable (Figure 2.7A). Thus, loss of both Dun1 and Rad53 FHA1 domain causes lethality in cells lacking *SGS1*. We note here that *sae2-2AQ* mutant is lethal in cells lacking both Sgs1 and Exo1 (Figure 2.3A). The stronger genetic interaction between *rad53 dun1Δ* with *sgs1Δ* could be attributed to that Rad53 and Dun1 FHA domains are known to have additional ligands besides Sae2.

To further explore the genetic relationships between *sae2-2AQ* with *rad53* and *dun1Δ* mutations, we examined the effect of *rad53* and *dun1Δ* mutations on CPT sensitivity of *sae2-2AQ* mutant. We found that *sae2-2AQ dun1Δ* double mutant has essentially the same sensitivity to CPT as *sae2-2AQ* mutant (Figure 2.7B), while *rad53-R70A,N107A sae2-2AQ* double mutant is modestly more sensitive to CPT than either *rad53-R70A,N107A* and *sae2-2AQ* single mutants (Figure 2.7C). The *sae2-2AQ rad53 dun1Δ* triple mutant is more sensitive to CPT than either *sae2-2AQ or rad53 dun1Δ* double mutant. Once again, we note here that this elevated CPT sensitivity of *sae2-2AQ rad53 dun1Δ* triple mutant could be complicated by that Rad53 and Dun1 FHA domains are known to have additional ligands.

Given that phosphorylation of T90 and T279 of Sae2 plays a role in preventing GCRs (Figure 2.3C, Table 2.2), we compared the rate of accumulating GCRs in *sae2-2AQ* mutant with those in *rad53* and *dun1Δ* mutants. As previously reported, deletion of *DUN1* causes an increase of GCRs

(~8-fold) compared to a wild-type strain *[7]*. Mutation of *rad53-R70A* resulted in a similar GCR rate to that of *sae2-2AQ* mutant, while the rate of accumulating GCRs in *dun1Δ rad53-R70A* double mutant is comparable to *dun1Δ, rad53* and *sae2-2AQ* single mutants (Figure 2.7D, Table 2.2). Thus, the rates of accumulating GCRs in these mutants are modest and comparable to each other.

2.3.7 Genetic relationships between *Xrs2 FHA domain with SGS1 and EXO1*

Sae2 is known to function together with the Mre11-Rad50-Xrs2 complex. It is interesting to detect a specific interaction between phosphorylated T90 and Xrs2 FHA domain here (Figures 2.4-2.6). To explore this further, we examined the effect of R32G and S47A mutations in Xrs2 FHA domain, which specifically disrupts its binding to phosphorylated T90 of Sae2. We found that this *xrs2* mutation does not cause an appreciable increase in sensitivity to a lower concentration (10 μM) of CPT treatment, although a higher sensitivity was observed at 20 μM CPT (Figure 2.8A). This *xrs2* mutation does not appreciably alter CPT sensitivity of *sgs1Δ*, unlike *sae2-2AQ* (Figure 2.8A), although we note here that Xrs2 FHA domain only interacts with phosphorylated T90 of Sae2. On the other hand, this *xrs2* FHA domain mutation does cause an elevated sensitivity to CPT in cells lacking Exo1 (Figure 2.8B), unlike *sae2-2AQ* (Figure 2.3D).

Taken together, the findings presented here suggest that phosphorylation of Sae2 and its recruitment of Rad53, Dun1 and Xrs2 might have multiple functions in DNA repair related processes.

2.4 Discussion

Sae2 and its ortholog CtIP have a key function in the initial processing of damaged DNA, which influences subsequent DNA repair pathway choices. A conserved feature of Sae2 and CtIP is their post-translational modifications, in particular, phosphorylation of Sae2/CtIP, has been shown to be critical for its functions in diverse organisms [34, 63, 65-68, 70, 80-82]. However, the molecular mechanism concerning phosphorylation regulation of Sae2 remains insufficiently understood. Here we showed that two conserved residues, threonine-90 and threonine-279, of Sae2 redundantly regulate its functions in the DNA damage response and suppression of gross chromosomal rearrangements. We further show that phosphorylation of these residues of Sae2 mediates specific interactions with multiple FHA-domain containing proteins, including Rad53, Dun1 and Xrs2, which are known to function in the DNA damage response. The initial analyses presented here reveal that these biochemical interactions are highly specific and they likely contribute to the function of Sae2 phosphorylation in not only DNA damage checkpoint but also DNA repair.

2.4.1 Conserved threonines of Sae2 have a redundant role in the DNA damage checkpoint and DNA repair

Among those Mec1 and Tel1 phosphorylation sites of Sae2, T279 is conserved in vertebrate CtIP, and phosphorylated by ATR and ATM, orthologs of Mec1 and Tel1, respectively. T90 of Sae2 is conserved among most fungal species, but not mammalian CtIP or *S. pombe* Ctp1. Despite this sequence divergence, T90 of Sae2 has a redundant role with T279 in regulating its functions in the DNA damage response. Mutations of both T90 and T279 of Sae2 cause a persistent and elevated Rad53 phosphorylation, similar to deletion of *SAE2* [34, 63]. The synthetic lethal interaction between *sae2-2AQ* mutation and *sgs1Δ exo1Δ* mutation is striking (Figure 2.3A), and it suggests that phosphorylation of Sae2 may have an important function in DNA end processing, consider the role of Sgs1 and Exo1 in DNA end processing. Further study is needed to address this more specifically.

Interestingly, despite *sae2-S249A* mutation has a significant effect on Sae2 electrophoretic mobility shift (Figure 2.1B), it does not cause any detectable phenotype in the assays performed in this study. This does not exclude the possibility that S249 phosphorylation of Sae2 might have another function yet to be identified. However, our findings here suggest that evolutionary conservation of the phosphorylated threonine residues of Sae2, rather than stoichiometry of phosphorylation, may provide a better prediction of potential functions of Sae2 phosphorylation.

2.4.2 Potential functions of Sae2-associated FHA domain-containing proteins

While it is evident that phosphorylation of Sae2 and its ortholog CtIP have important roles in regulating their functions in DNA damage checkpoint and DNA repair, the precise function of their phosphorylation has been insufficiently understood. Here we show that threonine-specific phosphorylation of Sae2 by Mec1 and Tel1 can recruit several FHA domain-containing proteins, including Rad53, Dun1, Xrs2, Dma1 and Dma2. The biochemical data presented here demonstrated the specificity of these phosphorylation-mediated interactions, consistent with the known ligand-binding property of FHA domains. It should be noted that these interactions are expected to have low micromolar affinity [78], thus requiring the use of recombinant FHA domain or abundant phosphopeptides of Sae2 to facilitate the detection of these interactions. For this reason, we cannot rule out the possibility that some of the binding interactions could occur as a biochemical artifact. On the other hand, similar FHA-mediated interactions have been shown to be important for the DNA damage checkpoint [73, 78, 82, 83]. Therefore, it is reasonable to suggest that some of these interactions may have important roles in Sae2 functions. Among them, Rad53, Dun1 and Xrs2 are particularly interesting, since they have known roles in the DNA damage response. Unlike genetic analysis of various *sae2* phosphorylation-defective mutants, analysis of *rad53, dun1Δ* and *xrs2* mutants could be complicated by the fact that FHA domains in these proteins are known

to have other ligands, which are critical for their diverse functions in the DNA damage response. For example, both FHA domains of Rad53 are known to interact with Rad9 and Mrc1, which are important for its activation [72, 73]. Additionally, many other ligands of Rad53 FHA1 domain have been identified [84]. Similarly, FHA domain of Dun1 is known to be critical for its interaction with Rad53 and trans-activation by Rad53 [83, 85]. Xrs2 FHA domain has also been shown to interact with Lif1 to promote NHEJ [86]. These other functions of Rad53, Dun1 and Xrs2 may complicate the genetic analysis here. Despite these caveats, several observations here suggest that Rad53 and Dun1 may be involved in the function of Sae2 phosphorylation in DNA repair. For example, *rad53 dun1Δ* mutation is synthetic lethal with *sgs1Δ*, although *sae2-2AQ* is lethal in cells lacking both Sgs1 and Exo1. Obviously, further studies are needed to dissect the functions of the biochemical interactions uncovered here, which point to a complex role of Sae2 phosphorylation in several processes.

We speculate that phosphorylated Sae2 may recruit Rad53, Dun1 and Xrs2 to the sites of DNA damage for different functions. Rad53 and Dun1 may phosphorylate proteins at the sites of DNA damage in a Sae2-dependent manner. For example, Dun1 was implicated in suppressing DSB-induced chromosomal translocations in the same study that demonstrated a role for Sae2 and its DNA damage-induced phosphorylation [64]. Clearly, identification of the relevant substrates of Rad53 and Dun1 that are specifically mediated by

Sae2 would be essential to understand the function of the interactions reported here.

2.5 Materials & Methods

2.5.1 Plasmids and yeast genetic methods

SAE2 plus 200 base pairs of upstream sequence was cloned into a pFA6a plasmid using PacI and AscI sites [87]. Sae2 and Rad9 were tagged in the C-terminus with a 6xHis-3xHA (3HA) epitope from pFA6a. FHA domains of Dma1, Dma2, Rad53-FHA1, Rad53-FHA2, and Dun1 were cloned into pGEX-4T1 plasmid such that an N-terminal GST tag is fused to each FHA domain. Xrs2-FHA domain was cloned into a C-terminal 6xHis-FLAG-TEV-Protein A (TAF) in pET21a plasmid [84]. All point mutations were introduced by site-directed mutagenesis and confirmed by DNA sequencing.

Yeast strains used are isogenic with W303 or S288c as shown in Table 2.1. Standard yeast genetic methods were used to introduce mutations into chromosomal loci, which were confirmed by DNA sequencing. For plate sensitivity, cells were grown to late log-phase and normalized before serial dilution and spotting onto YPD and drug plates with indicated concentrations. Cells were grown at 30°C and imaged after 2-3 days unless otherwise noted. For dose-dependent killing curve, cells in log-phase were split and treated with indicated doses of methyl methanesulfonate (MMS) for 1 hour. Cells were

added to an equal volume of 10% sodium thiosulfate to quench the MMS before serial dilution and plating onto YPD. Cells were incubated for 3 days at 30°C. Percent viability was calculated by dividing the number of viable colonies for each strain after the MMS treatment compared to no treatment and an average of three independent experiments was used. Camptothecin (CPT) sensitivity as measured by liquid culture was performed as previously described [71, 88]. Briefly, overnight cultures were diluted to YPD containing 2% DMSO to grow for 5 hours in log phase. For slow growing cultures this pre-growth was done overnight. Cultures were then diluted to an OD_{600} of 0.001 in YPD with 2% DMSO containing camptothecin at varying concentrations of 0 (untreated), 1, 5, 10, and 20 μM. Cultures were grown until the untreated control had reached 10 doublings before subsequent treated cultures were measured. The slope of the plot $\ln(A/A_0)$ was calculated, and the ratio of $Slope_C$ (treated) vs $Slope_{C=0}$ (untreated) from averages of three independent experiments is shown in the graphs. Fluctuation analysis used in analyzing GCRs was described previously [76].

2.5.2 Biochemical methods

For Western blot analysis, protein extracts were prepared using a TCA (trichloroacetic acid) method. To monitor Rad53 phosphorylation we used a mouse monoclonal α-Rad53, EL7E1 serum (Dr. Marco Foiani). To detect Sae2-3HA and Rad9-3HA, we used the 3F10 antibody (α-HA, Roche). For pull-down experiments, various Sae2-3HA cells were treated with 25 μg/mL phleomycin

for 1 hour. Native protein extracts from these cells were prepared using glass beads method described previously [89]. FHA-domain resins of Xrs2, Rad53-FHA1, and Dun1 were incubated with protein extracts derived from Sae2-3HA strain in TBS-N buffer (50mM Tris-HCl pH7.4, 0.5% NP-40, 150mM NaCl) for 2 hours at 4°C and washed several times. FHA binding proteins were eluted by boiling in 1% SDS or with cleavage by TEV protease. To dephosphorylate Sae2-3HA in cell extract, we incubated Sae2-3HA cell extract with 4000 units of Lambda phosphatase for 1 hour at 30 degree in the presence of 2 mM $MnCl_2$ without EDTA and beta-glycerophosphate. To preserve phosphorylation of Sae2, 5 mM EDTA and 5 mM beta-glycerophosphate were included to inhibit cellular phosphatases during the preparation of Sae2-3HA cell extract, which was not treated by Lambda phosphatase. Equal amounts of both cell extracts (with and without Lambda phosphatase treatment) were then used for FHA domain pull-down experiment. To prepare unphosphorylated peptide of Sae2, pT90 and pT279 containing phosphopeptides of Sae2 bound to neutravidin resins were dephosphorylated by 800 units of Lambda phosphatase before they were used for binding experiments with various FHA domains.

To prepare phosphopeptide resins, pT90- and pT279- containing phosphopeptides of Sae2 (Chi Scientific) with an N-terminal biotin were first immobilized on neutravidin resins (Thermo Scientific). Phosphopeptide resins or blank resins were incubated with native protein extracts, which were pre-treated with blank neutravidin resins to deplete endogenous biotinylated

proteins. The native cell lysates were prepared using glass beads method and cells grown using the Stable Isotope Labeling via Amino acid in Culture (SILAC) method [90]. After incubation, the phosphopeptide resins and blank resins were washed by the same TBS-N binding buffer. Phosphopeptide-binding proteins were eluted by incubation with 8M urea at 37°C for 30 minutes. Eluted proteins were reduced by 10mM DTT and alkylated with 30mM iodoacetamide before dilution and proteolysis with trypsin (Promega).

2.5.3 Methods used in quantitative mass spectrometry analyses

Trypsin-digested peptides were desalted using a Sep-Pak C18 cartridge and then resuspended in 80% acetonitrile/20% water to be fractionated on a TSKgel Amide-80 (1.0mm ID) column (TOSOH Bioscience) [91]. A total of 14 fractions were collected for LC-MS/MS analysis using an Orbitrap-LTQ mass spectrometer. MS data were searched using Sorcerer-SEQUEST as described previously [89]. The identified peptides were quantified using XPRESS. In cases where peptides in the mock sample were not identified, a minimal ion intensity of 1.0E4 was used to calculate the abundance ratio. Each protein was identified and quantified with at least three unique peptides. The average of their abundance ratios was used to calculate the abundance ratio for each protein for both replicate experiments.

2.6 Acknowledgements

This work was supported by funding from NIH GM080469 and Ludwig Cancer Research to H.Z. and R.S. J.L. was supported by NCI-training grant T32 CA009523. We thank Dr. Claudio Albuquerque for help with the MS analysis of phosphopeptide-binding proteins and Dr. Veronica Baldo for discussion and sharing yeast genetic techniques during the course of this study. We thank Dr. Marco Foiani for the anti-Rad53 antibody used in this study. We thank Dr. Lorraine Symington for helpful discussions and critical reading of the manuscript.

Chapter 2, in full, is a reprint of the material as it appears in Phosphorylation of Sae2 Mediates Forkhead-associated (FHA) Domain-specific Interaction and Regulates Its DNA Repair Function. *J Biol Chem*. 2015 Apr 24;290(17):10751-63, Liang J, Suhandynata RT, Zhou H. The dissertation author is the primary author for this paper.

Figure 2.1 T90 and T279 of Sae2 are specifically involved in its function in the DNA damage response

A) Sequence alignment of Sae2 orthologues revealed that T90 and T279 of Sae2 are conserved among various fungi, while T279 is also conserved in human CtIP as T859. B) Cell lysates derived from an untagged and the Sae2-3HA strain with various *sae2* (*2AQ-T90A,T279A; 3AQ-T90A,T279A,S249A*) mutants treated by 25 μg/mL phleomycin or 20μM camptothecin (CPT) for 1hr and analyzed by anti-HA immunoblotting. Ponceau stain shows equal loading. Asterisk denotes DNA damage-induced gel bands of Sae2-3HA. Strains used – HZY1078, JLY030, JLY032, JLY035, JLY048, JLY050 and JLY053. C) 10-fold serial dilution of wild-type strain and various *sae2* phosphorylation-defective mutants were plated on YPD plates containing no drug, 0.02% methyl methanesulfonate (MMS), DMSO, 30μM camptothecin (CPT), or 3μg/mL phleomycin for 3 days at 30°C. Strains used - HZY1078, HZY1235, HZY1236, HZY1239, HZY1240, HZY1241, HZY1242, HZY1243 and HZY1244. D) Camptothecin sensitivity of wild-type strain (open circle, HZY1077/HZY1078), the *sae2*Δ mutant (open square, HZY1239) and *sae2-2AQ* mutant (open triangle, HZY1244) were examined in liquid culture at various concentrations over 10 doubling times. The ratio of the slope of the curve between treated ($Slope_C$) and untreated ($Slope_{C=0}$) is plot for each concentration (See Materials & Method). The average result of three independent experiments is shown. E) Dose-dependent viability curve of *sae2* were analyzed using the same strains as in D. Cells were treated for 1 hour at the indicated MMS concentrations and then plated on YPD plates to measure the number of viable cells. The average result of three independent experiments is shown. Error bars represent the S.D.

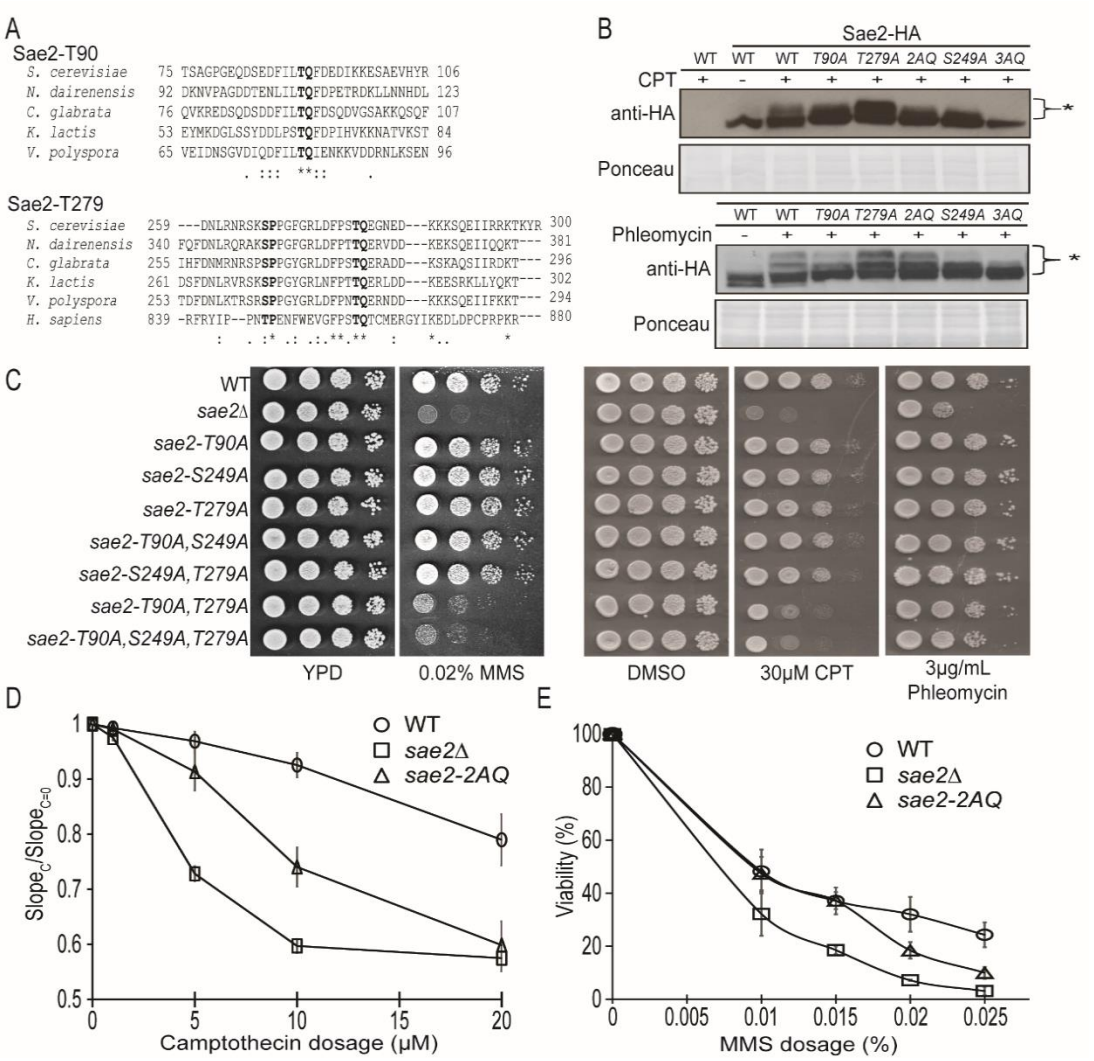
A
Sae2-T90
S. cerevisiae 75 TSAGPGEQDSEDFILTQFDEDIKKESAEVHYR 106
N. dairenensis 92 DKNVPAGDDTENLILTQFDPETRDKLLNNHDL 123
C. glabrata 76 QVKREDSQDSDDFILTQFDSQDVGSAKKQSQF 107
K. lactis 53 EYMKDGLSSYDDLPSTQFDPIHVKKNATVKST 84
V. polyspora 65 VEIDNSGVDIQDFILTQIENKKVDDRNLKSEN 96
Sae2-T279
S. cerevisiae 259 ---DNLRNRSKSPPGFGRLDFPSTQEGNED---KKKSQEIIRRKTKYR 300
N. dairenensis 340 FQFDNLRQRAKSPPGFGRLDFPTTQERVDD---KEKSQEIIQQKT--- 381
C. glabrata 255 IHFDNMRNRSPSPPGYGRLDFPSTQERADD---KSKAQSIIRDKT--- 296
K. lactis 261 DSFDNLRVRSKSPPGYGRLNFPTTQERLDD---KEESRKLLYQKT--- 302
V. polyspora 253 TDFDNLKTRSRSPPGYGRLDFPNTQERNDD---KKKSQEIIFKKT--- 294
H. sapiens 839 -RFRYIP--PNTPENFWEVGFPSTQTCMERGYIKEDLDPCPRPKR--- 880
B
Sae2-HA
WT WT WT T90A T279A 2AQ S249A 3AQ
CPT
anti-HA
Ponceau
Phleomycin
C
WT
sae2Δ
sae2-T90A
sae2-S249A
sae2-T279A
sae2-T90A,S249A
sae2-S249A,T279A
sae2-T90A,T279A
sae2-T90A,S249A,T279A
YPD
0.02% MMS
DMSO
30μM CPT
3μg/mL Phleomycin
D
WT
sae2Δ
sae2-2AQ
Slope_C/Slope_C=0
Camptothecin dosage (μM)
E
Viability (%)
MMS dosage (%)

Figure 2.2 Persistent Rad53 phosphorylated in the *sae2-2AQ* mutant following a transient DNA damage treatment

A) DNA damage checkpoint inactivation was examined using anti-Rad53 monoclonal antibody in wild-type and *sae2* mutants. Cells were treated for 1 hour with 0.01% MMS and subsequently resuspended into fresh YPD media. Cells were harvested at indicated time points to examine Rad53 phosphorylation. Representative loading control by Ponceau stain. Strains used – HZY1077, HZY1239, HZY1240, HZY1242 and HZY1244. B) Inactivation of Rad53 is correlated with dephosphorylation of HA-tagged *RAD9*. Rad9 phosphorylation was monitored at indicated time points similarly as in A with wild-type, *sae2-2AQ*, and *sae2*Δ cells. Strains used – JLY089, JLY091 and JLY093. C-D) Effect of combining the *rad9*Δ or *mrc1*Δ with *sae2-2AQ* mutations in causing DNA damage sensitivity. C) Camptothecin sensitivity at various concentrations. The ratio of the slope of the curve between treated ($Slope_C$) and untreated ($Slope_{C=0}$) is plot for each concentration (See Materials & Method). The average result of three independent experiments is shown with S.D. represented by error bars. D) Hydroxyurea sensitivity. Strains used for C and D – HZY1077/HZY1078, HZY1244, JLY158, JLY160, JLY161, JLY162, JLY163 and JLY164.

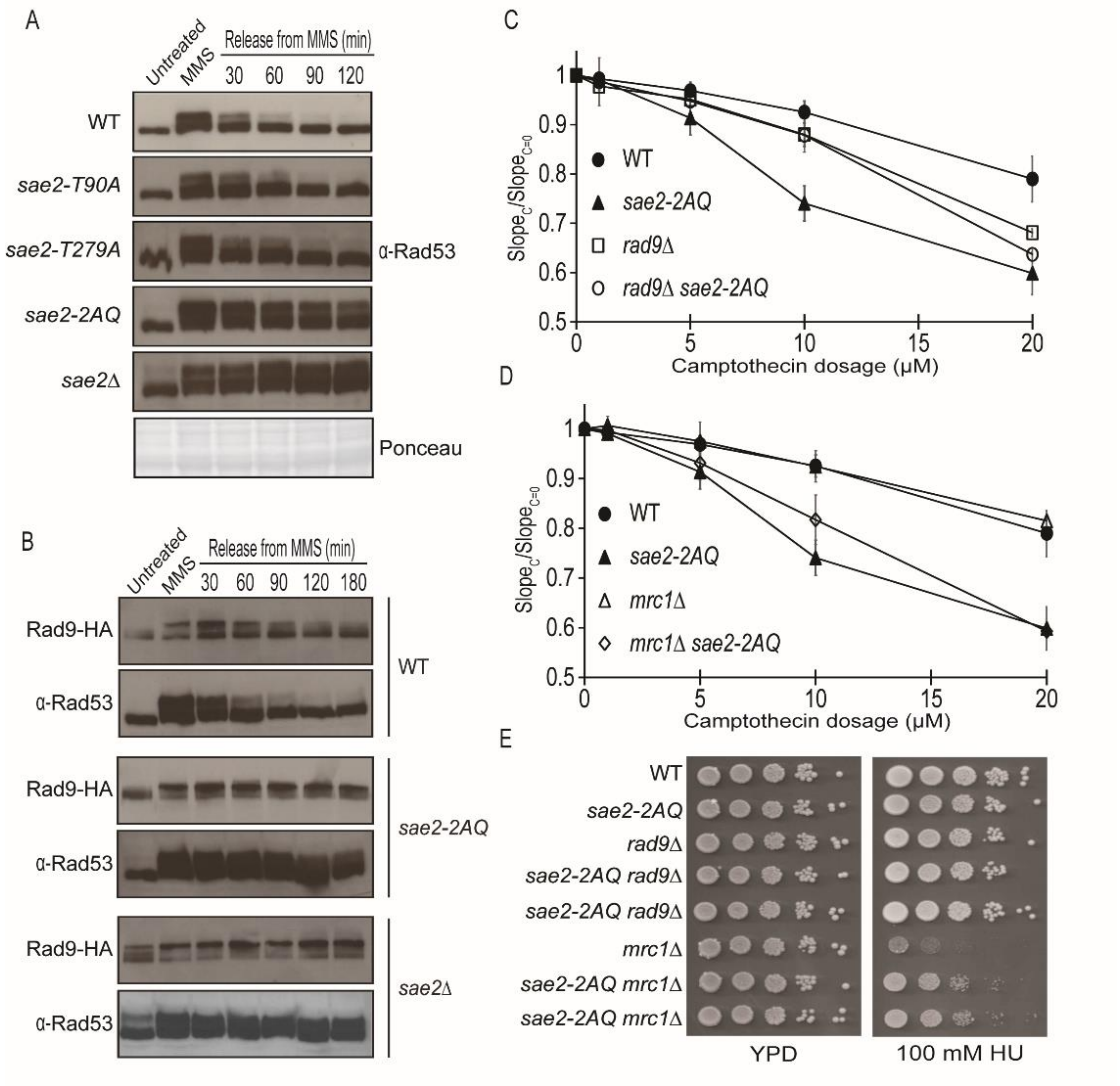
A
Untreated
MMS
Release from MMS (min)
30 60 90 120
WT
sae2-T90A
sae2-T279A
sae2-2AQ
sae2Δ
α-Rad53
Ponceau
B
Untreated
MMS
Release from MMS (min)
30 60 90 120 180
Rad9-HA
α-Rad53
WT
sae2-2AQ
sae2Δ
C
Slope_C/Slope_C=0
WT
sae2-2AQ
rad9Δ
rad9Δ sae2-2AQ
Camptothecin dosage (μM)
D
Slope_C/Slope_C=0
WT
sae2-2AQ
mrc1Δ
mrc1Δ sae2-2AQ
Camptothecin dosage (μM)
E
WT
sae2-2AQ
rad9Δ
sae2-2AQ rad9Δ
sae2-2AQ rad9Δ
mrc1Δ
sae2-2AQ mrc1Δ
sae2-2AQ mrc1Δ
YPD
100 mM HU

Figure 2.3 Genetic interactions between the *sae2-2AQ* mutation and mutations that affect DNA end resection, *sgs1Δ* and *exo1Δ*

A) Tetrad dissection of diploids containing heterozygous *sae2-2AQ*, *exo1Δ* and *sgs1Δ* mutations. Strains used – JLY229, JLY540 and JLY541. B) Camptothecin sensitivity of *sae2-2AQ* and *sgs1Δ* mutaitons at various concentrations. The ratio of the slope of the curve between treated ($Slope_C$) and untreated ($Slope_{C=0}$) is plot for each concentration (See Materials & Method). The average result of three independent experiments is shown with S.D. represented by error bars. Strains used – HZY1077, HZY1244, JLY233, and JLY235. C) Rates of accumulating GCRs in the *sae2* and *sgs1Δ* mutants using the *yel072w::CAN1/URA3* assay measured by fluctuation analysis (see Table 2.2). Strains used - HZY2672, HZY2709, HZY2801, and HZY2802. D) Camptothecin sensitivity shown the same as in B except with *sae2-2AQ* and *exo1Δ* mutations. Strains used – HZY1077, HZY1244, JLY230, JLY234 E) Graph of rate of accumulating GCRs shown the same as in C except with *sae2* and *exo1Δ* mutants. Strains used - HZY2672, HZY2709, HZY3041, and HZY3042.

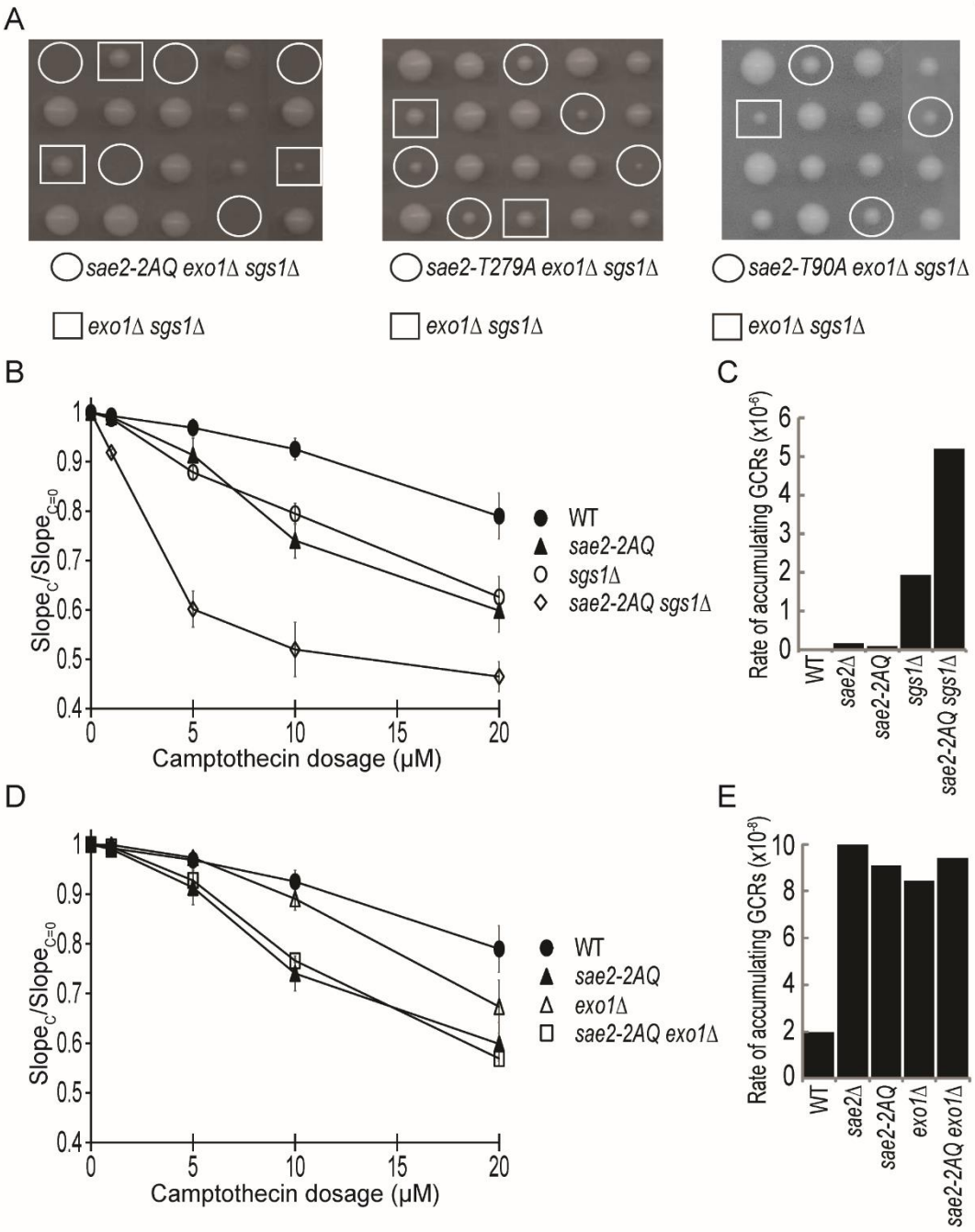
A
sae2-2AQ exo1Δ sgs1Δ
exo1Δ sgs1Δ
sae2-T279A exo1Δ sgs1Δ
exo1Δ sgs1Δ
sae2-T90A exo1Δ sgs1Δ
exo1Δ sgs1Δ
B
Slope_C/Slope_C=0
Camptothecin dosage (μM)
WT
sae2-2AQ
sgs1Δ
sae2-2AQ sgs1Δ
C
Rate of accumulating GCRs (x10^-6)
WT
sae2Δ
sae2-2AQ
sgs1Δ
sae2-2AQ sgs1Δ
D
Slope_C/Slope_C=0
Camptothecin dosage (μM)
WT
sae2-2AQ
exo1Δ
sae2-2AQ exo1Δ
E
Rate of accumulating GCRs (x10^-8)
WT
sae2Δ
sae2-2AQ
exo1Δ
sae2-2AQ exo1Δ

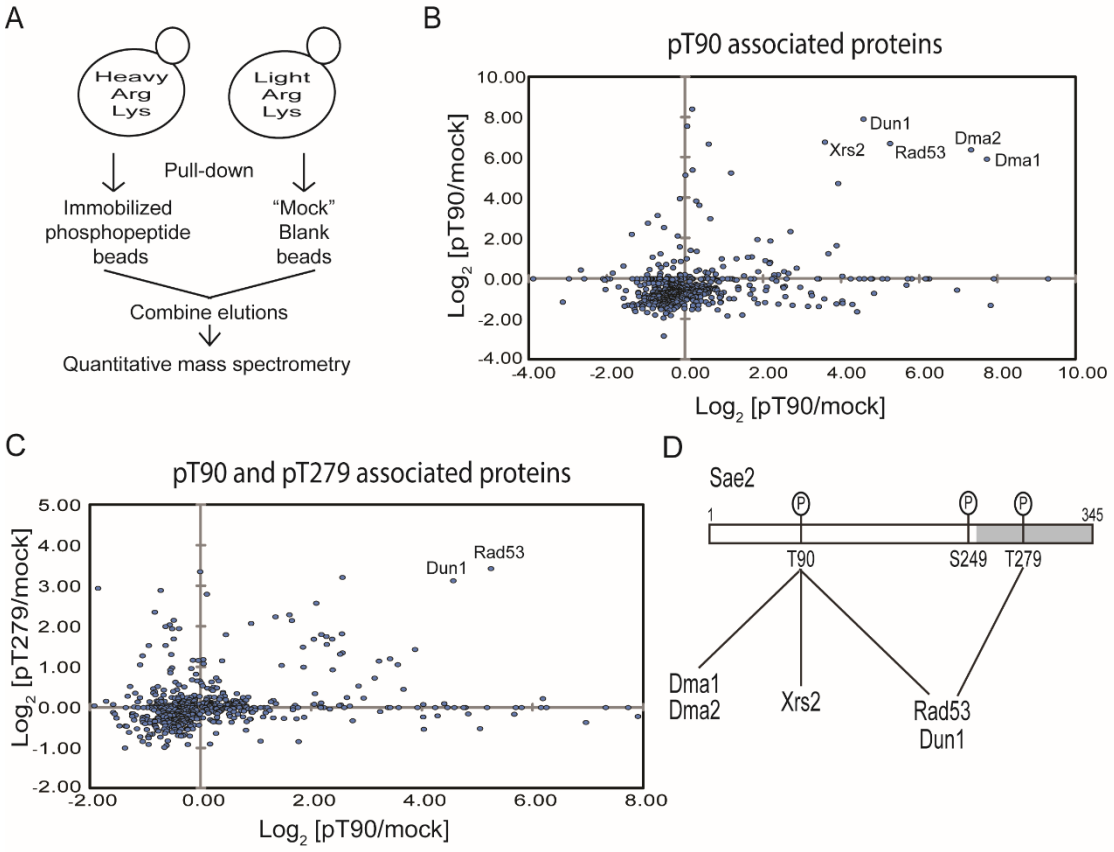

Figure 2.4 Phosphorylated T90 and T279 containing peptides of Sae2 interact with multiple FHA domain-containing proteins, including Rad53, Dun1, Xrs2, Dma1 and Dma2

A) Experimental method to identify the associated proteins of pT90- or pT279- containing phosphopeptide of Sae2 by SILAC-based quantitative MS. B) Relative abundance of proteins enriched by pT90-phosphopeptide resins compared to blank resins in two independent experiments. The abundance ratio of each protein was calculated using minimally three unique peptides per protein and shown in a $\log_2$ scale. The proteins clustered in the top right area were greatly enriched in both replicate experiments, thus considered as candidate binding proteins. C) Same as in B except comparing the relative abundance of proteins enriched by pT90-phosphopeptide resins or pT279-phosphopeptide resins compared to blank resins, each from independent experiments. Strain used – SCY249. D) Summary of candidate pT90- and pT279-associated proteins identified by quantitative MS.

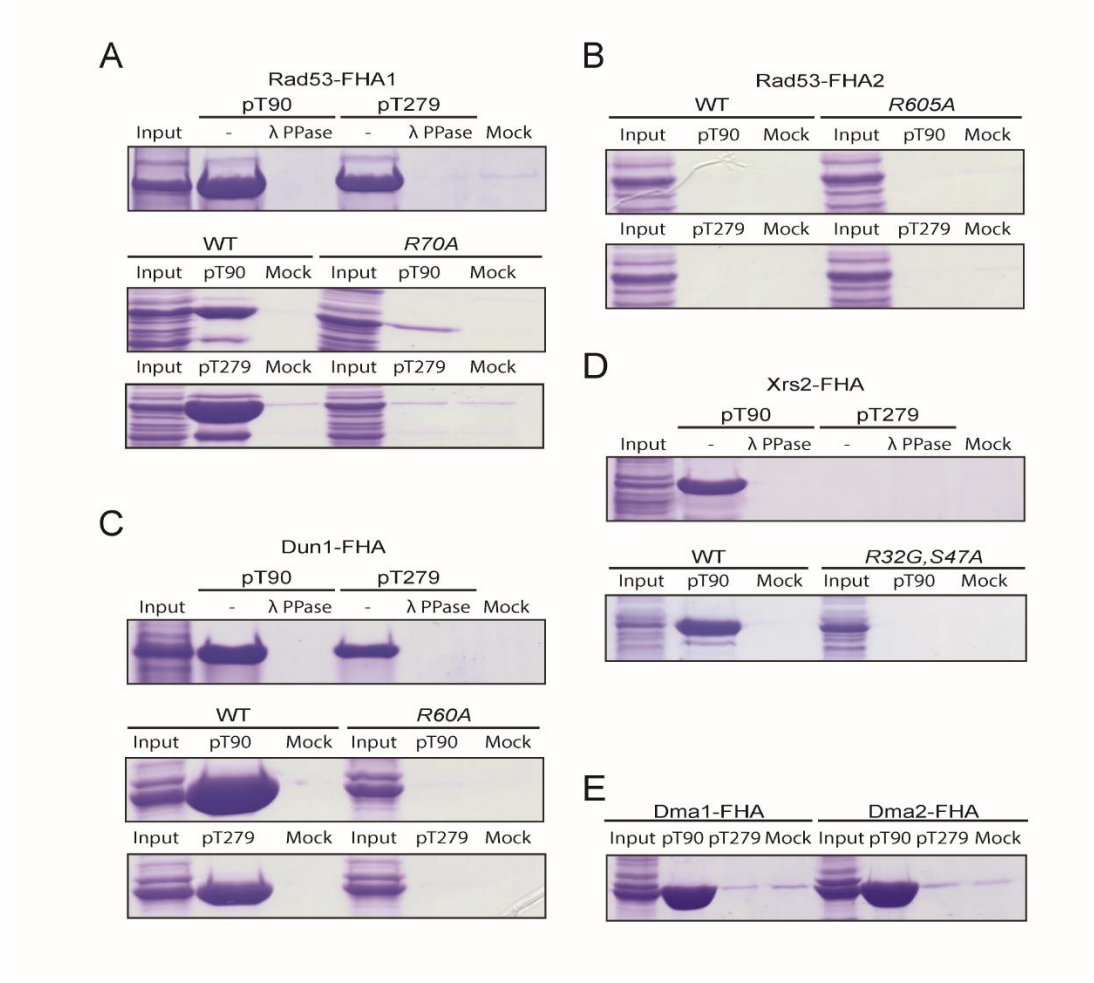

Figure 2.5 Phosphothreonine peptides of Sae2 interact directly with FHA domains or Rad53, Dun1, Xrs2, Dma1 and Dma2

A) Sae2-phosphopeptides containing either pT90 or pT279, treated with or without lambda phosphatase, and mock beads incubated with overexpressed Rad53-FHA1 from bacterial lysate (Top panel). pT90 or pT279 phosphopeptide and mock beads incubated with either overexpressed Rad53-FHA1 or its FHA mutant (Rad53-R70A-FHA1) from bacterial lysate (Bottom panel). B) pT90 or pT279 phosphopeptide and mock beads incubated with either overexpressed Rad53-FHA2 or its FHA mutant (Rad53-R605A-FHA2) from bacterial lysate. C) Same as in A, except with Dun1 FHA domain and its FHA mutant (Dun1-R60A-FHA). D) Xrs2-FHA domain overexpressed in bacterial lysate was incubated with pT90 or pT279, treated with or without lambda phosphatase, and mock beads (Top panel). pT90 phosphopeptide and mock beads were incubated with either overexpressed Xrs2-FHA or its FHA mutant (Xrs2-R32G,S47A-FHA) from bacterial lysate (Bottom panel). E) Sae2-phosphopeptides containing either pT90 or pT279, and mock beads incubated with either overexpressed Dma1-FHA or Dma2-FHA from bacterial lysate.

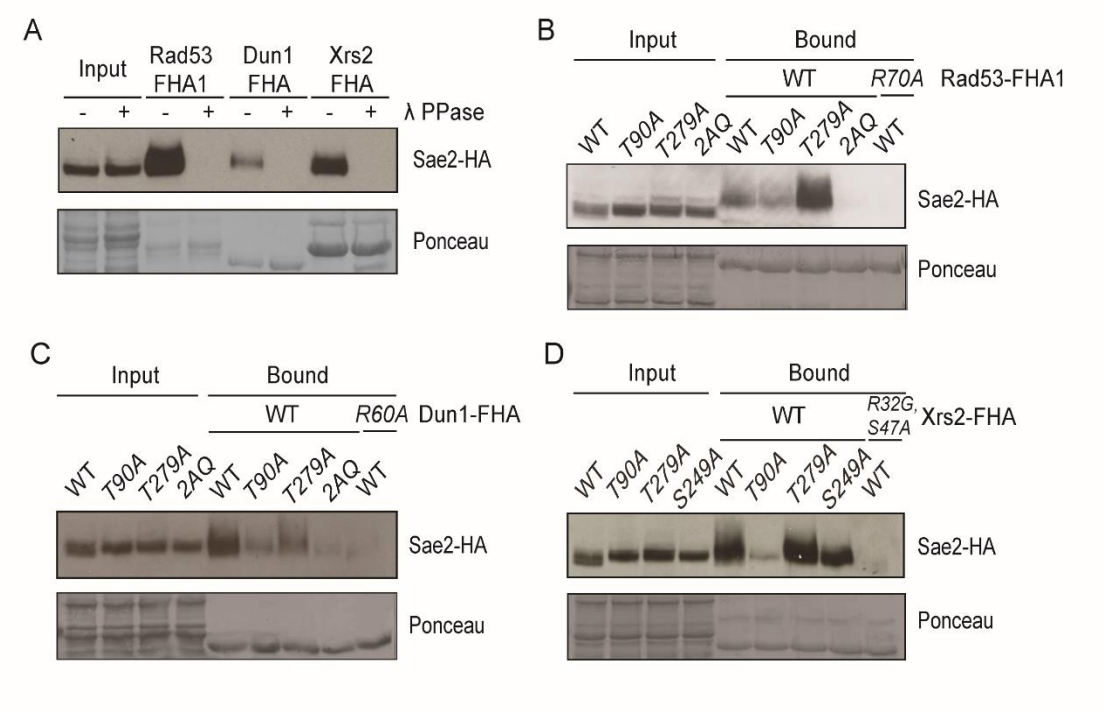

Figure 2.6 FHA domains of Rad53, Dun1 and Xrs2 specifically enriched phosphorylated Sae2 induced by phleomycin treatment in a T90- and T279- dependent manner

A) Pull-down of phleomycin-treated Sae2-3HA with recombinant Rad53-FHA1, Dun1-FHA, and Xrs2-FHA domains from lysates incubated with or without lambda phosphatase. B) Pull-down assay using recombinant GST-FHA1 of Rad53 (2-279 amino acids) to detect the specific enrichment of Sae2-3HA and various *sae2* mutant proteins, revealing the involvement of both T90 and T279 of Sae2 and that the binding is eliminated by the R70A mutation in the Rad53 FHA1 domain. C) Pull-down assay using GST-FHA (1-150 amino acids) of Dun1 to enrich Sae2 showed the involvement of both T90 and T279 of Sae2 and that this binding is essentially eliminated by the R60A mutation in the Dun1 FHA domain. D) Pull-down assay using Xrs2 FHA-BRCT-TAF (1-331 amino acids) showed the involvement of T90 of Sae2 and that this binding was diminished by the R32G and S47A mutations in the FHA domain of Xrs2. Strains used JLY030, JLY032, JLY048, JLY050, and JLY053.

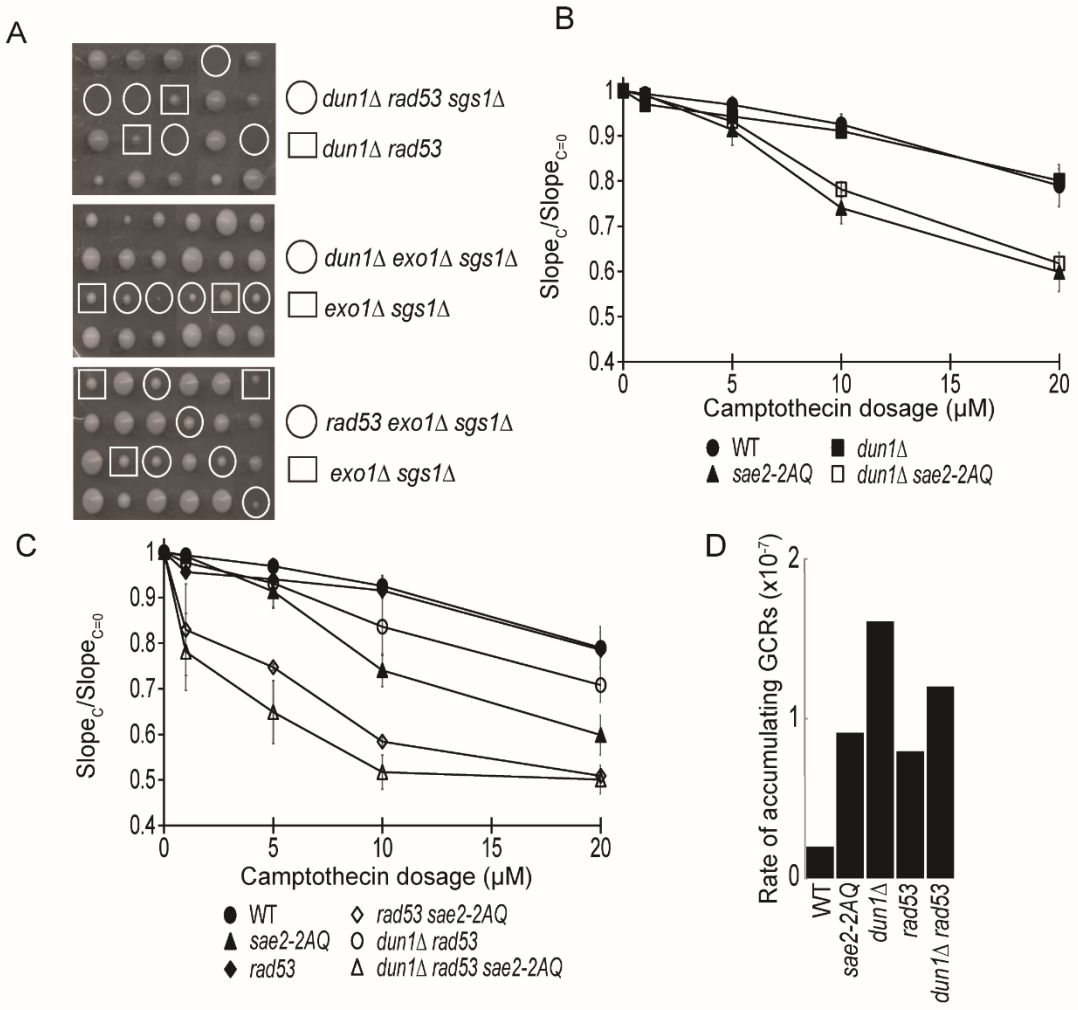

Figure 2.7 Genetic interactions between the *dun1Δ* and *rad53-R70A,N107A* mutations with the *sgs1Δ* and *exo1Δ* mutations

A) Tetrad dissection of diploids containing the following heterozygous mutations: *dun1Δ*, *rad53 (rad53-R70A,N107A)*, and *sgs1Δ*; *exo1Δ, sgs1Δ* and *dun1Δ*; *exo1Δ, sgs1Δ* and *rad53*. Strains used – JLY171, JLY496 and JLY497 B-C) Camptothecin sensitivity of *sae2-2AQ*, *dun1Δ*, *rad53 (rad53-R70A,N107A)* and their combined mutations at various concentrations. The ratio of the slope of the curve between treated ($Slope_C$) and untreated ($Slope_{C=0}$) is plot for each concentration (See Materials & Method). The average result of three independent experiments is shown with S.D. represented by error bars. Strains used – HZY1077, HZY1244, JLY221, JLY223, JLY635, JLY637, JLY639, and JLY641. D) Rates of accumulating GCRs comparing the *sae2-2AQ*, *dun1Δ*, and *rad53 (rad53-R70A)* mutants. Strains used – HZY2672, HZY2709, HZY2908, HZY2909, HZY2912 and HZY2913.

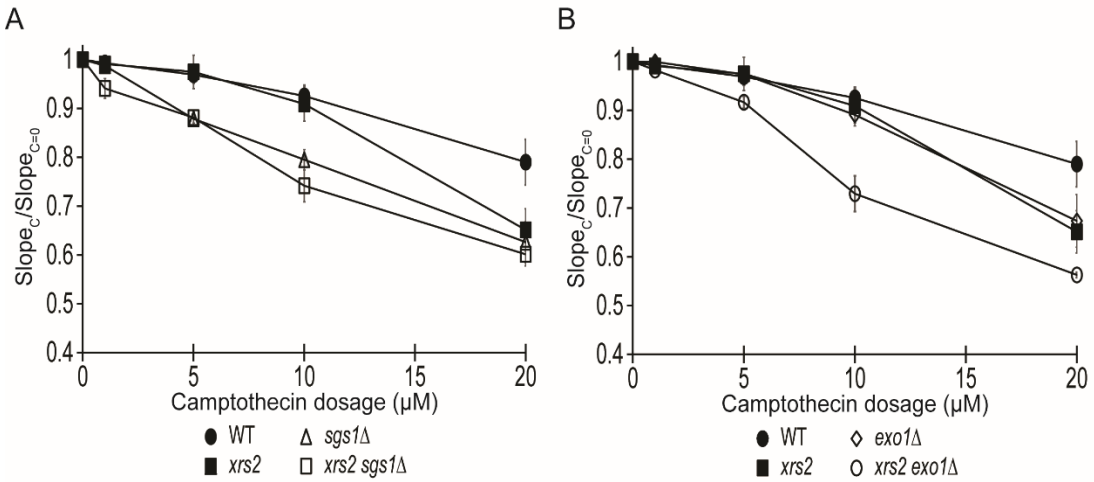

Figure 2.8 Genetic interaction between *xrs2-fha* mutation with *sgs1Δ* and *exo1Δ*

A-B) Camptothecin sensitivity of *xrs2 (xrs2-R32G,S47A)*, ***exo1Δ***, ***sgs1Δ*** and their combined mutations at various concentrations. The ratio of the slope of the curve between treated ($Slope_C$) and untreated ($Slope_{C=0}$) is plot for each concentration (See Materials & Method). Strains used – HZY1077, JLY391, JLY235, JLY335, JLY230, JLY395.

Table 2.1 Yeast strains used in Chapter 2

All W303 strains isogenic to HZY1077 and HZY1078
All S288c strains background *ura3-52 leu2Δ1 his3Δ200 lys2ΔBgl hom3-10 ade2Δ1 ade8*

Strain	Genotype	Background	Reference/ Source
HZY1077	MATa *ade2-1 can1-100 his3-1115 leu2-3,112 trp1-1 ura3-1 RAD5+*	W303	Xiaolan Zhao
HZY1078	MATα *ade2-1 can1-100 his3-1115 leu2-3,112 trp1-1 ura3-1 RAD5+*	W303	This study
HZY1239	MATα *sae2Δ::HIS3*	W303	This study
HZY1240	MATα *sae2-T90A::kanMX6*	W303	This study
HZY1241	MATα *sae2-S249A::kanMX6*	W303	This study
HZY1242	MATα *sae2-T279A::kanMX6*	W303	This study
HZY1243	MATα *sae2-T90A,S249A::kanMX6*	W303	This study
HZY1244	MATα *sae2-T90A,T279A::kanMX6*	W303	This study
HZY1235	MATα *sae2-S249A,T279A::kanMX6*	W303	This study
HZY1236	MATα *sae2-T90A,S249A,T279A::kanMX6*	W303	This study
JLY030	MATa *SAE2-3HA::HIS3MX6 bar1Δ::URA3*	W303	This study
JLY032	MATα *sae2-T90A,T279A-3HA:: HIS3MX6*	W303	This study
JLY035	MATα *sae2-T90A,S249A,T279A-3HA:: HIS3MX6*	W303	This study
JLY048	MATα *sae2-T90A-3HA::HIS3MX6*	W303	This study
JLY050	MATα *sae2-S249A-3HA::HIS3MX6*	W303	This study
JLY053	MATα *sae2-T279A-3HA::HIS3MX6*	W303	This study
SCY249	MATa *sml1Δ::TRP1 arg4Δ*	W303	This study
JLY089	MATα *RAD9-3HA::kanMX6*	S288c	Chen et al. (2010)
JLY091	MATα *RAD9-3HA::kanMX6 sae2Δ::HIS3*	W303	This study
JLY093	*MAT*α RAD9-3HA::HIS3MX6 *sae2-2AQ(T90A,T279A)::kanMX6*	W303	This study
JLY158	MATα *mrc1Δ::URA3*	W303	This study
JLY160	MATα *rad9Δ::URA3*	W303	This study
JLY161	MATα *sae2-2AQ::kanMX6 mrc1Δ::URA3*	W303	This study
JLY162	MATα *sae2-2AQ::kanMX6 mrc1Δ::URA3*	W303	This study
JLY163	MATα *sae2-2AQ::kanMX6 rad9Δ::URA3*	W303	This study
JLY164	MATα *sae2-2AQ::kanMX6 rad9Δ::URA3*	W303	This study
JLY230	MATa *exo1Δ::HIS3*	W303	This study
JLY235	MATα *sgs1Δ::URA3*	W303	This study
JLY233	MATα *sae2-2AQ::kanMX6 sgs1Δ::URA3*	W303	This study
JLY234	MATa *sae2-2AQ::kanMX6 exo1Δ::HIS3*	W303	This study
JLY221	MATa *dun1Δ::HIS3*	W303	This study
JLY223	MATα *rad53-R70A,N107A::kanMX6*	W303	This study
JLY641	MATa *rad53-R70A,N107A::kanMX6 dun1Δ::HIS3*	W303	This study
JLY635	MATa *sae2-2AQ(T90A,T279A)::URA3 dun1Δ::HIS3*	W303	This study
JLY637	MATα *sae2-2AQ(T90A,T279A)::URA3 rad53-R70A,N107A::kanMX6*	W303	This study

Table 2.1 Yeast Strains used in Chapter 2, continued

Strain	Genotype	Background	Reference/ Source
JLY639	MATa *sae2-2AQ(T90A,T279A)::URA3 dun1Δ::HIS3 rad53-R70A,N107A::kanMX6*	W303	This study
JLY391	MATα *xrs2-R32G,S47A::kanMX6*	W303	This study
JLY335	MATα *xrs2-R32G,S47A::kanMX6 sgs1Δ::URA3*	W303	This study
JLY395	MATα *xrs2-R32G,S47A::kanMX6 exo1Δ::natMX4*	W303	This study
JLY229	MATa/MATα *sae2-2AQ::kanMX6/SAE2 sgs1Δ::URA3/SGS1 exo1Δ::HIS3/EXO1*	W303	This study
JLY540	MATa/MATα *sae2-T90A::kanMX6/SAE2 sgs1Δ::URA3/SGS1 exo1Δ::natMX4/EXO1*	W303	This study
JLY541	MATa/MATα *sae2-T279A::kanMX6/SAE2 sgs1Δ::URA3/SGS1 exo1Δ::natMX4/EXO1*	W303	This study
JLY171	MATa/MATα *rad53-R70A,N107A:: kanMX6/RAD53 dun1Δ::HIS3/DUN1 sgs1Δ::URA3/SGS1*	W303	This study
JLY496	MATa/MATα *dun1Δ::HIS3/DUN1 sgs1Δ::URA3/SGS1 exo1Δ::natMX4/EXO1*	W303	This study
JLY497	MATa/MATα *rad53-R70A,N107A::kanMX6/RAD53 sgs1Δ::URA3/SGS1 exo1Δ::natMX4/EXO1*	W303	This study
HZY2672	MATα *sae2-2AQ::kanMX6 can1::hisG yel072w::CAN1/URA3 iYEL072W::hph*	S288c	This study
HZY2709	MATα *sae2-2AQ::natMX4 can1::hisG yel072w::CAN1/URA3 iYEL072W::hph*	S288c	This study
HZY2801	MATa *sae2-2AQ::natMX4 sgs1Δ::kanMX6 can1::hisG yel072w::CAN1/URA3 iYEL072W::hph*	S288c	This study
HZY2802	MATα *sae2-2AQ::natMX4 sgs1Δ::kanMX6 can1::hisG yel072w::CAN1/URA3 iYEL072W::hph*	S288c	This study
HZY3041	MATa *sae2-2AQ:: kanMX6 exo1Δ::natMX4 can1::hisG yel072w::CAN1/URA3 iYEL072W::hph*	S288c	This study
HZY3042	MATα *sae2-2AQ::kanMX6 exo1Δ::natMX4 can1::hisG yel072w::CAN1/URA3 iYEL072W::hph*	S288c	This study
HZY2908	MATa *rad53-R70A::kanMX6 can1::hisG yel072w::CAN1/URA3 iYEL072W::hph*	S288c	This study
HZY2909	MATα *rad53-R70A::kanMX6 can1::hisG yel072w::CAN1/URA3 iYEL072W::hph*	S288c	This study
HZY2912	MATa *rad53-R70A::kanMX6 dun1Δ::HIS3 can1::hisG yel072w::CAN1/URA3 iYEL072W::hph*	S288c	This study
HZY2913	MATα *rad53-R70A::kanMX6 dun1Δ::HIS3 can1::hisG yel072w::CAN1/URA3 iYEL072W::hph*	S288c	This study

Table 2.1 Yeast Strains used in Chapter 2, continued

Strain	Genotype	Background	Reference/ Source
HZY3377	MATa *rad53Δ::HIS3 sml1Δ::TRP1 can1::hisG yel072w::CAN1/URA3 iYEL072W::hph*	S288c	This study
HZY3378	MATα *rad53Δ::HIS3 sml1Δ::TRP1 can1::hisG yel072w::CAN1/URA3 iYEL072W::hph*	S288c	This study
HZY3192	MATα *exo1Δ::natMX4 sgs1Δ::TRP1 can1::hisG yel072w::CAN1/URA3 iYEL072W::hph*	S288c	This study
HZY3193	MATα *exo1Δ::natMX4 sgs1Δ::TRP1 can1::hisG yel072w::CAN1/URA3 iYEL072W::hph*	S288c	This study
JLY410	MATa *sae2-2AQ::natMX4 xrs2-R32G::kanMX6 can1::hisG yel072w::CAN1/URA3 iYEL072W::hph*	S288c	This study
JLY411	MATα *sae2-2AQ::natMX4 xrs2-R32G::kanMX6 can1::hisG yel072w::CAN1/URA3 iYEL072W::hph*	S288c	This study
JLY412	MATa *xrs2-R32G::kanMX6 can1::hisG yel072w::CAN1/URA3 iYEL072W::hph*	S288c	This study
JLY413	MATα *xrs2-R32G::kanMX6 can1::hisG yel072w::CAN1/URA3 iYEL072W::hph*	S288c	This study

Table 2.2 Rate of accumulating GCRs for mutations to *SAE2*, *RAD53*, *DUN1*, XRS2, *EXO1*, and *SGS1*

* Rate of accumulating Can 5-FOA progeny. Number in the parenthesis is the fold increase relative to wild-type *yel068c::CAN1/URA3* strain (2.27×10^{-9})
** Rates taken from Putnam et al., 2009 study.

Genotype	***yel072w::CAN1/URA3* GCR rate***	**Reference**
Wild type**	1.97×10^{-8} (8.7)	Putnam et al., 2009
*sae2Δ***	1.65×10^{-7} (73)	Putnam et al., 2009
rad53Δ sml1Δ	2.8×10^{-7} (123)	This study
rad53-R70A	7.94×10^{-8} (35)	This study
*dun1Δ***	1.61×10^{-7} (71)	Putnam et al., 2009
rad53-R70A dun1Δ	1.2×10^{-7} (53)	This study
sae2-2AQ	9.1×10^{-8} (40)	This study
*sgs1Δ***	1.93×10^{-6} (850)	Putnam et al., 2009
sae2-2AQ sgs1Δ	5.2×10^{-6} (2291)	This study
*exo1Δ***	8.44×10^{-8} (37)	Putnam et al., 2009
sae2-2AQ exo1Δ	9.4×10^{-8} (41)	This study
exo1Δsgs1Δ	8.31×10^{-7} (41)	This study
xrs2-R32G	2.14×10^{-8} (9.4)	This study
sae2-2AQ xrs2-R32G	3.61×10^{-8} (16)	This study

CHAPTER 3

SUMO isopeptidases Ulp1 and Ulp2 control sumoylation homeostasis and suppress aberrant genome rearrangements

3.1 Summary

SUMO E3 ligases are known to have a major role in preventing gross chromosomal rearrangements (GCRs); however, relatively little is known about the role of SUMO isopeptidases in genome maintenance and their role in controlling intracellular sumoylation homeostasis. Here we show the SUMO isopeptidase Ulp2 in *Saccharomyces cerevisiae* has a minor role in preventing the accumulation of GCRs and interestingly, its loss causes subunit-specific changes of sumoylated MCM helicase in addition to drastic accumulation of sumoylated nucleolar RENT and inner kinetochore complexes. In contrast, loss of Ulp1 or its mis-localization from the nuclear periphery causes substantial accumulations of GCRs and elevated sumoylation of most proteins except for Ulp2 targets. Interestingly, the E3 ligase Mms21, which has a major role in genome maintenance, preferentially controls the sumoylation of Mcm3 during DNA replication. These findings reveal distinct roles for Ulp1 and Ulp2 in controlling homeostasis of intracellular sumoylation and show that sumoylation of MCM is controlled in a subunit-specific and cell cycle dependent manner.

3.2 Introduction

Protein sumoylation is an essential post-translational modification in eukaryotes [92, 93]. Two families of enzymes control reversible sumoylation of specific substrates, including SUMO (Small Ubiquitin-like MOdifier) E3 ligases

and SUMO isopeptidases. Three SUMO E3 ligases Siz1, Siz2 and Mms21 have been identified in *S. cerevisiae* and shown to have distinct, but partially overlapping roles in catalyzing substrate-specific sumoylation [19, 94-96]. Siz1 and Siz2 are paralogs and they redundantly catalyze the bulk of sumoylation in cells [19, 94]. Mms21 catalyzes sumoylation of fewer substrates, but plays a more important role in genome maintenance than Siz1 and Siz2 [94, 97]. Deletion of *SIZ1* and *SIZ2* is lethal in cells lacking Mms21 E3 ligase activity [19, 96]. Moreover, deletion of either *SIZ1* or *SIZ2* causes further accumulation of gross chromosome rearrangements (GCRs) in cells lacking Mms21 E3 ligase activity [94]. These findings suggest that the functions of these E3 ligases are partially redundant, which correlate with their partially overlapping roles in catalyzing intracellular sumoylation [19, 94].

Besides SUMO E3 ligases, homeostasis of intracellular sumoylation is also regulated by SUMO isopeptidases, which catalyze the removal of SUMO from its targets. Two SUMO isopeptidases Ulp1 and Ulp2 have been identified in *S. cerevisiae [7, 44, 98]*. Ulp2 is not required for cell viability; however, its loss causes accumulation of poly-SUMO chains, resulting in pleiotropic effects including slow growth and sensitivity to higher temperature [7, 99]. Moreover, over-expression of *ULP2* (also known as *SMT4*) suppresses defects in chromosome condensation and segregation, suggesting its role in regulating chromosome segregation [98, 100]. This role of Ulp2 in chromosome segregation appears to be conserved in higher eukaryotes including *C. elegans*

and human cells, although its targets are poorly known [101, 102]. Consistent with its nuclear function, Ulp2 has been shown to localize throughout the nucleus and occasionally the nucleolus [43, 103]. On the other hand, Ulp1 is essential for cell viability and localizes at the nuclear periphery via the nuclear pore complex (NPC) [44, 104-108]. Ulp1 has been shown to interact with Kap95 and Kap60 via its N-terminal NPC-targeting domain (1-340 amino acids) [107]. Removal of the NPC-targeting domain of Ulp1, or the loss of NPC components Nup60 and Mlp1/Mlp2 [104, 106, 108], attenuates its localization at the nuclear periphery and causes the accumulation of Rad52 foci, which is indicative of endogenous DNA damage and repair [106]. These studies suggest that localization of Ulp1 at the nuclear periphery has an important role in protecting genome integrity, possibly by preventing Ulp1 from desumoylating nucleoplasmic proteins yet to be determined. The distinct localization patterns of Ulp1 and Ulp2 likely contribute to their substrate selectivity in cells, which has been poorly understood.

In this study, we first characterized the function of Ulp1 and Ulp2 in preventing the accumulation of GCRs and identified a genetic basis for the essential function of Ulp1. To identify the substrates of Ulp1 and Ulp2, we applied quantitative mass spectrometry (MS) to analyze the effect of *ulp1* and *ulp2* mutations on intracellular sumoylation. These studies led to the finding that Ulp2 has highly specific desumoylation activity *in vivo*, while Ulp1 has a broader specificity towards many substrates. Interestingly, loss of Ulp1 or its mis-

localization from the nuclear periphery causes specific and aberrant desumoylation of Ulp2 targets, including the essential replicative MCM helicase [109]. Furthermore, Mms21, the E3 ligase with a major role in preventing the accumulation of GCRs [94], preferentially catalyzes sumoylation of specific MCM subunits.

3.3 Results

3.3.1 The roles of Ulp1 and Ulp2 in preventing GCR and maintaining viability

Considering the known roles of Ulp1 in SUMO maturation and Ulp2 in disassembly of poly-SUMO chains [44, 99], we first examined the effect of *smt3GG* and *4R-smt3GG* mutations on the rate of accumulating GCRs using the *yel072w::URA3/CAN1* assay [7]. The *smt3GG* mutation supplies cells with mature SUMO [44], while the *4R-smt3GG* mutation additionally eliminates the bulk of poly-SUMO chains [99]. Both *smt3GG* and *4R-smt3GG* mutations cause a modest change in the rate of accumulating GCRs (Figure 3.1A), suggesting that the removal of poly-SUMO chains does not appreciably affect the accumulation of GCRs. Next we examined the effect of *ulp2Δ* mutation and found that the loss of Ulp2 has a minimal effect on the rate of accumulating GCRs in wild-type, *smt3GG* and *4R-smt3GG* mutants. Thus, neither the accumulation of poly-SUMO chains in cells lacking Ulp2, nor the lack of poly-

SUMO chains appreciably alters the accumulation of GCRs measured by the *yel072w::URA3/CAN1* assay.

The essential function of Ulp1 has been attributed to its role in SUMO maturation and desumoylating other proteins in cells whose identities have been unknown [44]. We reasoned that the latter function of Ulp1 could be bypassed by mutations that down-regulate intracellular sumoylation. Since Siz1 and Siz2 are known to have a major role in intracellular sumoylation [19, 94, 95], we tested whether loss of Siz1 and/or Siz2 could suppress the lethality of *ulp1Δ* by performing tetrad dissection of diploid cells containing heterozygous *ulp1Δ*, *siz1Δ* and *siz2Δ* mutations, as well as a homozygous *smt3GG* mutation to supply mature Smt3. As shown in Figure 3.1B, deletion of *SIZ1* and *SIZ2*, but neither one alone, suppresses the lethality of *ulp1Δ*. In contrast, loss of Mms21 E3 ligase activity does not rescue the lethality of *ulp1Δ* (Figure 3.1B). This suggests that an essential function of Ulp1 is to desumoylate the bulk of intracellular sumoylation, catalyzed by Siz1 and Siz2.

Interestingly, the loss of Ulp1 in the *siz1Δ siz2Δ* mutant causes a significant increase in the rate of accumulating GCRs, which is comparable to that of an *mms21-CH* mutant and is considerably higher than that of the *siz1Δ siz2Δ* mutant (Figure 3.1C). By comparison, the loss of Ulp2 in the *siz1Δ siz2Δ* mutant causes a smaller increase in the rate of accumulating GCRs. The *ulp1-N338Δ* mutation has been shown to compromise the localization of Ulp1 at the nuclear periphery without affecting cell viability [105, 107, 108]. We found this

ulp1-N338Δ mutation causes a significant increase in the rate of accumulating GCRs comparable to that of the *mms21-CH* mutant and is independent of Ulp2 (Figure 3.1C). This suggests that mis-localized Ulp1 could either directly desumoylate Mms21 targets or indirectly down-regulate Mms21 activity to cause accumulation of GCRs. Distinguishing these possibilities would require knowledge of Ulp1 and Ulp2 targets and how they are regulated by the localization of Ulp1.

3.3.2 Ulp2 has a specific role in desumoylating proteins at the rDNA, centromere and origins of DNA replication

To identify the *in vivo* targets of Ulp1 and Ulp2, we chose to use our quantitative MS approach as previously described [94]. In this approach, following purification of sumoylated proteins, Ulp1 is used to elute sumoylated proteins for MS analysis. This approach provides information on the amount of sumoylated proteins, but does not distinguish whether they are poly-sumoylated or mono-sumoylated at one or more lysines, which can be studied using alternative methods. Using this quantitative MS approach, we found that deletion of *ULP2* in the *4R-smt3GG* strain causes substantial increases in three protein complexes located in distinct chromosomal regions, including rDNA (the RENT complex), centromere (inner kinetochore complex) and origins of DNA replication (the MCM complex) (Figure 3.2A and Table 3.2). Among them, loss of Ulp2 causes accumulation of approximately 20-fold more sumoylated Net1, Cdc14 and Tof2, subunits of the RENT complex in the nucleolus [110, 111].

Similarly, the loss of Ulp2 also causes accumulation of approximately 20-fold more sumoylated Ame1, Mcm21, Okp1, Mcm16 and Mcm22, which are components of the inner kinetochore complex [106, 107, 112]. This drastic accumulation of sumoylated RENT and inner kinetochore complexes is consistent with them being Ulp2 targets.

Loss of Ulp2 also causes significant accumulations of sumoylated subunits of the MCM complex, the essential replicative DNA helicase [52, 104, 108, 109]. However, unlike the RENT and inner kinetochore complexes, the effect of Ulp2 removal on MCM sumoylation is subunit-specific. As shown in Figure 3.2A, loss of Ulp2 results in relatively modest changes in the amount of sumoylated Mcm2 and Mcm6 but causes a 4- to 10-fold accumulation of sumoylated Mcm3, Mcm4, Mcm5 and Mcm7. In addition to these increases in sumoylation, loss of Ulp2 reduces the amount of most other sumoylated proteins (Figure 3.2A and Table 3.2), which is unlikely a direct effect of Ulp2 removal. Since Ulp1 is the remaining SUMO isopeptidase, its activity could be up regulated to compensate for the loss of Ulp2. Alternatively, loss of Ulp2 may down regulate the activity of SUMO E3 ligases in cells; although this possibility is difficult to reconcile with the drastic accumulation of sumoylated RENT, kinetochore and MCM complexes upon Ulp2 removal, which is largely unaffected by the *4R-smt3GG* mutation (Table 3.3). Loss of Ulp2 has been shown to cause excessive poly-sumoylation and slow growth [99]. However, we found that deletion of *ULP2* in the *HF-SUMO* and *HF-4R-smt3* strains did not

cause detectable changes to their cell cycle profile or growth rate (Figure 3.7). One possible explanation is that the N-terminal HF tag on Smt3 in these cells may partially compromise poly-SUMO formation in the absence of Ulp2, although this tag has little appreciable effect on cell growth or GCR phenotype in wild type background [94]. For this reason all subsequent biochemical experiments were performed using the *HF-SUMO* strain background unless noted otherwise.

To rule out the possibility that the observed changes of sumoylated proteins are due to a change in protein expression and to validate the MS findings, we chose to analyze selected Ulp2 targets further. To this end, we used Ni-NTA and anti-FLAG affinity resins to purify total sumoylated proteins from HF-SUMO (6xHIS-3xFLAG-Smt3) strain, which additionally contains Net1-6xHIS-3xHA, and then probed for the presence of sumoylated Net1 using an anti-HA antibody. As shown in Figure 3.2B, loss of Ulp2 causes a drastic accumulation of slower migrating and sumoylated species of Net1 in purified sumoylated proteins, while the abundance of un-modified Net1 in the cell lysate is unaffected, indicating a specific role of Ulp2 in desumoylating Net1. To study MCM sumoylation, we first evaluated the effect of epitope-tagging of MCM subunits on the rate of accumulating GCRs using the *yel072w::CAN1/URA3* assay [7, 94]. Since C-terminal tagging of Mcm3 compromises its function [113], a 6xHIS-3xHA tag was introduced to the N-terminus of Mcm3 at its endogenous locus, while the same 6xHIS-3xHA tag was fused to the C-termini of other MCM

subunits. We found a modest accumulation of GCRs caused by epitope-tagging of most MCM subunits except for Mcm5, whose tagging resulted in a drastic accumulation of GCRs (Figure 3.8). Although this finding implicated a role of MCM in preventing the accumulation of GCRs, sumoylation of Mcm5 was not analyzed further. Moreover, N-terminal tagging of Mcm3 causes a relatively stronger, albeit modest accumulation of GCRs, which prompted us to develop an anti-Mcm3 antibody for its analysis.

Following purification of sumoylated proteins in the indicated strains (all containing HF-SUMO), we probed for the presence of sumoylated Mcm2, Mcm3, Mcm4, Mcm6, and Mcm7, using either an anti-HA or an anti-Mcm3 antibody. As shown in Figure 3.2C, sumoylated Mcm2 in unperturbed wild type cells was not detected in this experiment and there is no evidence for its accumulation upon the loss of Ulp2. Sumoylated Mcm6 was readily detected in wild type cells and is partially reduced by the loss of Ulp2 (Figure 3.2D). In contrast, two major sumoylated species of Mcm3 are present in wild type cells and both are strongly induced upon the loss of Ulp2 (Figure 3.2E). Like Mcm2, sumoylated Mcm4 and Mcm7 in wild type cells were not readily detected [52]. However, the loss of Ulp2 causes significant accumulations of sumoylated Mcm4 and Mcm7 (Figures 3.2F and 3.2G). In each case, the abundance of each MCM subunit is unaffected by the loss of Ulp2 and sumoylated species of MCM subunits are undetectable in cell lysate without enrichment. Un-sumoylated MCM could still be seen after anti-FLAG immuno-purification due to the

relatively low stoichiometry of MCM sumoylation. Together, these findings are in general agreement with the MS findings (Figure 3.2A). It should be noted here that a previous study using C-terminal tagged Mcm3 did not detect sumoylated Mcm3 in unperturbed wild type cells [52]. However, C-terminal tagging of Mcm3 has been found to compromise its function [113].

3.3.3 Ulp1 has a broad role in intracellular desumoylation distinct from Ulp2

To identify Ulp1 targets, we applied the same quantitative MS assay to measure the effect of deleting ULP1 on sumoylated proteins in the siz1Δ siz2Δ mutant, in which Ulp1 is not essential. As shown in Figures 3.3A (Tables 3.4 and 3.5), losses of Ulp1, Siz1 and Siz2 cause drastic accumulations of the majority of sumoylated proteins compared to wild type and siz1Δ siz2Δ mutant, indicating a broad role of Ulp1 for desumoylating most proteins in cells. Interestingly, sumoylation of Net1 is strongly reduced by the loss of Ulp1 (Figure 3.3A), which we confirmed by Western blotting to detect sumoylated Net1 (Figure 3.3B). Since Ulp2 has a highly specific role in desumoylating Net1 (Figure 3.2A), we hypothesized that this reduction of sumoylated Net1 could be explained by elevated Ulp2 activity to compensate for the loss of Ulp1.

In cells lacking Siz1 and Siz2, Mms21 and/or the E2 enzyme Ubc9 are expected to be responsible for the accumulation of sumoylation caused by the loss of Ulp1 (Figure 3.3A). However, other Ulp2 targets including MCM were below the detection limit of these MS experiments, perhaps due to elevated

Ulp2 activity. To investigate the relative specificity of Ulp1 and Ulp2 in desumoylating MCM, we purified total sumoylated proteins and analyzed the presence of sumoylated MCM subunits. As shown in Figures 3.3C, loss of Ulp2, Siz1, and Siz2 results in a drastic accumulation of sumoylated Mcm2, which is below the detection limit in wild type and the ulp1Δ siz1Δ siz2Δ mutant. Similarly, loss of Ulp2, but not Ulp1, causes a more drastic accumulation of sumoylated Mcm3, Mcm4, and Mcm6 (Figures 3.3D-3.3F). These findings show that Ulp2 has a more specific role than Ulp1 in desumoylating MCM in cells lacking Siz1 and Siz2, while Ulp1 has a broad role in desumoylating non-Ulp2 targets in cells.

3.3.4 Localization of Ulp1 prevents its desumoylation of Ulp2-specific targets

Ulp1 and Ulp2 are known to have different subcellular localizations [43, 103, 105, 107], which may contribute to their distinct substrate specificity. To test this we investigated the role of the NPC-targeting domain of Ulp1 (N-terminal 338 amino acid), which directs Ulp1 to the nuclear periphery [105, 107, 108]. We found that removal of the Ulp1 NPC-targeting domain causes an approximately 20-fold reduction of sumoylated Net1 and about 4-fold reduction of sumoylated Mcm2 and Mcm3 (Figure 3.4A and Table 3.6). In contrast, there are significant accumulations of many sumoylated proteins in the ulp1-N338Δ mutant, including Pol30, Smc5 and others. This finding shows that mis-localized Ulp1 does not non-specifically desumoylate all nucleoplasmic proteins, but instead specifically reduces the amount of sumoylated Net1 and MCM subunits.

The reduction of sumoylated Net1 raises a possibility that Ulp2 could be involved. To test this, we compared sumoylated proteins in ulp1-N338Δ ulp2Δ and ulp2Δ mutants using quantitative MS and found that removal of the Ulp1 NPC-targeting domain results in significant reductions of sumoylated Net1, Tof2, Cdc14, various kinetochore and MCM subunits in cells lacking Ulp2 (Figure 3.4B and Table 3.7). The accumulations of many other sumoylated proteins in the *ulp1-N338Δ ulp2Δ* mutant indicate that Ulp1-N338Δ does not non-specifically desumoylate proteins in the nucleoplasm.

In agreement with these MS findings, removal of the Ulp1 NPC-targeting domain largely eliminates sumoylated Net1 and this occurs independent of Ulp2 (Figure 3.4C). Similarly, sumoylated Mcm6 is strongly reduced upon removal of the Ulp1 NPC-targeting domain, again in an Ulp2-independent manner (Figure 3.4D). Interestingly, removal of the Ulp1 NPC-targeting domain specifically reduces the amount of slower migrating sumoylated species of Mcm3, which is independent of Ulp2, while the faster migrating sumoylated species of Mcm3 is relatively unaffected. Together, these results show that the localization of Ulp1 at the nuclear periphery prevents it from desumoylating Ulp2 targets including Net1 and MCM as well as being necessary for proper desumoylation of other targets.

3.3.5 Roles of E3 ligases Siz1, Siz2 and Mms21 in sumoylating Ulp2 targets

Considering that the accumulations of GCRs in cells lacking Ulp1 or its NPC-targeting domain are comparable to that caused by the loss of Mms21 E3

ligase activity (Figure 3.1), we reasoned that these *ulp1* mutations might reduce the amount of sumoylated Mms21 targets. While the loss of Ulp1 could do so by up-regulating Ulp2 activity to desumoylate Ulp2 targets (Figure 3.3), mis-localized Ulp1 could achieve the same task directly (Figure 3.4). If so, the question is whether Mms21 preferentially sumoylates Ulp2 targets. To address this, we quantified sumoylated proteins in *ulp2Δ mms21-CH* and *ulp2Δ siz1Δ siz2Δ* mutants using MS. As shown in Figure 3.5A and Table 3.8, sumoylated Septins and Pol30, known Siz1/Siz2 targets, are considerably more abundant in the *ulp2Δ mms21-CH* mutant than in the *ulp2Δ siz1Δ siz2Δ* mutant as expected. On the other hand, known Mms21 targets including the SMC family proteins are more abundant in the *ulp2Δ siz1Δ siz2Δ* mutant than in the *ulp2Δ mms21-CH* mutant [94]. Among Ulp2 targets, the amount of sumoylated Net1, Cdc14, Tof2, and kinetochore subunits are comparable in cells lacking Siz1/Siz2 or Mms21 E3 ligase activity (Figure 3.5A). Interestingly, sumoylation of essentially all MCM subunits is considerably more abundant in the *ulp2Δ siz1Δ siz2Δ* mutant than the *ulp2Δ mms21-CH* mutant (Figure 3.5A), indicating that sumoylation of MCM is preferentially controlled by Mms21 albeit in cells lacking Ulp2.

To investigate whether Mms21 preferentially controls the sumoylation of MCM in cells containing intact Ulp1 and Ulp2, we next quantified sumoylated proteins in *siz1Δ siz2Δ* and *mms21-CH* mutants by MS. As shown in Figure 3.5B and Table 3.9, the amount of sumoylated SMCs are more abundant in cells

lacking Siz1/Siz2 compared to cells lacking Mms21 E3 ligase activity, while sumoylation of Septins and Pol30 are strongly Siz1/Siz2-dependent [94]. Interestingly, sumoylation of MCM subunits show a varying dependency on these E3 ligases. For example, sumoylation of Mcm2 and Mcm3 are more dependent on Mms21, while sumoylation of Mcm6 is more specific to Siz1/Siz2 as previously reported [94]. In agreement with these MS findings, sumoylated Mcm2 is reduced more by the *mms21-CH* mutation compared to the loss of Siz1 and Siz2 (Figure 3.5C). Between the two major sumoylated species of Mcm3, the slower migrating species of Mcm3 is specifically reduced by the *mms21-CH* mutation, while the loss of Siz1 and Siz2 has little effect (Figure 3.5D). On the other hand, sumoylated Mcm6 is more strongly reduced by the loss of Siz1 and Siz2 compared to the *mms21-CH* mutation (Figure 3.5E). These findings reveal that Mms21 more specifically controls the sumoylation of Mcm2 and Mcm3, while Siz1 and Siz2 preferentially control the sumoylation of Mcm6.

3.3.6 Regulation of MCM sumoylation in response to DNA replication stress

A previous study showed that a DNA alkylating agent could induce the sumoylation of MCM, including Mcm2, Mcm4, Mcm5 and Mcm6, but not Mcm3 and Mcm7 [52]. To explore a role for MCM sumoylation during DNA replication, we asked whether MCM sumoylation could be induced by hydroxyurea (HU) treatment, which causes stalled DNA replication forks without extensive DNA damages. As shown in Figure 3.6A, HU treatment has little effect on sumoylated

Mcm2, Mcm4, Mcm6, and Mcm7; however, it causes a significant accumulation of the slower migrating sumoylated species of Mcm3, whereas the faster migrating species of sumoylated Mcm3 is relatively unaffected (Figure 3.6A). Moreover, Mms21, but not Siz1 and Siz2, is required for the HU-induced sumoylated species of Mcm3, detected by anti-Mcm3 and anti-HA antibodies (Figure 3.6B). It is presently unknown whether this HU-induced sumoylation of Mcm3 by Mms21 is a consequence of stalled DNA replication fork or it helps to stabilize stalled replication forks. Nevertheless, this finding suggests that Mms21-dependent sumoylation of Mcm3 might occur during DNA replication. To test this we examined the timing of Mcm3 and Mcm6 sumoylation during the cell cycle. As shown in Figure 3.6C, the faster migrating species of Mcm3 is relatively unchanged during the cell cycle, while the slower migrating species of Mcm3 accumulates during the S phase and it is largely absent in the G1 and G2-M phases. In contrast, sumoylated Mcm6 is already present in G1 cells, persists as cells enter S phase and disappears during the G2-M phase (Figure 3.6C).

3.4 Discussion

Protein sumoylation is essential for cell viability and regulates many nuclear processes [92, 93]. Recent studies have revealed a major role for Mms21 in DNA recombination repair and preventing the accumulation of GCRs [52, 94, 97]; however, relatively little has been known about the function and

substrates of SUMO isopeptidases in genome maintenance. The NPC has been shown to contribute to genome maintenance and regulates the localization of Ulp1, although the mechanism has been insufficiently understood [96, 104-108]. Here we report several advances in addressing these questions, using *Saccharomyces cerevisiae* as a model organism.

First, we identified an essential function of Ulp1 in desumoylating the bulk of intracellular sumoylation, which is rescued by the removal of Siz1 and Siz2. Concerning the role of Ulp1 and Ulp2 in genome maintenance, we found that the loss of Ulp2 or elimination of the bulk of poly-sumoylation in cells does not cause appreciable accumulation of GCRs (Figure 3.1A). Interestingly, either deleting Ulp1 or disrupting its localization at the nuclear periphery causes substantial accumulation of GCRs (Figure 3.1C). Considering the major role of Mms21 in preventing the accumulation of GCRs [94], reduced sumoylation of certain Mms21 targets might have occurred in these *ulp1* mutants. While disrupting Ulp1 localization at the nuclear periphery could lead to its aberrant desumoylation of Mms21 targets in the nucleoplasm, reducing sumoylated Mms21 targets by the loss of Ulp1 is expected to be indirect.

Second, understanding the functions of Ulp1 and Ulp2 requires knowledge of their substrates. Here we found that the loss of Ulp2 causes a drastic and specific accumulation of sumoylated proteins at three chromosomal regions, including the RENT complex in the nucleolus, the inner kinetochore complexes at centromeres and specific subunits of the MCM helicase at DNA

replication forks (Figures 3.2A and 3.6D). On the other hand, Ulp1 broadly desumoylates many proteins in cells except for these Ulp2 targets (Figure 3.3A). Interestingly, Ulp1 and Ulp2 appear to compensate for the loss of each other. For example, a broad reduction in many sumoylated proteins caused by the loss of Ulp2 could be explained by elevated Ulp1 activity, while reduced sumoylated Net1 in cells lacking Ulp1 is best explained by elevated Ulp2 activity. The distinct substrate specificity of Ulp1 and Ulp2 is further illustrated by their roles in regulating the desumoylation of various MCM subunits (Figure 3.3).

Third, the NPC has been shown to regulate Ulp1 localization at the nuclear periphery [96, 104-108]. Given the broad specificity of Ulp1 towards many sumoylated proteins, one might speculate that the NPC may restrict the access of Ulp1 towards proteins in the nucleoplasm to prevent aberrant desumoylation. Interestingly, we found that removal of the NPC-targeting domain of Ulp1 causes a specific loss of sumoylated Ulp2 targets including MCM in an Ulp2-independent manner, and this is accompanied by the accumulation of many sumoylated proteins in the nucleoplasm (Figure 3.4). This observation argues against the model that mis-localized Ulp1 may non-specifically desumoylate all proteins in the nucleoplasm. The accumulation of most sumoylated proteins in cells lacking the NPC-targeting domain could be due to elevated activities of SUMO E3 ligases to counter the activity of mis-localized Ulp1, a characteristic feature of sumoylation homeostasis in which a relatively small number of enzymes could compensate for each other.

Finally, we and others have shown that sumoylation of the SMC family proteins are preferentially controlled by Mms21 [94, 96, 110]. Sumoylation of MCM has been reported previously [52, 94], although how the SUMO pathway regulates MCM sumoylation is largely unknown. Interestingly, epitope-tagging of most MCM subunits causes varying degrees of GCR accumulation (Figure 3.8), suggesting a properly functioning MCM is needed to prevent genome rearrangements, which could be compromised by improper epitope-tagging. Here we have characterized sumoylation of MCM in greater detail and found that Mms21 preferentially controls the sumoylation of Mcm2 and Mcm3 (Figure 3.5). Interestingly, between the two major sumoylated species of Mcm3 found, Mms21 specifically controls the accumulation of the slower migrating sumoylated species of Mcm3 (Figure 3.5), which occurs during S phase and is further induced in response to DNA replication stress (Figure 3.6). On the other hand, Siz1 and Siz2 have a stronger role in regulating sumoylation of Mcm6, which occurs during the G1 and S phases but disappears during the G2-M phase. While Ulp2 has a more important role in desumoylating MCM (Figure 3.3), the association of Ulp1 with the nuclear periphery is necessary to prevent its aberrant desumoylation of MCM (Figure 3.4), which could contribute to the role of the NPC in genome maintenance [106, 112].

Taken together, our findings here have identified Ulp1 and Ulp2 substrates and revealed that sumoylation of MCM is controlled in a subunit-specific and cell cycle dependent manner. These findings further raise a

hypothesis that sumoylation of Mms21 targets including Mcm2 and Mcm3 may contribute to the suppression of genome rearrangements.

3.5 Materials & Methods

3.5.1 Yeast genetics

All yeast strains used for MS and biochemical experiments were derived from the *HF-SMT3* (*HF-SUMO*) strain, in which a 6xHIS-3xFLAG tag was integrated into the N-terminus of *SMT3* in its chromosomal locus [94]. The strains used to study GCRs were derived from RDKY6678, which contains the *yel072w::CAN1/URA3* assay [7]. All tagged MCM strains and indicated mutations were integrated into the chromosomal locus of the gene of interest (Table 1), using standard yeast genetic methods unless otherwise noted. The yeast strains used here also have their 2-micron circles removed, according to a previous study [98]. Fluctuation analysis of GCRs was performed as previously described [76]. At least 16 isolates were examined per mutant to calculate the median rate of accumulating GCRs. Error bars in the graph represent the upper and lower limits determined by the 95% confidence intervals of the median. (https://epilab.ich.ucl.ac.uk/coursematerial/statistics/non_parametric/confidence_interval.html). *p* values were calculated using the two-tailed Mann-Whitney *U* test as previously described [77]

3.5.2 MS and biochemical methods

For quantitative MS analysis, each mutant strain was grown in synthetic media containing either light or heavy stable isotope-labeled Lysine and Arginine. A two-liter culture was used for each strain, which was grown to an optical density (600 nm) near 0.5 and then harvested. Cell pellets of the two yeast strains to be compared were combined and used to purify sumoylated proteins under denaturing conditions using methods described previously [94]. The methods used in the MS experiments and data analysis have been described previously [94]. The complete list of sumoylated proteins and their abundance changes are shown in Tables 3.2-3.9. Each sumoylated protein was quantified based on the median of the abundance ratios of at least three unique peptides per protein.

To detect Net1 and MCM sumoylation, the same denaturing method using Ni-NTA and anti-FLAG affinity resins was used to purify sumoylated proteins from the same amount (200 milliliters) of yeast culture during logarithmic growth [94]. After cell lysis, Bradford assay was used to ensure the same amount of total proteins was used to purify sumoylated proteins. To elute sumoylated proteins from anti-FLAG affinity resins, Buffer containing 50 mM Tris, pH8.0, 10 mM EDTA and 1% SDS was added to the anti-FLAG resins, which were heated to 100 °C for 10 min. The eluted sample was analyzed using an appropriate antibody as indicated. To induce DNA replication stress, 0.1 M HU was added to a logarithmic growing YPD culture (optical density at 0.5) for

2 hours. For cells growing in synthetic media, 0.1 M HU was added for 3 hours. To analyze Mcm3 and Mcm6 sumoylation during the cell cycle, Mcm6-6xHIS-3HA cells (Bar1-deficient) were arrested by adding either 30 nM alpha-factor (G1 arrest) or 7.5 μg/ml nocodazole (M-phase arrest) for 3 hours at 26°C. To prepare S-phase cells, G1-arrested cells were washed with fresh YPD and then released into fresh YPD media for 40 min at 26°C. The G1, S and G2-M phase cells used for pull-down experiment were confirmed by FACS analysis. Full length recombinant Mcm3 purified from bacteria was used to immunize rabbits (Covance) and serum containing anti-Mcm3 polyclonal antibody was used to detect Mcm3 [113].

3.6 Acknowledgements

We thank Drs. Richard Kolodner and Xiaolan Zhao for communicating unpublished results, Dr. Daniel Kaplan for anti-Mcm2 antibody, and members of Zhou lab for suggestions. This work was supported by NCI training grant T32 CA009523 to JL and funding from Ludwig Cancer Research and NIGMS GM116897 to HZ.

Chapter 3, in full, is a reprint of the material as it appears in Molecular Circuitry of the SUMO (Small Ubiquitin-like Modifier) Pathway in Controlling Sumoylation Homeostasis and Suppressing Genome Rearrangements. *J Biol Chem*. 2016 Apr 15;291(16):8825-35, de Albuquerque CP, Liang J, Gaut NJ, Zhou H. The dissertation author is primary co-author for this paper.

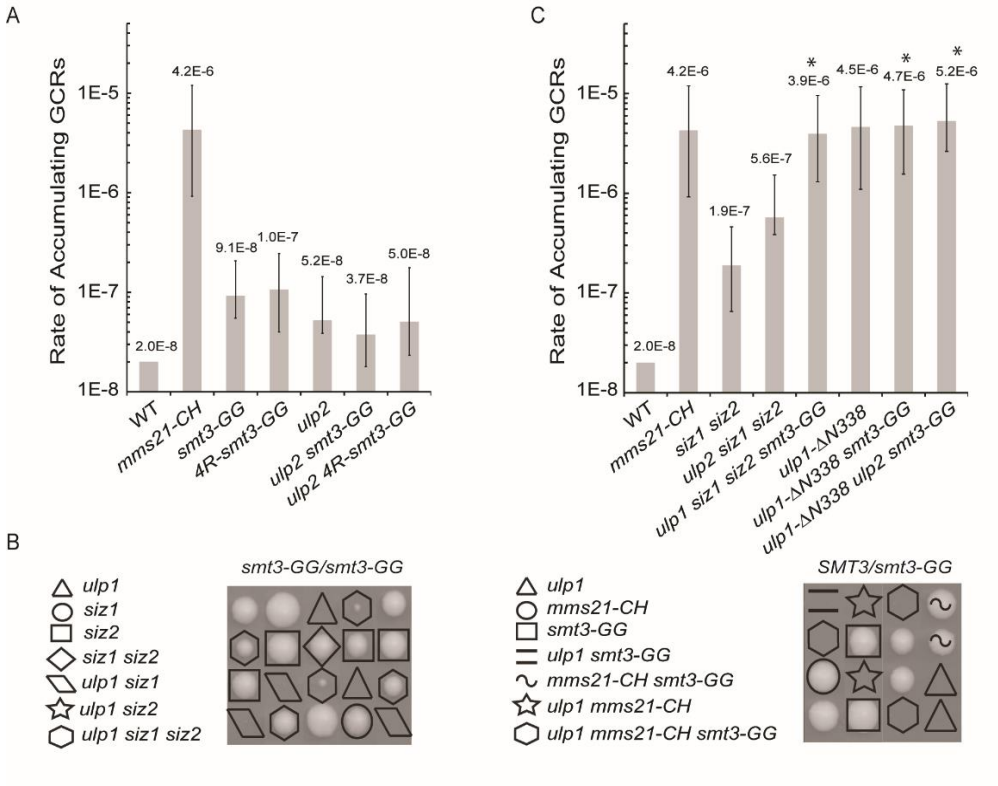

Figure 3.1 Characterization of the functions of Ulp1 and Ulp2 in genome maintenance and cell viability

A) Rate of accumulating GCRs in cells lacking Ulp2 or poly-sumoylation using the *yel072w::CAN1/URA3* assay. B) Tetrad analysis shows the lethality of *ulp1Δ* is suppressed by the removal of both Siz1 and Siz2, but not Mms21 E3 ligase activity. C) Rate of accumulating GCRs in cells lacking Ulp1 or the NPC-targeting domain of Ulp1 using the *yel072w::CAN1/URA3* assay. Error bars represent the upper and lower limits of the 95% confidence intervals of the median.

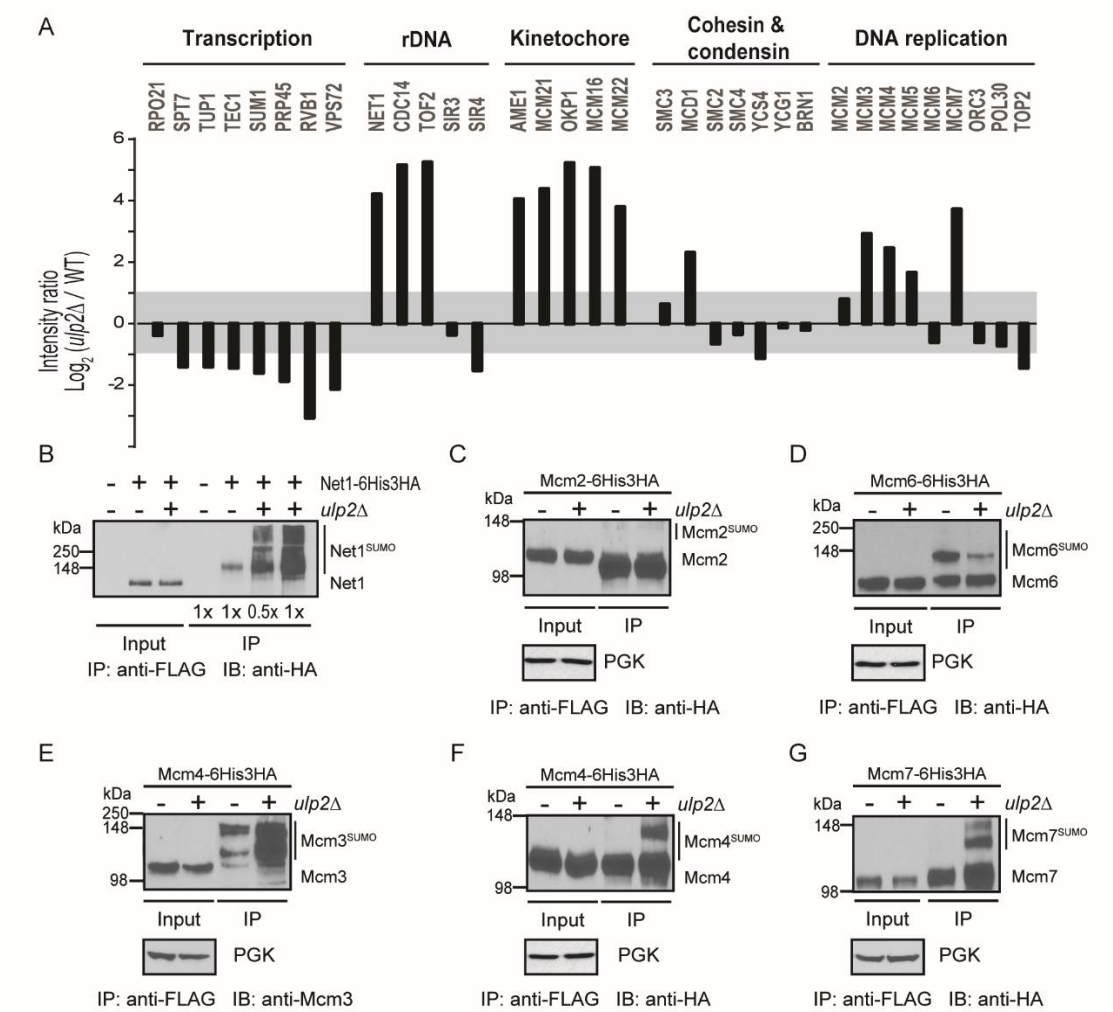

Figure 3.2 Effect of the loss of Ulp2 on intracellular protein sumoylation

A) Effect of loss of Ulp2 on the relative abundance of sumoylated proteins by comparing *ulp2Δ* mutant to the parental strain. B) Sumoylated Net1-6xHIS-3xHA in wild-type or *ulp2Δ* mutant was purified by anti-FLAG affinity resins and then probed by anti-HA antibody. Sumoylated Net1 is indicated showing slower electrophoretic mobility compared to un-sumoylated Net1. C-G) Sumoylated Mcm2, Mcm3, Mcm4, Mcm6 and Mcm7 in wild type and *ulp2Δ* mutant are analyzed using the same approach. In each case, sumoylated MCM subunits in the anti-FLAG affinity-purified sample show a slower electrophoretic mobility compared to unmodified MCM subunits, which occasionally appear as a contaminant.

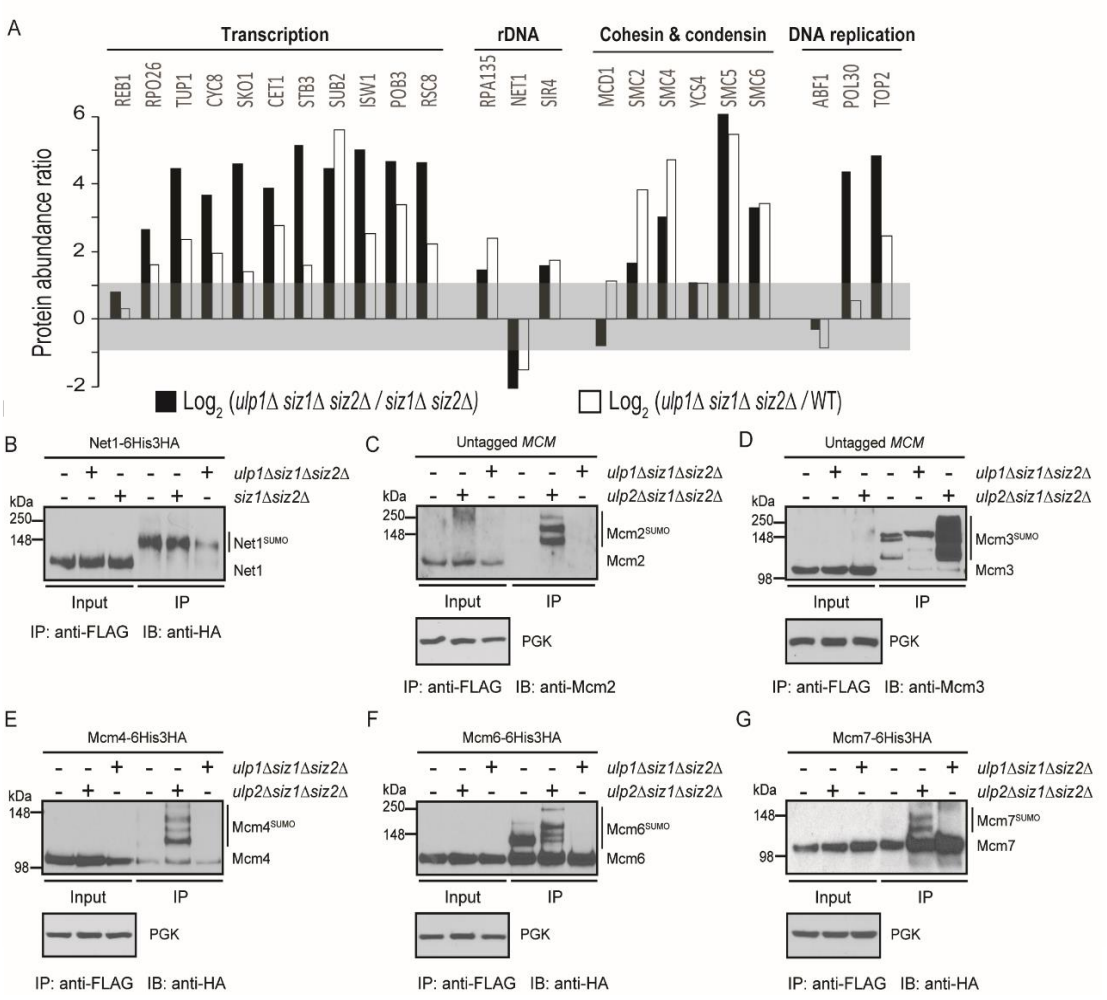

Figure 3.3 Ulp1 has a broad role in intracellular desumoylation distinct from Ulp2

A) Effect of the losses of Ulp1, Siz1 and Siz2 on sumoylated proteins measured by quantitative MS. White bar: abundance ratio of sumoylated proteins between *ulp1Δ siz1Δ siz2Δ* and wild-type strains. Black bar: abundance ratio of sumoylated proteins between *ulp1Δ siz1Δ siz2Δ* and *siz1Δ siz2Δ* mutants. B) Effects of deleting Ulp1, Siz1 and Siz2 on sumoylated Net1. C-F) Effects of deleting Ulp1 or Ulp2 on sumoylated MCM subunits in cells lacking Siz1 and Siz2. Sumoylated proteins were purified and analyzed by various antibodies as indicated, using the same method as in Figure 3.2B.

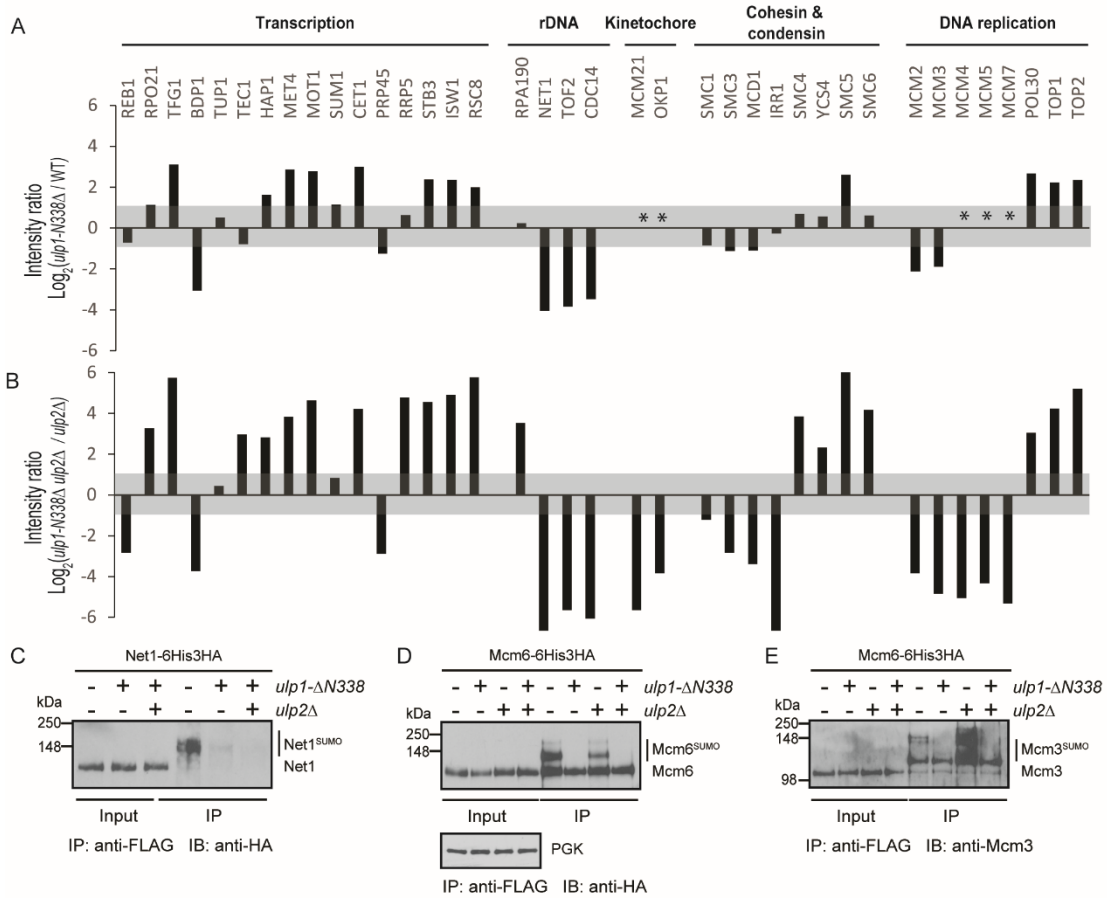

Figure 3.4 Loss of Ulp1 NPC-targeting domain causes specific desumoylation of Ulp2-specific targets

A) Effect of *ulp1-N338Δ* on intracellular protein sumoylation measured by quantitative MS. Asterisk indicates the protein was not identified. B) Effect of *ulp1-N338Δ* on intracellular protein sumoylation in cells lacking Ulp2 measured by quantitative MS. C-E) Effect of *ulp1-N338Δ* and *ulp2Δ* mutations on sumoylated Net1, Mcm6 and Mcm3, using the same method as in Figure 3.2B.

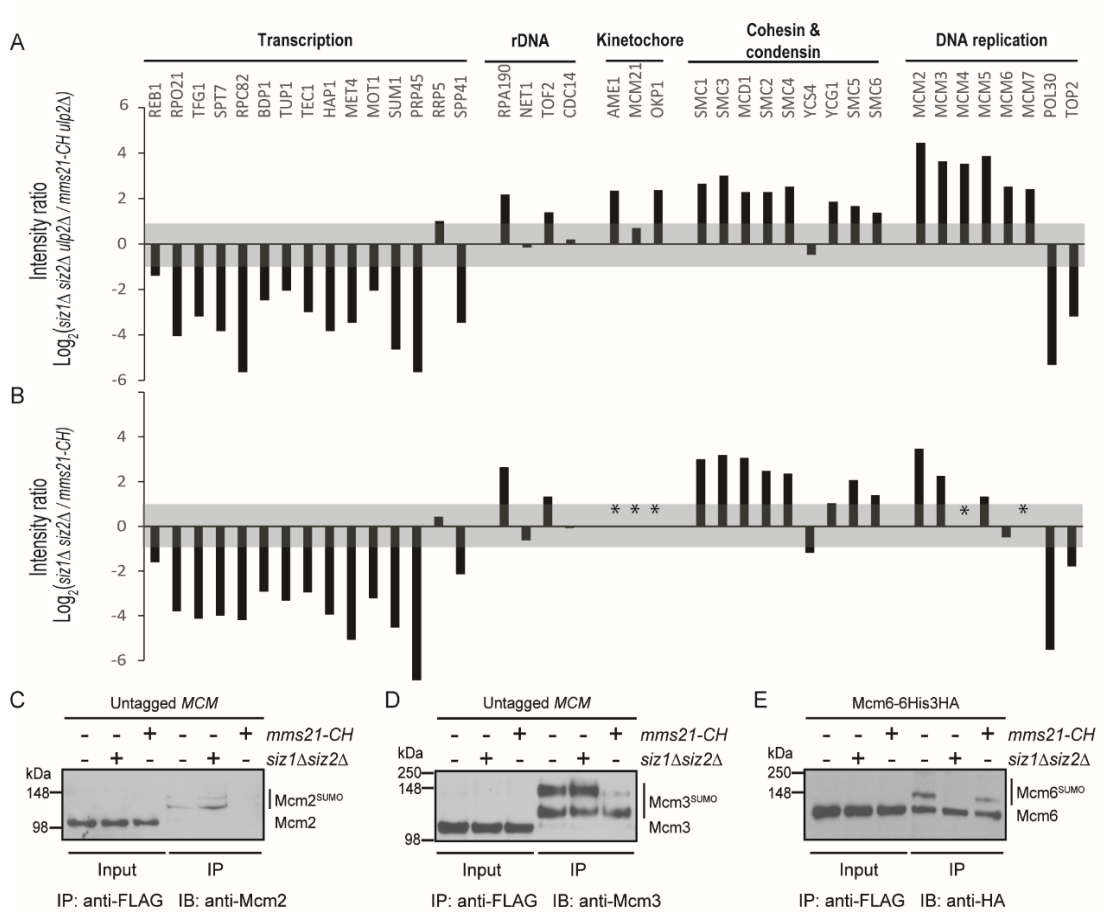

Figure 3.5 Comparison between *siz1Δ siz2Δ* and *mms21-CH* mutants reveals MCM as a target of Mms21

A) Relative abundance of sumoylated proteins in *ulp2Δ siz1Δ siz2Δ* and *ulp2Δ mms21-CH* mutants measured by quantitative MS. B) Relative abundance of sumoylated proteins in *siz1Δ siz2Δ* and *mms21-CH* mutants measured by quantitative MS. Asterisks indicate the protein was not identified. C-E) Effect of *siz1Δ siz2Δ* and *mms21-CH* mutations on sumoylated Mcm2, Mcm3 and Mcm6, using the same method as in Figure 3.2B.

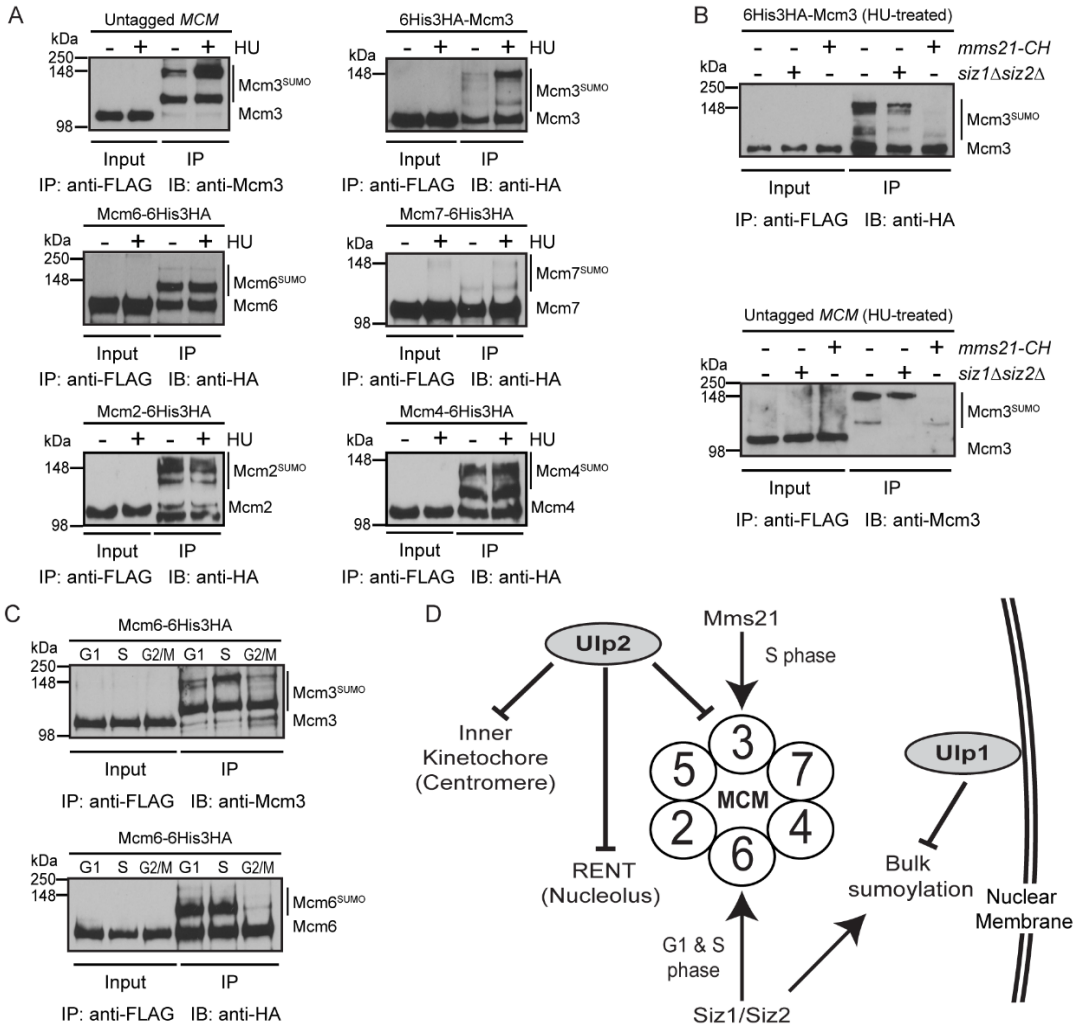

Figure 3.6 Regulation of MCM sumoylation in response to DNA replication stress and during the cell cycle

A) Effect of hydroxyurea (HU) treatment on sumoylated MCM subunits. B) Effect of *siz1Δ siz2Δ* and *mms21-CH* mutations on HU-induced sumoylated Mcm3 detected by anti-HA and anti-Mcm3 antibodies. C) Cell cycle dynamics of sumoylated Mcm3 and Mcm6 following G1 release into S and G2/M phase. In each case, sumoylated MCM subunits were analyzed using the same method as in Figure 3.22B. D) Regulation of sumoylation of MCM and other Ulp2 targets by the SUMO-pathway.

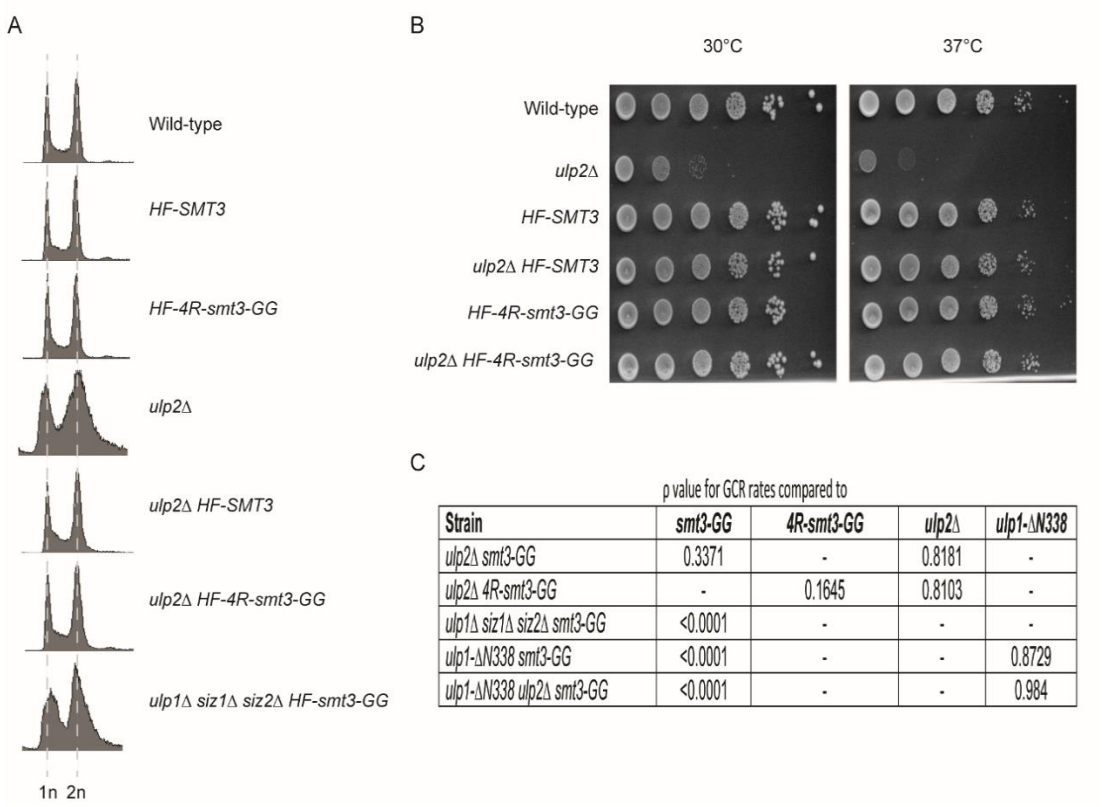

C

ρ value for GCR rates compared to

Strain	smt3-GG	4R-smt3-GG	ulp2Δ	ulp1-ΔN338
ulp2Δ smt3-GG	0.3371	-	0.8181	-
ulp2Δ 4R-smt3-GG	-	0.1645	0.8103	-
ulp1Δ siz1Δ siz2Δ smt3-GG	<0.0001	-	-	-
ulp1-ΔN338 smt3-GG	<0.0001	-	-	0.8729
ulp1-ΔN338 ulp2Δ smt3-GG	<0.0001	-	-	0.984

Figure 3.7 Growth effects in *ulp2Δ* mutants

A) FACs profile of the parental strain and strains with or without *HF-SMT3 or HF-4R-smt3-GG*. B) Plating of *ulp2* mutant strains with or without *HF-SMT3* or *HF-4R-smt3-GG*. Cells were normalized and serial diluted 1:10 before plating. Cells were grown at 30°C and 37°C for 3 days before imaging. C) Table of ρ-values of GCR rates for *ulp1* and *ulp2* mutants from Figure 3-1A and C.

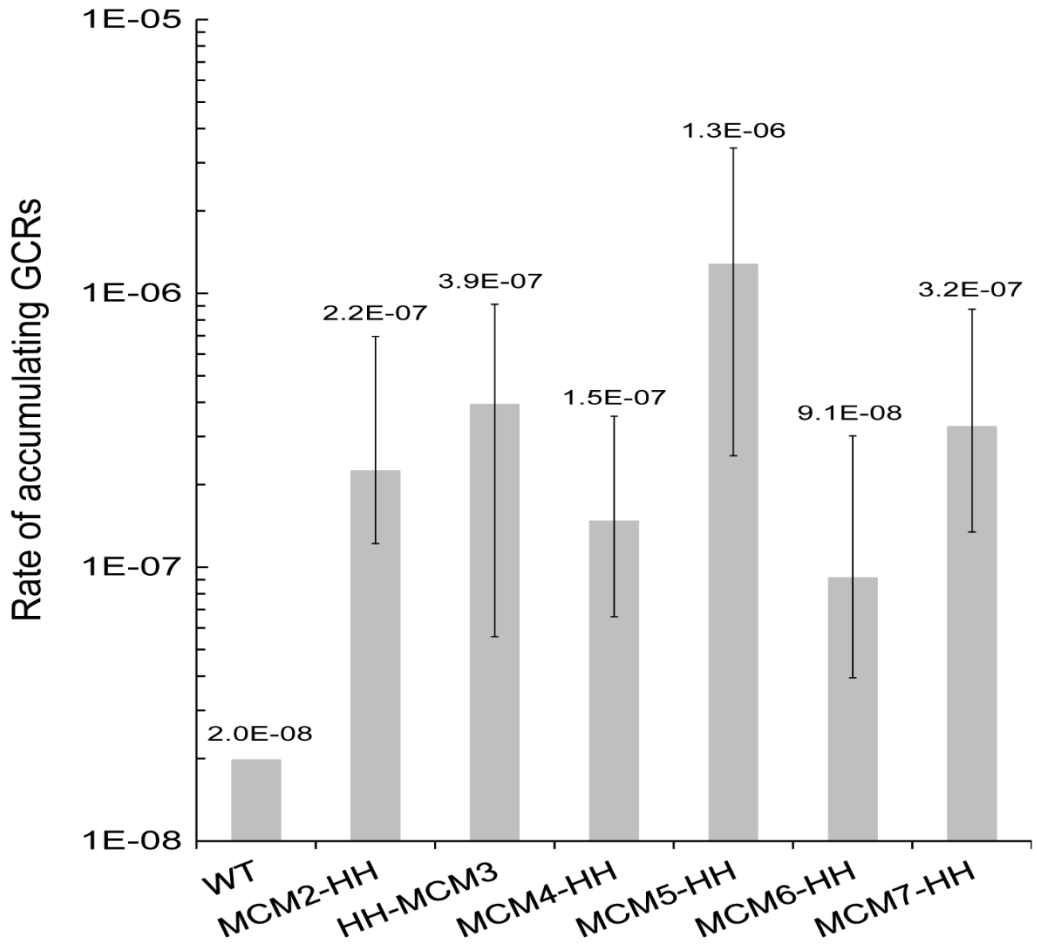

Figure 3.8 Rate of accumulating GCRs in MCM-HH tagged strains

Rate of accumulating GCRs of cells tagged with a 6xHis-3HA epitope at each individual *MCM* gene in the *yel072w::CAN1/URA3* assay. Error bars represent the upper and lower limits of the 95% confidence intervals of the median.

Table 3.1 Yeast strains used in Chapter 3
HF-SMT3 refers *to 6xHIS-3xFLAG-SMT3*. HH tag refers to 6xHIS-3xHA tag. *4R-smt3 – smt3-(K11R, K15R, K19R and K27R), while smt3GG* indicates mature SUMO with the C-terminal three amino acids of Smt3 removed.

Strain name	Genotype	Source
RDKY6678	MATa, *leu2Δ1 trp1Δ63 his3Δ200 lys2ΔBgl hom3-10 ade2Δ ade8 ura3-52 iYEL072W::hph can1::hisG yel072w::CAN1/URA3*	Putnam, et al, Nature 2009
RDKY6677	MATa, *leu2Δ1 trp1Δ63 his3Δ200 lys2ΔBgl hom3-10 ade2Δ ade8 ura3-52 iYEL072W::hph can1::hisG yel068c::CAN1/URA3*	Putnam, et al, Nature 2009
HZY3392	MATa, *smt3GG::kanMX6*, isogenic to RDKY6678	This study
HZY3451	MATa, *4R-smt3GG::KanMX6*, isogenic to RDKY6678	This study
HZY3443	MAT a, *ulp2Δ::HIS3 4R-smt3GG::kanMX6*, isogenic to RDKY6678	This study
HZY3860	MATa, *ulp2Δ::HIS3 smt3GG::TRP*, isogenic to RDKY6678	This study
HZY3864	MATα, *ulp2Δ::HIS3*, isogenic to RDKY6678	This study
HZY3865	MATa, *ulp2Δ::HIS3 siz1Δ::TRP1 siz2Δ::NAT*, isogenic to RDKY6678	This study
HZY3644	MATa, *ulp1Δ::kanMX6 siz1Δ::HIS3 siz2Δ::NAT smt3GG::TRP1*, isogenic to RDKY6678	This study
HZY3785	MATa, *ulp1-N338Δ::kanMX6 smt3GG::TRP1*, isogenic to RDKY6678	This study
HZY3998	MATa, *ulp1-N338Δ::kanMX6 ulp2Δ::HIS3 smt3GG::TRP*, isogenic to RDKY6678	This study
HZY2786	MATa, *MCM2-HH::HisMX6*, isogenic to RDKY6678	This study
HZY4252	MATa, *HH-MCM3 sml1Δ::TRP1*, isogenic to RDKY6678	This study
HZY4046	MATα, *MCM4-HH::kanMX6*, isogenic to RDKY6678	This study
HZY2788	MATa, *MCM5-HH::HisMX6*, isogenic to RDKY6678	This study
HZY2789	MATa, *MCM6-HH::HisMX6*, isogenic to RDKY6678	This study
HZY2790	MATa, *MCM7-HH::HisMX6*, isogenic to RDKY6678	This study
HZY2101	MATa, *HF-SMT3 sml1Δ::TRP1 arg4Δ ura3-52 leu2Δ1 trp1Δ63 his3Δ200 lys2ΔBgl hom3-10 ade2Δ ade8*, 2-micron removed.	Albuquerque, et al, PLoS genetics 2013
HZY2109	MATa, *siz1Δ::HIS3 siz2Δ::URA3, HF-SMT3,* isogenic to HZY2101	Albuquerque, et al, PLoS genetics 2013
HZY2136	MATa, *mms21-CH::kanMX6, HF-SMT3,* isogenic to HZY2101	Albuquerque, et al, PLoS genetics 2013
HZY3393	MATa, *HF-4R-smt3GG::kanMX6,* isogenic to HZY2101	This study
HZY3485	MATa, *ulp1Δ::HIS3 siz1Δ::URA3 siz2Δ::NAT HF-smt3GG::kanMX6,* isogenic to HZY2101	This study
HZY3710	MATa, *ulp2Δ::HIS3 HF-4R-smt3GG::kanMX6,* isogenic to HZY2101	This study
HZY3252	MATa, *siz1Δ::URA3 siz2Δ::NAT HF-smt3GG::kanMX6*, isogenic to HZY2101	This study

Table 3.1 Yeast strains used in Chapter 3, continued

Strain name	Genotype	Source
HZY3716	MATα, *ulp2Δ::HIS3 siz1Δ::NAT siz2Δ::URA3 HF-4R-smt3GG::kanMX6,* isogenic to HZY2101	This study
HZY3752	MATa, *ulp2Δ::NAT HF-SMT3,* isogenic to HZY2101	This study
HZY3766	MATa, *ulp2Δ::NAT siz1Δ::HIS3 siz2Δ::URA3 HF-SMT3,* isogenic to HZY2101	This study
HZY3870	MATα, *ulp2Δ::HIS3 mms21-CH:kanMX6 HF-4R-smt3GG::URA3,* isogenic to HZY2101	This study
HZY3896	MATa, *ulp1-N338Δ::kanMX6 HF-SMT3,* isogenic to HZY2101	This study
HZY3934	MATa, *ulp2Δ::NAT ulp1-N338Δ::kanMX6 HF-SMT3,* isogenic to HZY2101	This study
HZY3721	MATa, *NET1-HH::kanMX6 HF-SMT3,* isogenic to HZY2101	This study
HZY3725	MATa, *NET1-HH::kanMX6 ulp2Δ::HIS3,* isogenic to HZY2101	This study
HZY4139	MATα, *NET1-HH::HisMX6 ulp1-N338Δ::kanMX6 HF-SMT3,* isogenic to HZY2101	This study
HZY4140	MATa, *NET1-HH::HisMX6 ulp1-N338Δ::kanMX6 ulp2Δ::NAT HF-SMT3,* isogenic to HZY2101	This study
HZY1706	MATa, *NET1-HH::kanMX6 siz1Δ::HIS3 siz2Δ::URA3 HF-SMT3,* isogenic to HZY2101	This study
HZY1708	MATa, *NET1-HH::kanMX6 ulp1Δ::HIS3 siz1Δ::URA3 siz2Δ::NAT HF-SMT3,* isogenic to HZY2101	This study
HZY2791	MATα, *MCM2-HH::kanMX6 HF-SMT3,* isogenic to HZY2101	This study
HZY1982	MATa, *MCM2-HH::kanMX6 ulp2Δ::NAT HF-SMT3,* isogenic to HZY2101	This study
HZY4213	MATα, *HH-MCM3*, *HF-SMT3,* isogenic to HZY2101	This study
HZY4217	MATa, *URA3::HH-MCM3 mms21-CH::kanMX6 HF-SMT3,* isogenic to HZY2101	This study
HZY4222	MATa, *URA3::HH-MCM3 siz1Δ::HIS3 siz2Δ::kanMX6, HF-SMT3,* isogenic to HZY2101	This study
HZY3875	MATα, *MCM4-HH::kanMX6 HF-SMT3,* isogenic to HZY2101	This study
HZY3876	MATa, *MCM4-HH::kanMX6 ulp2Δ::NAT HF-SMT3,* isogenic to HZY2101	This study
HZY3880	MATa, *MCM4-HH::kanMX6 ulp2Δ::NAT siz1Δ::HIS3 siz2Δ::URA3 HF-SMT3,* isogenic to HZY2101	This study
HZY1716	MATα, *MCM4-HH::kanMX6 ulp1Δ::HIS3 siz1Δ::URA3 siz2Δ::NAT HF-SMT3,* isogenic to HZY2101	This study
HZY2795	MATα, *MCM6-HH::kanMX6 HF-SMT3,* isogenic to HZY2101	This study
HZY1902	MATa, *MCM6-HH::HisMX6 bar1Δ::URA3 HF-SMT3,* isogenic to HZY2101	This study
HZY1997	MATα, *MCM6-HH:: kanMX6 ulp1Δ::HIS3 siz1Δ::URA3 siz2Δ::NAT HF-smt3GG::kanMX6*	This study

Table 3.1 Yeast strains used in Chapter 3, continued

Strain name	Genotype	Source
HZY4027	MATa, *MCM6-HH::kanMX6 siz1Δ::HIS3 siz2Δ::URA3 HF-SMT3,* isogenic to HZY2101	This study
HZY4029	MATa, *MCM6-HH::kanMX6 ulp2Δ::NAT HF-SMT3,* isogenic to HZY2101	This study
HZY4031	MATα, *MCM6-HH::kanMX6 siz1Δ::HIS3 siz2Δ::URA3 ulp2Δ::NAT HF-SMT3,* isogenic to HZY2101	This study
HZY4033	MATa, *MCM6-HH::kanMX6 mms21-CH::KanMX6 HF-SMT3,* isogenic to HZY2101	This study
HZY4037	MATa, *MCM6-HH::kanMX6 ulp1-N338Δ::kanMX6 HF-SMT3,* isogenic to HZY2101	This study
HZY4039	MATa, *MCM6-HH::kanMX6 ulp2Δ::NAT ulp1-N338Δ::kanMX6 HF-SMT3,* isogenic to HZY2101	This study
HZY4198	MATα, *MCM7-HH::kanMX6*, *HF-SMT3,* isogenic to HZY2101	This study
HZY1704	MATα, *MCM7-HH::kanMX6 ulp2Δ::NAT*, *HF-SMT3,* isogenic to HZY2101	This study

Table 3.2 Abundance of sumoylated protein identified and quantified by comparing *ulp2*Δ *HF-4R-smt3GG* (HZY3710) and *HF-4R-smt3GG* (HZY3393) strains

Gene	ORF	Median ratio (HZY3710/HZY3393)	# of peptides found
ABF1	YKL112W	0.63	35
ABP1	YCR088W	0.57	8
AME1	YBR211C	16.53	10
AOS1	YPR180W	1.91	3
BIR1	YJR089W	0.35	30
BOP3	YNL042W	0.50	26
BRF1	YGR246C	0.75	3
BRN1	YBL097W	0.87	12
BUD3	YCL014W	0.25	6
BUD4	YJR092W	0.58	9
CBF1	YJR060W	3.99	13
CBF2	YGR140W	1.75	31
CDC11	YJR076C	0.42	12
CDC14	YFR028C	35.50	19
CDC3	YLR314C	0.60	22
CDC48	YDL126C	2.05	39
CET1	YPL228W	1.24	17
CIN5	YOR028C	0.56	7
CRZ1	YNL027W	0.41	4
CST6	YIL036W	0.87	3
CYC8	YBR112C	0.33	24
GCN5	YGR252W	0.44	7
GCR1	YPL075W	0.17	20
GCR2	YNL199C	0.32	4
HPC2	YBR215W	0.23	8
HRP1	YOL123W	0.61	4
HTA2|HTA1	YBL003C|YDR225W	8.05	3
HTB2|HTB1	YBL002W|YDR224C	2.89	7
ISW1	YBR245C	0.56	7
ISW1|ISW2	YBR245C|YOR304W	0.61	3
ITC1	YGL133W	0.32	3
MAD1	YGL086W	0.38	10
MCD1	YDL003W	4.95	33
MCM16	YPR046W	33.44	4
MCM2	YBL023C	1.74	6
MCM21	YDR318W	22.33	15
MCM22	YJR135C	13.88	6
MCM3	YEL032W	7.56	5
MCM4	YPR019W	5.50	12
MCM5	YLR274W	3.16	3
MCM6	YGL201C	0.66	10
MCM7	YBR202W	13.17	15
MET4	YNL103W	0.77	10
MLP1	YKR095W	0.47	154

Table 3.2 Abundance of sumoylated protein identified and quantified by comparing *ulp2Δ HF-4R-smt3GG* (HZY3710) and *HF-4R-smt3GG* (HZY3393) strains, continued

Gene	ORF	Median ratio (HZY3710/HZY3393)	# of peptides found
MLP2	YIL149C	0.68	59
MOT1	YPL082C	1.18	4
NET1	YJL076W	18.71	225
NGG1	YDR176W	0.54	5
NPL6	YMR091C	0.36	7
NUP2	YLR335W	0.31	13
NUT1	YGL151W	0.47	21
OKP1	YGR179C	37.37	3
ORC3	YLL004W	0.66	3
PAA1	YDR071C	0.44	3
POB3	YML069W	0.71	22
POL30	YBR088C	0.61	25
PRP45	YAL032C	0.28	22
RAP1	YNL216W	0.66	18
REB1	YBR049C	0.72	10
RIF1	YBR275C	0.38	5
RPA43	YOR340C	1.21	5
RPB4	YJL140W	0.48	7
RPC37	YKR025W	1.14	17
RPC82	YPR190C	1.51	5
RPO21	YDL140C	0.77	65
RPO26	YPR187W	0.77	7
RSC8	YFR037C	0.33	28
RTT102	YGR275W	0.37	6
RVB1	YDR190C	0.12	15
RVB2	YPL235W	0.26	4
SEF1	YBL066C	0.32	5
SHS1	YDL225W	0.51	37
SIN3	YOL004W	0.34	30
SIR3	YLR442C	0.78	7
SIR4	YDR227W	0.35	17
SIZ1	YDR409W	0.98	22
SKO1	YNL167C	0.52	11
SLK19	YOR195W	0.79	11
SMC2	YFR031C	0.64	4
SMC3	YJL074C	1.55	14
SMC4	YLR086W	0.79	5
SPC24	YMR117C	0.58	7
SPP41	YDR464W	0.51	5
SPT15	YER148W	3.70	6
SPT7	YBR081C	0.38	52
STB3	YDR169C	0.50	13
STE12	YHR084W	0.38	7
STU1	YBL034C	0.46	15

Table 3.2 Abundance of sumoylated protein identified and quantified by comparing *ulp2Δ HF-4R-smt3GG* (HZY3710) and *HF-4R-smt3GG* (HZY3393) strains, continued

Gene	ORF	Median ratio (HZY3710/HZY3393)	# of peptides found
SUB2	YDL084W	0.44	4
SUM1	YDR310C	0.33	13
SWC5	YBR231C	0.57	3
SWI3	YJL176C	0.61	28
TAF12	YDR145W	0.61	7
TAF2	YCR042C	0.63	3
TAF3	YPL011C	0.45	5
TAF5	YBR198C	0.41	3
TEC1	YBR083W	0.37	23
TFC7	YOR110W	0.44	16
TIF2|TIF1	YJL138C|YKR059W	0.42	24
TOA1	YOR194C	1.24	9
TOF2	YKR010C	43.17	38
TOP2	YNL088W	0.37	11
TUP1	YCR084C	0.38	72
TYE7	YOR344C	0.59	12
UAF30	YOR295W	5.11	5
UBA2	YDR390C	0.68	43
UBC9	YDL064W	0.38	21
VHR1	YIL056W	0.48	5
VID21	YDR359C	0.67	3
VPS72	YDR485C	0.23	7
YCG1	YDR325W	0.92	31
YCS4	YLR272C	0.46	56
YMR111C	YMR111C	1.24	20

Table 3.3 Abundance of sumoylated proteins identified and quantified by comparing *ulp2*Δ *HF-SMT3* (HZY3752) strain and *ulp2*Δ *HF-4R-smt3GG* (HZY3710) strains

Gene	ORF	Median ratio (HZY3752/HZY3710)	# of peptides found
AOS1	YPR180W	7.94	3
BDP1	YNL039W	5.44	41
BIR1	YJR089W	2.29	31
BOP3	YNL042W	3.53	29
BRF1	YGR246C	3.67	9
BRN1	YBL097W	3.64	12
BUD4	YJR092W	8.675	4
BUR6	YER159C	1.75	4
CBF1	YJR060W	2.92	18
CBF2	YGR140W	3.29	12
CDC3	YLR314C	2.37	39
CDC48	YDL126C	2.32	47
CET1	YPL228W	7.06	3
CIN5	YOR028C	14.335	16
CST6	YIL036W	3.065	6
CTI6	YPL181W	6.905	6
CYC8	YBR112C	5.76	3
HAP1	YLR256W	6.79	4
HIR2	YOR038C	3.82	5
HPC2	YBR215W	6.03	38
HTA2|HTA1	YBL003C|YDR225W	3.475	10
HTB2|HTB1	YBL002W|YDR224C	3.135	10
IRR1	YIL026C	2.07	7
ISW1	YBR245C	4.31	7
MCD1	YDL003W	2.27	31
MCM16	YPR046W	2.71	3
MCM21	YDR318W	2.23	3
MCM22	YJR135C	3.785	2
MCM3	YEL032W	1.76	14
MCM4	YPR019W	1.455	2
MCM7	YBR202W	2.51	3
MET4	YNL103W	8.98	8
MLP1	YKR095W	1.13	99
MLP2	YIL149C	1.7	31
MOT1	YPL082C	4.605	6
NET1	YJL076W	2.87	399
NGG1	YDR176W	5.8	10
OKP1	YGR179C	2.025	6
POB3	YML069W	2.88	6
POL30	YBR088C	4.07	30
PRP45	YAL032C	1.9	18
RAP1	YNL216W	5.035	8
REB1	YBR049C	3.42	21

Table 3.3 Abundance of sumoylated proteins identified and quantified by comparing *ulp2*Δ *HF-SMT3* (HZY3752) strain and *ulp2*Δ *HF-4R-smt3GG* (HZY3710) strains, continued

Gene	ORF	Median ratio (HZY3752/HZY3710)	# of peptides found
RET1	YOR207C	3.475	4
RPB4	YJL140W	4.55	13
RPC37	YKR025W	7.01	15
RPC53	YDL150W	6.94	31
RPC82	YPR190C	6.34	16
RPO21	YDL140C	3.9	32
RPO26	YPR187W	5.62	7
RRP5	YMR229C	2.37	5
RSC2	YLR357W	10.875	14
RSC8	YFR037C	3.77	8
SHS1	YDL225W	2.1	23
SIN3	YOL004W	3.355	4
SIR3	YLR442C	5.535	32
SIR4	YDR227W	6.01	31
SIZ1	YDR409W	1.53	24
SKO1	YNL167C	8.7	21
SLI15	YBR156C	1.77	4
SMC1	YFL008W	1.915	8
SMC2	YFR031C	2.14	4
SMC3	YJL074C	2.425	14
SMC4	YLR086W	3.515	16
SPC24	YMR117C	1.2	3
SPP41	YDR464W	4.46	51
SPT15	YER148W	3.42	3
SPT7	YBR081C	8.535	30
STB3	YDR169C	3.77	6
STH1	YIL126W	5.81	9
SUM1	YDR310C	9.745	70
SWI3	YJL176C	5.65	10
SWR1	YDR334W	6.45	4
TEC1	YBR083W	8.29	21
TFC7	YOR110W	4.38	5
TFG1	YGR186W	6.775	16
TIF2|TIF1	YJL138C|YKR059W	1.365	6
TOA1	YOR194C	8.93	11
TOF2	YKR010C	6.14	117
TOP2	YNL088W	1.77	27
TUP1	YCR084C	6.39	37
TYE7	YOR344C	7.195	46
UAF30	YOR295W	3.19	13
UBA2	YDR390C	1.3	34
UBC9	YDL064W	1.095	28
UPC2	YDR213W	9.045	6
YCG1	YDR325W	4.075	6

Table 3.3 Abundance of sumoylated proteins identified and quantified by comparing *ulp2*Δ *HF-SMT3* (HZY3752) strain and *ulp2*Δ *HF-4R-smt3GG* (HZY3710) strains, continued

Gene	ORF	Median ratio (HZY3752/HZY3710)	# of peptides found
YCS4	YLR272C	2.425	12
YMR111C	YMR111C	4.21	25

Table 3.4 Abundance of sumoylated proteins identified and quantified by comparing *ulp1*Δ *siz1*Δ *siz2*Δ *HF-smt3GG* (HZY3485) and *HF-SMT3* (HZY2101) strains

Gene	ORF	Median ratio (HZY3485/HZY2101)	# of peptides found
ABF1	YKL112W	0.545	24
AOS1	YPR180W	179.495	36
BIR1	YJR089W	0.28	5
BUD3	YCL014W	0.17	3
BUD4	YJR092W	0.07	11
CBF2	YGR140W	1.53	8
CDC11	YJR076C	0.07	11
CDC3	YLR314C	0.115	34
CET1	YPL228W	6.75	22
CYC8	YBR112C	3.87	17
GCR1	YPL075W	0.5	5
HRP1	YOL123W	2285	4
ISW1	YBR245C	5.73	3
MCD1	YDL003W	2.185	8
MET4	YNL103W	0.38	3
MLP1	YKR095W	1.005	44
NET1	YJL076W	0.35	7
NUP2	YLR335W	39.775	14
POB3	YML069W	10.38	25
POL30	YBR088C	1.44	13
REB1	YBR049C	1.225	4
RPA135	YPR010C	5.27	6
RPC37	YKR025W	0.905	6
RPO21	YDL140C	0.47	29
RPO26	YPR187W	3.03	5
RSC58	YLR033W	15.74	4
RSC8	YFR037C	4.67	37
RTT102	YGR275W	13.19	5
RVB1	YDR190C	3.23	17
SEF1	YBL066C	3.54	3
SHS1	YDL225W	0.095	36
SIN3	YOL004W	1.195	6
SIR4	YDR227W	3.33	3
SIZ1	YDR409W	0.105	14
SKO1	YNL167C	2.65	4
SMC2	YFR031C	14.115	18
SMC4	YLR086W	26.215	30
SMC5	YOL034W	44	21
SMC6	YLR383W	10.585	4
SPT7	YBR081C	0.17	21
STB3	YDR169C	2.955	14
STE12	YHR084W	1	3
STU1	YBL034C	0.96	3

Table 3.4 Abundance of sumoylated proteins identified and quantified by comparing *ulp1*Δ *siz1*Δ *siz2*Δ *HF-smt3GG* (HZY3485) and *HF-SMT3* (HZY2101) strains, continued

Gene	ORF	Median ratio (HZY3485/HZY2101)	# of peptides found
SUB2	YDL084W	48.47	14
SWI3	YJL176C	2.12	11
TEC1	YBR083W	1.01	7
TOA1	YOR194C	2.835	4
TOP2	YNL088W	5.51	3
TUP1	YCR084C	5.15	49
TYE7	YOR344C	0.115	4
UBA2	YDR390C	4.72	62
UBC9	YDL064W	2.42	17
YCG1	YDR325W	4.01	6
YCS4	YLR272C	2.09	19

Table 3.5 Abundance of sumoylated proteins identified and quantified by comparing *ulp1*∆ *siz1*∆ *siz2*∆ *HF-smt3GG* (HZY3485) and *siz1*∆ *siz2*∆ *HF-smt3GG* (HZY3252) strains

Gene	ORF	Median ratio (HZY3485/HZY3252)	# of peptides found
ABF1	YKL112W	0.8	41
AOS1	YPR180W	58.77	33
AZF1	YOR113W	3.16	3
BRN1	YBL097W	1.58	3
CDC3	YLR314C	4.44	7
CET1	YPL228W	14.635	8
CRZ1	YNL027W	53.265	4
CYC8	YBR112C	12.84	8
HAP1	YLR256W	6.25	4
HPC2	YBR215W	4.37	3
HRP1	YOL123W	37.44	3
HTB2|HTB1	YBL002W|YDR224C	1.095	4
ISW1	YBR245C	32.15	9
ISW1|ISW2	YBR245C|YOR304W	19.44	3
MCD1	YDL003W	0.57	5
MCM2	YBL023C	0.14	1
MLP1	YKR095W	1.78	5
NET1	YJL076W	0.235	36
NUP2	YLR335W	13.45	5
PAF1	YBR279W	11.27	7
POB3	YML069W	25.375	18
POL30	YBR088C	20.66	7
RAD16	YBR114W	47.215	10
REB1	YBR049C	1.74	11
RPA135	YPR010C	2.73	3
RPA190	YOR341W	8.215	18
RPC53	YDL150W	3.8	5
RPO26	YPR187W	6.3	4
RRP5	YMR229C	6.1	19
RSC58	YLR033W	34.65	6
RSC8	YFR037C	25.22	13
RVB1	YDR190C	24.94	4
SIR3	YLR442C	1.35	3
SIR4	YDR227W	3.02	15
SKO1	YNL167C	24.495	4
SMC1	YFL008W	1.08	5
SMC2	YFR031C	3.21	22
SMC3	YJL074C	0.915	12
SMC4	YLR086W	8.225	70
SMC5	YOL034W	67.54	78
SMC6	YLR383W	9.85	7
SPN1	YPR133C	24.69	3

Table 3.5 Abundance of sumoylated proteins identified and quantified by comparing *ulp1*Δ *siz1*Δ *siz2*Δ *HF-smt3GG* (HZY3485) and *siz1*Δ *siz2*Δ *HF-smt3GG* (HZY3252) strains, continued

Gene	ORF	Median ratio (HZY3485/HZY3252)	# of peptides found
SPP41	YDR464W	2.37	3
SPT5	YML010W	6.3	6
STB3	YDR169C	35.56	7
STH1	YIL126W	6.83	5
SUB2	YDL084W	22.4	7
SUM1	YDR310C	4.225	4
TFG1	YGR186W	25.3	12
TOF2	YKR010C	0.37	6
TOP1	YOL006C	22.125	22
TOP2	YNL088W	28.795	60
TUP1	YCR084C	21.96	48
UBA2	YDR390C	4.23	52
UBC9	YDL064W	0.5	29
YCS4	YLR272C	2.11	7

Table 3.6 Abundance of sumoylated proteins identified and quantified by comparing *ulp1-N338*Δ (HZY3896) and *HF-SMT3* (HZY2101) strains

Gene	ORF	Median ratio (HZY3896/HZY2101)	# of peptides found
ABF1	YKL112W	0.56	22
ABP1	YCR088W	2.93	7
AOS1	YPR180W	16.18	13
ASF2	YDL197C	0.15	4
AZF1	YOR113W	6.07	6
BDP1	YNL039W	0.12	13
BIR1	YJR089W	1.19	14
BOP3	YNL042W	1.09	14
BRN1	YBL097W	0.815	6
BUD3	YCL014W	14.01	15
BUD4	YJR092W	12.23	35
BUR6	YER159C	10.71	3
CBF1	YJR060W	1.33	4
CDC11	YJR076C	5.715	14
CDC14	YFR028C	0.09	1
CDC3	YLR314C	3.92	43
CDC48	YDL126C	14.575	62
CET1	YPL228W	7.995	16
CIN5	YOR028C	1.78	3
CRZ1	YNL027W	6.13	15
CST6	YIL036W	4.67	19
CYC8	YBR112C	1.405	6
GCN5	YGR252W	1.39	5
GCR1	YPL075W	0.17	8
GIN4	YDR507C	12.65	34
HAP1	YLR256W	3.06	3
HIR2	YOR038C	0.97	19
HMS1	YOR032C	1.22	3
HPC2	YBR215W	1.26	29
HRP1	YOL123W	5.58	4
HSL1	YKL101W	3.995	4
HTA2|HTA1	YBL003C|YDR225W	0.255	4
IRR1	YIL026C	0.83	3
ISW1	YBR245C	5.12	33
ISW1|ISW2	YBR245C|YOR304W	5.43	3
ITC1	YGL133W	3.79	11
KRE33	YNL132W	0.6	3
MAD1	YGL086W	0.29	3
MCD1	YDL003W	0.465	4
MCM2	YBL023C	0.23	1
MCM3	YEL032W	0.27	1
MET4	YNL103W	7.225	10
MLP1	YKR095W	0.14	89

Table 3.6 Abundance of sumoylated proteins identified and quantified by comparing *ulp1-N338*Δ (HZY3896) and *HF-SMT3* (HZY2101) strains, continued

Gene	ORF	Median ratio (HZY3896/HZY2101)	# of peptides found
MLP2	YIL149C	0.13	48
MOT1	YPL082C	6.79	23
NET1	YJL076W	0.06	60
NFI1	YOR156C	5.85	12
NGG1	YDR176W	1.35	10
NUP2	YLR335W	1.82	7
NUT1	YGL151W	9.06	5
PAF1	YBR279W	6.565	4
POB3	YML069W	7.94	21
POL30	YBR088C	6.33	13
PRP45	YAL032C	0.42	15
RAD16	YBR114W	3.81	9
RAP1	YNL216W	1.28	12
REB1	YBR049C	0.61	15
RET1	YOR207C	1.82	4
RPA135	YPR010C	5.61	12
RPA190	YOR341W	1.18	7
RPB4	YJL140W	2.01	5
RPC37	YKR025W	2.105	8
RPC53	YDL150W	3.12	15
RPC82	YPR190C	1.21	7
RPO21	YDL140C	2.19	44
RPO26	YPR187W	1.28	3
RRP5	YMR229C	1.55	21
RSC2	YLR357W	1.87	12
RSC8	YFR037C	3.96	21
SEF1	YBL066C	1.18	4
SHS1	YDL225W	6.365	38
SIN3	YOL004W	1.73	15
SIR3	YLR442C	1.02	20
SIR4	YDR227W	0.79	25
SIZ1	YDR409W	2.99	31
SKO1	YNL167C	1.41	16
SMC1	YFL008W	0.555	4
SMC3	YJL074C	0.46	6
SMC4	YLR086W	1.615	12
SMC5	YOL034W	6.09	40
SMC6	YLR383W	1.515	6
SPP41	YDR464W	1.46	16
SPT5	YML010W	3.9	26
SPT7	YBR081C	0.85	21
STB3	YDR169C	5.19	21
STH1	YIL126W	1.93	16

Table 3.6 Abundance of sumoylated proteins identified and quantified by comparing *ulp1-N338*Δ (HZY3896) and *HF-SMT3* (HZY2101) strains, continued

Gene	ORF	Median ratio (HZY3896/HZY2101)	# of peptides found
STU1	YBL034C	7.39	21
SUB2	YDL084W	5.395	8
SUM1	YDR310C	2.2	59
SWI3	YJL176C	2.34	9
SWR1	YDR334W	0.94	5
TAF2	YCR042C	3.49	5
TEC1	YBR083W	0.58	11
TFC4	YGR047C	0.31	4
TFC7	YOR110W	0.71	3
TFG1	YGR186W	8.58	39
TIF2|TIF1	YJL138C|YKR059W	5.905	18
TOA1	YOR194C	5.675	6
TOF2	YKR010C	0.07	32
TOP1	YOL006C	4.71	21
TOP2	YNL088W	5.08	61
TUP1	YCR084C	1.43	27
TYE7	YOR344C	5.63	11
UBA2	YDR390C	2.98	34
UBC9	YDL064W	11.47	33
UPC2	YDR213W	2.92	4
VHR1	YIL056W	0.59	3
VPS72	YDR485C	0.74	3
YBR025C	YBR025C	2.26	3
YCS4	YLR272C	1.48	7
YER064C	YER064C	3.745	6
YMR111C	YMR111C	1.19	20

Table 3.7 Abundance of sumoylated proteins identified and quantified by comparing *ulp1-N338*Δ *ulp2*Δ (HZY3934) and *ulp2*Δ (HZY3752) strains

Gene	ORF	Median ratio (HZY3934/HZY3752)	# of peptides found
AOS1	YPR180W	53.5	15
AZF1	YOR113W	25.1	4
BDP1	YNL039W	0.075	12
BIR1	YJR089W	0.155	26
BOP3	YNL042W	0.41	27
BRN1	YBL097W	0.49	9
BUD3	YCL014W	20.5	13
BUD4	YJR092W	67.15	32
CBF1	YJR060W	0.06	7
CBF2	YGR140W	0.05	22
CDC11	YJR076C	17.7	18
CDC14	YFR028C	0.015	24
CDC3	YLR314C	9.04	51
CDC48	YDL126C	9.655	50
CET1	YPL228W	18.5	15
CIN5	YOR028C	0.14	3
CRZ1	YNL027W	34.95	12
CST6	YIL036W	10.6	21
CYC8	YBR112C	3.82	5
FOB1	YDR110W	98.2	4
GCN5	YGR252W	0.24	5
GCR2	YNL199C	10.9	3
GIN4	YDR507C	21.4	20
HAP1	YLR256W	7.04	9
HIR2	YOR038C	4.47	18
HMS1	YOR032C	0.91	9
HPC2	YBR215W	2.15	23
HRP1	YOL123W	44.9	5
HSL1	YKL101W	14.65	10
HTA2|HTA1	YBL003C|YDR225W	0	3
HTB2|HTB1	YBL002W|YDR224C	0.045	6
IRR1	YIL026C	0.01	17
ISW1	YBR245C	29.8	33
ISW1|ISW2	YBR245C|YOR304W	503	4
ITC1	YGL133W	20.2	8
KRE33	YNL132W	12.2	11
MCD1	YDL003W	0.095	20
MCM16	YPR046W	0.23	3
MCM2	YBL023C	0.07	9
MCM21	YDR318W	0.02	7
MCM3	YEL032W	0.035	28
MCM4	YPR019W	0.03	6
MCM5	YLR274W	0.05	2

Table 3.7 Abundance of sumoylated proteins identified and quantified by comparing *ulp1-N338*Δ *ulp2*Δ (HZY3934) and *ulp2*Δ (HZY3752) strains, continued

Gene	ORF	Median ratio (HZY3934/HZY3752)	# of peptides found
MCM7	YBR202W	0.025	8
MET4	YNL103W	14.2	9
MLP1	YKR095W	0.06	102
MLP2	YIL149C	0.14	50
MOT1	YPL082C	24.7	37
NET1	YJL076W	0.01	219
NFI1	YOR156C	10.15	8
NUP2	YLR335W	32.45	12
NUT1	YGL151W	11	5
OKP1	YGR179C	0.07	6
ORC3	YLL004W	36.9	3
PAF1	YBR279W	53.65	6
POB3	YML069W	69.65	20
POL30	YBR088C	8.23	19
PRP45	YAL032C	0.135	12
RAD16	YBR114W	17.7	11
RAP1	YNL216W	3.86	11
REB1	YBR049C	0.14	11
RET1	YOR207C	86.76	4
RIF1	YBR275C	1.3	5
RPA135	YPR010C	43.7	25
RPA190	YOR341W	11.5	27
RPB4	YJL140W	2.91	5
RPC37	YKR025W	8.11	6
RPC53	YDL150W	29.8	15
RPC82	YPR190C	2.235	18
RPO21	YDL140C	9.64	61
RPO26	YPR187W	1.55	3
RRP5	YMR229C	27.4	32
RSC2	YLR357W	6.39	13
RSC58	YLR033W	13.6	4
RSC8	YFR037C	54.4	24
RVB1	YDR190C	13.88	4
SHS1	YDL225W	14.2	35
SIN3	YOL004W	2.21	7
SIR3	YLR442C	1.165	36
SIR4	YDR227W	3.77	37
SIZ1	YDR409W	5.67	27
SKO1	YNL167C	1.29	14
SMC1	YFL008W	0.43	20
SMC2	YFR031C	11.5	15
SMC3	YJL074C	0.14	29
SMC4	YLR086W	14.4	43
SMC5	YOL034W	64.2	61

Table 3.7 Abundance of sumoylated proteins identified and quantified by comparing *ulp1-N338*Δ *ulp2*Δ (HZY3934) and *ulp2*Δ (HZY3752) strains, continued

Gene	ORF	Median ratio (HZY3934/HZY3752)	# of peptides found
SMC6	YLR383W	17.95	20
SNF2	YOR290C	3.36	7
SNF5	YBR289W	11.9	3
SPP41	YDR464W	0.5	24
SPT15	YER148W	0.095	8
SPT5	YML010W	16.5	15
SPT7	YBR081C	0.28	23
STB3	YDR169C	23.5	14
STH1	YIL126W	13.2	15
STU1	YBL034C	41.05	44
SUB2	YDL084W	17	4
SUM1	YDR310C	1.78	47
SWI4	YER111C	4.2	3
SWR1	YDR334W	10.625	6
TAF2	YCR042C	26.95	12
TEC1	YBR083W	7.77	8
TFC7	YOR110W	7.1	3
TFG1	YGR186W	53.3	33
TIF2|TIF1	YJL138C|YKR059W	436	28
TOA1	YOR194C	20	5
TOF2	YKR010C	0.02	41
TOP1	YOL006C	18.85	20
TOP2	YNL088W	36.85	86
TUP1	YCR084C	1.35	28
TYE7	YOR344C	7.54	14
UAF30	YOR295W	0.01	5
UBA2	YDR390C	10.65	56
UBC9	YDL064W	74.9	33
VHR1	YIL056W	1.08	7
YCG1	YDR325W	90.945	6
YCS4	YLR272C	5	15
YMR111C	YMR111C	11.3	21

Table 3.8 Abundance of sumoylated proteins identified and quantified by comparing *ulp2*Δ *siz1*Δ *siz2*Δ *HF-4R-smt3GG* (HZY3716) and *ulp2*Δ *mms21-CH HF-4R-smt3GG* (HZY3870) strains

Gene	ORF	Median ratio (HZY3716/HZY3870)	# of peptides found
ABF1	YKL112W	1.095	62
AME1	YBR211C	5.06	3
BDP1	YNL039W	0.18	21
BIR1	YJR089W	0.04	11
BOP3	YNL042W	0.065	12
BRF1	YGR246C	0.52	5
BRN1	YBL097W	1.96	5
BUD3	YCL014W	0.055	8
BUD4	YJR092W	0.025	18
CBF1	YJR060W	1.27	7
CBF2	YGR140W	1.11	11
CDC11	YJR076C	0.01	14
CDC14	YFR028C	1.14	29
CDC3	YLR314C	0.015	50
CDC48	YDL126C	0.125	24
CRZ1	YNL027W	0.03	8
FOB1	YDR110W	3.54	5
GIN4	YDR507C	0.045	6
HAP1	YLR256W	0.07	6
HPC2	YBR215W	0.12	7
HTA2|HTA1	YBL003C|YDR225W	2.025	8
HTB2|HTB1	YBL002W|YDR224C	6.45	9
IRR1	YIL026C	5.775	28
MCD1	YDL003W	4.86	19
MCM2	YBL023C	21.685	22
MCM21	YDR318W	1.61	3
MCM3	YEL032W	12.405	40
MCM4	YPR019W	11.55	25
MCM5	YLR274W	14.52	5
MCM6	YGL201C	5.71	5
MCM7	YBR202W	5.33	17
MET4	YNL103W	0.09	3
MLP1	YKR095W	0.19	45
MLP2	YIL149C	0.93	17
MOT1	YPL082C	0.24	4
NET1	YJL076W	0.9	207
NFI1	YOR156C	0.01	3
OKP1	YGR179C	5.13	3
POB3	YML069W	0.16	9
POL30	YBR088C	0.025	18
PRP45	YAL032C	0.02	12
REB1	YBR049C	0.38	9

Table 3.8 Abundance of sumoylated proteins identified and quantified by comparing *ulp2*Δ *siz1*Δ *siz2*Δ *HF-4R-smt3GG* (HZY3716) and *ulp2*Δ *mms21-CH HF-4R-smt3GG* (HZY3870) strains, continued

Gene	ORF	Median ratio (HZY3716/HZY3870)	# of peptides found
RPA190	YOR341W	4.5	5
RPC53	YDL150W	0.065	18
RPC82	YPR190C	0.02	7
RPO21	YDL140C	0.06	25
RRP5	YMR229C	2.01	5
RSC2	YLR357W	0.1	3
RSC8	YFR037C	0.15	5
SHS1	YDL225W	0.01	32
SIR3	YLR442C	0.345	20
SIR4	YDR227W	0.82	13
SIZ1	YDR409W	0.02	17
SKO1	YNL167C	0.08	3
SMC1	YFL008W	6.23	32
SMC2	YFR031C	4.86	9
SMC3	YJL074C	8	47
SMC4	YLR086W	5.705	12
SMC5	YOL034W	3.16	8
SMC6	YLR383W	2.58	3
SPP41	YDR464W	0.09	8
SPT15	YER148W	2.25	4
SPT7	YBR081C	0.07	11
STU1	YBL034C	0.03	4
SUM1	YDR310C	0.04	21
TEC1	YBR083W	0.125	6
TFG1	YGR186W	0.11	11
TIF2|TIF1	YJL138C|YKR059W	0.92	3
TOF2	YKR010C	2.62	79
TOP2	YNL088W	0.11	38
TUP1	YCR084C	0.24	28
TYE7	YOR344C	0.02	16
UAF30	YOR295W	2.55	6
UBA2	YDR390C	1.31	59
UBC9	YDL064W	2.6	25
VHR1	YIL056W	0.04	3
WTM1	YOR230W	0.09	3
YCG1	YDR325W	3.59	6
YCS4	YLR272C	0.72	5
YER064C	YER064C	0.03	4
YMR111C	YMR111C	0.03	19

Table 3.9 Abundance of sumoylated proteins identified and quantified by comparing untreated *siz1*Δ *siz2*Δ (HZY2109) and *mms21-CH* (HZY2136) strains

Gene	ORF	Median ratio (HZY2109/HZY2136)	# of peptides found
ABF1	YKL112W	20.94	25
ABP1	YCR088W	1.39	3
AOS1	YPR180W	1.035	6
ASF2	YDL197C	0.24	5
BDP1	YNL039W	7.535	8
BIR1	YJR089W	29.26	10
BOP3	YNL042W	30.67	16
BRF1	YGR246C	3.395	8
BRN1	YBL097W	1.04	13
BUD3	YCL014W	96.285	4
BUD4	YJR092W	142.8	25
CBF1	YJR060W	6.29	5
CBF2	YGR140W	1.575	4
CDC11	YJR076C	101.03	23
CDC14	YFR028C	1.05	3
CDC3	YLR314C	99.95	48
CDC48	YDL126C	4.255	40
CET1	YPL228W	14.9	7
CST6	YIL036W	25.97	8
CYC8	YBR112C	6.06	11
FOB1	YDR110W	0.225	8
GCN5	YGR252W	6.91	10
GCR1	YPL075W	3.025	10
HAP1	YLR256W	15.4	12
HIR2	YOR038C	2.67	5
HMS1	YOR032C	42.14	12
HSP104	YLL026W	1.825	14
HTB2|HTB1	YBL002W|YDR224C	0.64	7
ISW1	YBR245C	3.49	16
ISW1|ISW2	YBR245C|YOR304W	3.545	4
MAD1	YGL086W	2.27	7
MCD1	YDL003W	0.12	17
MCM2	YBL023C	0.09	13
MCM3	YEL032W	0.21	2
MCM4	YPR019W	0.535	2
MCM5	YLR274W	0.4	3
MCM6	YGL201C	1.405	6
MCM7	YBR202W	0.29	1
MET4	YNL103W	33.52	7
MLP1	YKR095W	14.75	165
MLP2	YIL149C	7.22	69
MOT1	YPL082C	9.23	15
NET1	YJL076W	1.545	26

Table 3.9 Abundance of sumoylated proteins identified and quantified by comparing untreated *siz1*Δ *siz2*Δ (HZY2109) and *mms21-CH* (HZY2136) strains, continued

Gene	ORF	Median ratio (HZY2109/HZY2136)	# of peptides found
NFI1	YOR156C	32.05	5
NGG1	YDR176W	1.935	8
NUT1	YGL151W	16.96	7
PAF1	YBR279W	2.5	3
POB3	YML069W	7.58	19
POL30	YBR088C	45.71	15
PRP45	YAL032C	117.515	26
RAP1	YNL216W	2.95	9
REB1	YBR049C	3.045	26
RET1	YOR207C	10.55	4
RIF1	YBR275C	4.73	6
RPA135	YPR010C	0.065	18
RPA190	YOR341W	0.16	20
RPA43	YOR340C	0.22	7
RPB4	YJL140W	13.795	10
RPC37	YKR025W	9.37	11
RPC82	YPR190C	18.135	14
RPO21	YDL140C	13.88	63
RPO26	YPR187W	1.45	4
RRP5	YMR229C	0.745	6
RSC1	YGR056W	1.775	6
RSC2	YLR357W	9.38	18
RSC58	YLR033W	1.17	6
RSC8	YFR037C	5.05	19
RVB1	YDR190C	2.8	5
SEF1	YBL066C	1.675	4
SHS1	YDL225W	208	43
SIN3	YOL004W	4.65	15
SIR3	YLR442C	2.81	26
SIR4	YDR227W	1.67	4
SIZ1	YDR409W	200.82	19
SKO1	YNL167C	16.095	6
SLK19	YOR195W	13.105	10
SMC1	YFL008W	0.125	32
SMC2	YFR031C	0.18	21
SMC3	YJL074C	0.11	36
SMC4	YLR086W	0.195	38
SMC5	YOL034W	0.24	43
SMC6	YLR383W	0.38	21
SPC24	YMR117C	23.015	4
SPP41	YDR464W	4.4	3
SPT15	YER148W	1.69	5
SPT5	YML010W	4.87	26

Table 3.9 Abundance of sumoylated proteins identified and quantified by comparing untreated *siz1*Δ *siz2*Δ (HZY2109) and *mms21-CH* (HZY2136) strains, continued

Gene	ORF	Median ratio (HZY2109/HZY2136)	# of peptides found
SPT7	YBR081C	15.88	31
STB3	YDR169C	48.06	15
STE12	YHR084W	1.995	4
STH1	YIL126W	3.17	3
STU1	YBL034C	23.27	26
SUB2	YDL084W	1.4	6
SUM1	YDR310C	22.895	22
SWI3	YJL176C	4.52	14
SWR1	YDR334W	3.95	5
TAF2	YCR042C	8.84	7
TAF3	YPL011C	30.3	3
TEC1	YBR083W	7.705	22
TFC4	YGR047C	7.57	4
TFC7	YOR110W	5.825	4
TFG1	YGR186W	17.33	16
TIF2|TIF1	YJL138C|YKR059W	1.38	16
TOA1	YOR194C	37.815	6
TOF2	YKR010C	0.4	15
TOP2	YNL088W	3.46	3
TUP1	YCR084C	10.03	45
TYE7	YOR344C	23.865	8
UBA2	YDR390C	0.77	34
UBC9	YDL064W	0.44	33
VHR1	YIL056W	18.01	11
VID21	YDR359C	4.57	5
VPS72	YDR485C	5.4	3
WTM1	YOR230W	17.44	7
YBR025C	YBR025C	1.62	3
YCG1	YDR325W	0.49	7
YCS4	YLR272C	2.27	17
YER064C	YER064C	21.34	13
YMR111C	YMR111C	37.615	16

CHAPTER 4

Monopolin stabilizes rDNA silencing complexes through direct recruitment of SUMO isopeptidase Ulp2

4.1 Summary

The integrity of ribosomal DNA (rDNA) repeats in the nucleolus is maintained by assembly of multiple protein complexes that inhibit aberrant recombination and promote gene silencing, but the regulation of these complexes has remained insufficiently understood. Here we describe a novel role of the SUMO isopeptidase Ulp2 in promoting rDNA silencing by stabilizing silencing complexes. Using progressive truncations of the poorly-characterized Ulp2 C-terminus, we identified a conserved region that directly interacts with the monopolin/cohibin complex protein Csm1. Using x-ray crystallography, we show that Csm1 binds Ulp2 in a structurally equivalent manner to its interaction with the monopolin complex subunit Mam1. Truncation of the Ulp2 C-terminus or mutation of its Csm1-binding region cause a defect in rDNA silencing and show elevated sumoylation of nucleolar Ulp2 substrates including Net1 and Tof2. We find that increased Tof2 sumoylation correlates with a marked reduction in its cellular abundance, and that this reduction depends on Slx5, a subunit of the SUMO-targeted ubiquitin ligase Slx5-Slx8. Moreover, mutation of the SUMO-interacting motif of Slx5 also rescues the abundance loss of Tof2 in Ulp2 mutants, suggesting that sumoylated Tof2 is ubiquitinated and targeted for degradation by Slx5-Slx8. Taken together, our findings demonstrate that Ulp2 is recruited to the nucleolus by Csm1 and ensures rDNA silencing by desumoylating, and thereby stabilizing, Tof2 and other critical rDNA silencing factors.

4.2 Introduction

Protein sumoylation regulates numerous nuclear processes including gene transcription, nuclear transport and DNA metabolism [40, 93]. Like ubiquitin, SUMO (Small Ubiquitin-like MOdifier) is attached to lysine residues of target proteins via an enzymatic cascade consisting of an E1-activating enzyme (Aos1-Uba2 in *Saccharomyces cerevisiae*), an E2-conjugating enzyme (Ubc9) and a number of SUMO E3 ligases [17-19, 60]. SUMO can also be cleaved off its target proteins by SUMO-specific isopeptidases, of which *S. cerevisiae* possesses two: Ulp1 and Ulp2 [44, 45]. Hundreds of proteins have been found to be sumoylated and their sumoylation is strongly affected by various environmental stimuli [52, 55]. Moreover, homeostasis of protein sumoylation in cells is controlled by multiple E3 ligases and isopeptidases in a substrate-specific manner [19, 60, 114]. Despite recent advances in understanding these pathways, the substrate specificity of the enzymes involved in reversible sumoylation, and in most cases the biological function of the SUMO modification itself, remains to be determined.

A major biological role for ubiquitin modification is the targeting of substrate proteins to the proteasome for degradation. While SUMO modification does not directly target proteins for degradation, the recent discovery of a family of SUMO-targeted ubiquitin ligases (STUbls) suggests that SUMO could promote target degradation indirectly through STUbl-dependent ubiquitination of sumoylated proteins [115]. Extensive genetic studies of an *S. cerevisiae*

STUbl comprising Slx5 and Slx8 have suggested that Slx5 has a prominent role in regulating the abundance of SUMOylated proteins [60, 116-119]. While one Slx5 substrate, Pli1 (ortholog of Siz1/PIAS in fission yeast), has been shown to undergo SUMO-dependent protein degradation [120], a general mechanism for Slx5 regulation of sumoylated protein abundance has remained unclear.

Recently, we used quantitative mass spectrometry (MS) to show that deletion of the SUMO isopeptidase Ulp2 results in a strong increase in sumoylation of several nucleolar proteins including Net1, Tof2 and the Cdc14 phosphatase [114]. These proteins are part of a complex called RENT (Regulator of Nucleolar silencing and Telophase exit) that regulates DNA replication, recombination, and silencing in the ribosomal DNA (rDNA) repeats that comprise the bulk of nucleolar chromatin [111, 121, 122]. The rDNA comprises ~200 copies of a 9.1 kb repeat that includes an origin of replication and genes coding for the 5S and 35S ribosomal RNAs (Figure 4.1B). A specialized locus in the non-transcribed region #1 (*NTS1*) binds the replication fork blocking protein Fob1, which in turn recruits Net1, Tof2, Cdc14, and the Sir2 histone deacetylase complex. Recently, the monopolin complex subunits Csm1 and Lrs4 (Csm1:Lrs4 is referred to as cohibin when localized to the nucleolus) have also been found to associate with the RENT complex [121, 123]. Together, this protein network mediates silencing of the rDNA loci and also suppresses illegitimate recombination between rDNA repeats [121, 123, 124].

Our prior finding that Ulp2 regulates the sumoylation of several RENT complex subunits suggested a direct role in the regulation of the rDNA repeats in the nucleolus. Ulp2 has recently been shown to interact with the Csm1:Lrs4 complex, suggesting a mechanism for direct recruitment of Ulp2 to the rDNA [125]. Here, we show that Ulp2 is involved in maintaining rDNA silencing, and that its recruitment to the nucleolus depends on a direct interaction with Csm1. Disruption of the Ulp2-Csm1 interaction causes an increase in SUMOylation, and a dramatic decrease in abundance, of the RENT subunit Tof2. Both the rDNA silencing defect and the decrease in Tof2 abundance are suppressed by deletion of Slx5, supporting a model in which SUMOylation of RENT subunits targets them for degradation by Slx5-mediated ubiquitination. Specific localization of the SUMO isopeptidase Ulp2 to RENT, through the Csm1:Lrs4 complex, is thus required to maintain RENT complex stability by deSUMOylating several of its critical structural components to inhibit their Slx5-dependent degradation.

4.3 Results

4.3.1 Ulp2 has a specific role in promoting rDNA silencing, mediated by its C-terminal domain

Our identification of several RENT complex subunits as substrates of Ulp2 [114] and a more recent finding that RENT complex subunits' rDNA

localization is defective in the *ulp2Δ* strain [126], prompted us to investigate whether Ulp2 functions with RENT in rDNA silencing. As shown in Figure 4.1A, the isopeptidase domain of Ulp2 is flanked by poorly-characterized N- and C-terminal regions. While the N-terminal region of Ulp2 contains nuclear localization signals [43], the only known features of its C-terminal region are several putative SUMO interacting motifs (SIMs) (Figure 4.1A). To gain a better understanding of the roles of Ulp2 C-terminus, we progressively truncated the protein at residues 707, 781 and 873, and examined effects on gene silencing at several chromosomal locations, including the *NTS1* and *NTS2* regions in the rDNA and at the *LEU2* locus (Figure 4.1B). We found that while loss of the histone deacetylase Sir2 disrupts rDNA silencing at both the *NTS1* and *NTS2* regions in the rDNA, the *ulp2Δ* mutation causes a specific defect in silencing at *NTS1* (Figure 4.1C). *NTS1*-specific loss of silencing is also observed in *fob1Δ*, *tof2Δ*, *csm1Δ*, and *lrs4Δ* mutants [121, 122], suggesting that Ulp2 may function with these proteins in the rDNA. When examining our *ULP2* truncation mutants we found that silencing at *NTS1* is unaffected by the *ulp2-873Δ* mutation, but is disrupted by both *ulp2-707Δ* and *ulp2-781Δ* mutations (Figure 4.1D). *ULP2* mutants had no effect on silencing at NTS2 (Figure 4.1C,E). These results suggest that the region between amino acids 781 and 873 of Ulp2 has a specific role in promoting silencing at *NTS1*, potentially by mediating an interaction with the RENT complex.

4.3.2 Ulp2$^{781-873}$ is required for desumoylation of Tof2 and for maintaining its abundance

We recently showed that loss of Ulp2 causes a dramatic accumulation of sumoylation of proteins associated with three distinct chromosomal regions, including the rDNA, the centromere, and origins of DNA replication [114]. To determine the role of the Ulp2 C-terminal domain in substrate targeting, we compared the relative abundance of sumoylated proteins in wild-type and *ulp2-781Δ* strains, using the quantitative MS approach described previously [60]. As shown in Figure 4.2A and Table 4.3, while most sumoylated proteins show a modest reduction in their levels of sumoylation in the *ulp2-781Δ* mutant, a subset of previously-identified Ulp2 substrates shows 2-4 fold elevation of sumoylation in this mutant. These substrates include Net1, Tof2 and Cdc14 in the nucleolus and Mcm21, Okp1 and Mcm22 in the kinetochore. In contrast, we observed no such accumulation in sumoylated MCM complex proteins in the *ulp2-781Δ* mutant, as previously observed in the *ulp2Δ* mutant. These findings suggest that the region of Ulp2 spanning residues 781-873 specifically mediates its ability to desumoylate nucleolar and centromeric substrates.

Considering the role of the Ulp2 C-terminus in rDNA silencing, we chose to analyze the nucleolar substrates of Ulp2 further. First, we purified total sumoylated proteins using the previously-described *HF-SUMO* strain (*HIS$_6$-3xFLAG-SMT3*; [60]) in strains containing HA-tagged *TOF2* and various mutations to *ULP2*. We first observed that the overall abundance of Tof2 is

reduced in the *ulp2Δ* and *ulp2-781Δ* mutants compared to wild-type cells (Figure 4.2B; “Input”). By purifying sumoylated proteins using Ni^{2+}-NTA and anti-FLAG chromatography, we further found that loss of Ulp2 causes a drastic accumulation of higher molecular weight and poly-sumoylated Tof2 (Figure 4.2B; “Ni^{2+}/αFLAG Elution”). The *ulp2-781Δ* mutation causes a similar accumulation of poly-sumoylated Tof2, albeit less dramatic than in *ulp2Δ*. These findings are in agreement with the MS finding confirming that the C-terminal region of Ulp2 contributes to the ability of Ulp2 to desumoylate Tof2. We have previously shown that loss of Ulp2 also causes a drastic accumulation of poly-sumoylated Net1; however, unlike Tof2, there is no detectable change to Net1 abundance upon the loss of Ulp2 (Figure 4.2 [114]).

4.3.3 Ulp2 residues 781-873 bind to Csm1 in a Mam1-like manner

A prior mass spectrometry-based examination of protein-protein interactions in the *S. cerevisiae* SUMO system identified an association between Ulp2 and the Csm1:Lrs4 complex [125]. We therefore tested whether deletion of *CSM1* would affect the sumoylation and abundance of Tof2. Similar to the *ulp2Δ* and *ulp2-781Δ* mutations, the *csm1Δ* mutant causes an increase in Tof2 poly-sumoylation and a reduction in its abundance (Figure 4.2D). This suggests that the role of Ulp2 residues 781-873 may mediate a direct interaction with Csm1, thereby recruiting Ulp2 to the rDNA to desumoylate RENT complex subunits. To test for such an interaction, we purified GST-$Ulp2^{781-873}$ and tested its ability to bind Csm1 using a GST pull-down assay. While GST alone failed to

interact with Csm1, GST-Ulp2$^{781-873}$ robustly bound both full-length Csm1 and its globular C-terminal domain (residues 69-181) (Figure 4.7C) [124]. Using isothermal titration calorimetry, we found that Ulp2$^{781-873}$ binds Csm1$^{69-190}$ with a K_d of 0.9 μM and a stoichiometry of ~1 Ulp2 per Csm1 chain (Figure 4.7E). Ulp2 binding is not disrupted by mutations in a conserved hydrophobic surface (Figure 4.7A,B) of Csm1 (Figure 4.7D) that we previously showed mediates interactions with the kinetochore protein Dsn1 and rDNA regulator Tof2 [124], indicating that a separate surface of Csm1 likely mediates Ulp2 binding. We next co-expressed Ulp2$^{781-873}$ with Csm1$^{69-181}$, and found that they form a stable 2:2 complex (Figure 4.8B). We progressively truncated Ulp2 based on sequence conservation, finally identifying a minimal Csm1-interacting region comprising Ulp2 residues 821-847 (Figure 4.8A).

We identified conditions for crystallization of the Ulp2$^{821-847}$:Csm1$^{69-181}$ complex, and determined its structure to a resolution of 2.15 Å (Table 4.1). In agreement with our isothermal titration calorimetry findings, the structure shows a Csm1 dimer bound to two copies of Ulp2, each of which wrap around one side of the Csm1 dimer (Figure 4.3A, 4.8C). Ulp2 buries several conserved hydrophobic residues against Csm1, including Y826 and F827, which insert into a pocket on Csm1 lined with hydrophobic residues, and L832, F839, and V842 (Figure 4.3B). Additionally, Ulp2 R835 forms a salt bridge with Csm1 residue D117. As expected from our binding assays, Ulp2 does not interact with the conserved hydrophobic surface on Csm1 that mediates its interaction with Tof2.

To validate our structural findings, we performed GST pulldown assays with GST-Ulp2$^{781-873}$ containing mutations in key hydrophobic residues that interact with Csm1: F827, L832, and F839. While mutation of L832 had no detectable effect, mutation of either F827 or F839 to a negatively-charged residue (aspartate) completely disrupted Ulp2 binding to Csm1 (Figure 4.3C). Single mutations of these residues to alanine had a more subtle effect, but mutation of both phenylalanine residues to alanine (2A mutant; F827A/F839A) also completely disrupts binding (Figure 4.3D). By isothermal titration calorimetry, we found that the Ulp2 F839D mutant caused a 20-fold weakening of the binding affinity of Ulp2$^{781-873}$ for Csm1$^{69-190}$ (18.3 μM versus 0.9 μM; Figure 4.7E).

Strikingly, the structure of Ulp2$^{821-847}$:Csm1$^{69-181}$ closely resembles our previous structure of Csm1 bound to the monopolin complex subunit Mam1 (Figure 4.3E,F) [127]. While Mam1 forms a more extensive interface with Csm1 that includes a short C-terminal α-helix packing against the Csm1 β-sheet, the bulk of Mam1's interface with Csm1 overlays closely with that of Ulp2. Each conserved residue in Ulp2 that interacts with Csm1 has an analog in Mam1, including all of the buried hydrophobic residues plus the arginine residue (Ulp2 R835, Mam1 R234) making a salt-bridge with Csm1 D117 (Figure 4.3E). When combined with our data indicating that Tof2 and the kinetochore protein Dsn1 interact with the same conserved hydrophobic surface on Csm1 ([127] and below), a picture emerges wherein Csm1 uses a common set of protein-protein

interfaces to nucleates assembly of functionally-divergent protein complexes at the kinetochore and in the rDNA repeats.

To verify the biological significance of the Ulp2-Csm1 interface we identified, we next tested the effect of the Ulp2 residues F827 and F839 on Tof2 abundance and sumoylation, and on rDNA silencing at NTS1. While neither *ulp2-F827D* nor *ulp2-F839D* has a strong effect on Tof2 abundance compared to *ulp2-781Δ*, both mutations caused a marked increase in Tof2 sumoylation (Figure 4.4A). This effect was more pronounced in the *ulp2-F839D* mutant than the *ulp2-F827D* mutant. Additionally, mutation to both F827 and F839 to alanine also increased Tof2 sumoylation while only having a small effect on Tof2 abundance (Figure 4.4B). In keeping with these results, we found that both *ulp2-F839D* and *ulp2-2A* mutants have a silencing defect at NTS1, but not the *ulp2-F827D* mutant (Figure 4.4C). These results confirm that Ulp2 binds Csm1 to localize to rDNA and desumoylate and stabilize the RENT complex, and show that Ulp2 F839 plays a more prominent role in in Csm1 binding than F827.

4.3.4 Slx5 and its SUMO-interacting motif are required for the reduction of Tof2 abundance

Our finding that increased Tof2 sumoylation is accompanied by a marked loss in protein abundance raised the possibility that Tof2 sumoylation may act as a signal to induce its degradation via a SUMO-tageted ubiquitin ligase (STUbl) (Figure 4.5). Slx5 is the founding member of the STUbl family in *S. cerevisiae [115]*, so we next tested whether Slx5 plays a role in regulating Tof2

sumoylation and abundance. We first examined Tof2 abundance in *ulp2Δ*, *slx5Δ*, and *ulp2Δ slx5Δ* double mutant. While *slx5Δ* mutant alone has little to no effect on Tof2 sumoylation or abundance, it strongly suppresses the loss of Tof2 abundance and decreased its sumoylation in *ulp2Δ* cells (Figure 4.5A). The same effect was also observed in *ulp2-781Δ slx5Δ* double mutants (Figure 4.5B). We next tested more specifically the role of the Slx5 SUMO-interacting motifs, which recognize SUMO-conjugated substrates [51]. We found that a *slx5-sim* mutant, with these motifs disrupted, strongly suppresses the loss of Tof2 abundance seen in the *ulp2-781Δ* mutant, indicating that specific recognition of sumoylated Tof2 by Slx5 is required for its loss of abundance (Figure 4.5E). These results stongly support a model in which Slx5-Slx8 recognizes and ubiqutinates sumoylated Tof2, targeting the protein for degradation. Finally, we examined the effect of *slx5Δ* on rDNA silencing. While the *slx5Δ* mutant did not have an effect on silencing at NTS1, it did rescue the silencing defect of a *ulp2-F839D* mutant Figure 4.5C,D).

4.4 Discussion

Protein sumoylation is a critically-important post-translational modification for a wide range of cellular pathways, but how specific substrate proteins' sumoylation is regulated in both space and time is still poorly understood. *S. cerevisiae* Ulp1 and Ulp2 are the two founding members of the SUMO isopeptidase family whose orthologues are found in higher eukaryotes

[128]. We previously showed that Ulp1 and Ulp2 have distinct specificities, with Ulp1 responsible for the bulk of desumoylation in the cell and Ulp2 showing a strong bias towards desumoylation of substrates associated with several regions of the chromosome [114]. Here, we identify a new mechanism for regulating Ulp2 substrate specificity, through direct localization to the rDNA-associated RENT silencing complex. A direct interaction between Ulp2 and the monopolin complex subunit Csm1 targets Ulp2 activity to Tof2 and RENT complex subunits, stabilizes Tof2 by suppressing Slx5-Slx8-mediated degradation, and is required for robust rDNA silencing. While binding of Ulp2 to Csm1 is required for its activity on both nucleolar and kinetochore-associated substrates (see below), it is not required for activity on other substrates including the MCM proteins. This suggests that Csm1 binding is only one of several means by which Ulp2 activity is regulated.

The Csm1:Lrs4 complex has long been known to lead a double life, mediating rDNA silencing during interphase as part of the RENT complex, and re-localizing to kinetochores in both meiotic prophase and mitotic anaphase. Our structural and biochemical data show that Csm1 nucleates functionally-diverse complexes in these different contexts using a common set of protein-protein interfaces. Ulp2 and the monopolin complex subunit Mam1 bind Csm1 in a strikingly similar manner, and Tof2 likely binds Csm1 equivalently to the kinetochore protein Dsn1. In multiple structures of Csm1 bound to different proteins, we have observed the conserved Dsn1/Tof2 binding hydrophobic

surface interacting with phenylalanine residues [124], Figure 4.7B). While our structures now show that Mam1 and Ulp2 share sequence features in their Csm1-binding regions, there is no clear similarity between the Csm1-binding regions of Tof2/Net1 and Dsn1. Further work will be required to determine if these proteins bind Csm1 in a structurally similar manner.

While Csm1:Lrs4 nucleates distinct complexes at rDNA and meiotic kinetochores, the complex also localizes to kinetochores in mitotic anaphase where it contributes to the fidelity of chromosome segregation in an unknown manner. Our data showing an increase in sumoylation of the inner-kinetochore proteins Mcm21, Okp1, and Mcm22 in mutants where Ulp2-Csm1 binding is disrupted suggests that Csm1 may recruit Ulp2 to kinetochores in mitotic cells. Additionally, we cannot fully discount the possibility that a subset of monopolin complexes also recruit Ulp2 to kinetochores in meiotic prophase. How Ulp2 localization and desumoylation of kinetochore proteins might contribute to chromosome segregation fidelity, in both mitosis and meiosis, will be an intriguing avenue for future research.

4.5 Materials & Methods

4.5.1 Protein Expression and Purification

Ulp2 C-terminal domain, Ulp2$^{781-873}$, was cloned into a pET3a-derived vector containing an N-terminal His$_6$-GST tag and expressed in *E. coli* Rosetta

2 DE3 pLysS cells (EMD Millipore). Ulp2 point-mutations were cloned by PCR mutagenesis. The recombinant Ulp2 C-terminal domain (full-length and point-mutants) was purified using glutathione affinity sepharose resin (GE Healthcare Life Sciences) followed by cation-exchange (HiTrap SP HP, GE Healthcare Life Sciences) chromatography before pooling fractions and concentrating. We expressed Csm1 as previously described [124]. Briefly, we cloned full-length *S. cerevisiae* Csm1 (or the 69-190 or 69-181 truncations) into a pET3a-derived vector containing an N-terminal His_6-tag, expressed the protein in *E. coli* Rosetta2 DE3 pLysS cells (EMD Millipore) at 20°C for 16 hours in 2XYT media by induction with 0.25 mM IPTG. We purified Csm1 using Ni^{2+} affinity (Qiagen Ni-NTA Superflow) anion-exchange (HiTrap Q HP, GE Life Sciences), and size-exclusion (Superdex 200, GE Life Sciences) chromatography, then concentrated the protein and snap-froze aliquots for biochemical assays. For Ulp2:Csm1 complexes, we generated a coexpression vector with Ulp2 fragments fused to a TEV protease-cleavable N-terminal His_6-SUMO-tag and untagged $Csm1^{69-181}$ (for crystallography) or $Csm1^{69-190}$ (for Tof2 binding assays). We purified the complexes with Ni^{2+} affinity chromatography, followed by tag cleavage with TEV protease, removal of tags and uncleaved protein with Ni^{2+} resin, then passed over a Superdex 200 size-exclusion column in a final buffer of 20mM Tris-HCl pH 7.5, 300mM NaCl. The protein was concentrated and stored at 4°C for crystal trays.

4.5.2 Binding Assays

To analyze the interaction between Ulp2 and Csm1 by pulldown, either GST-Ulp2$^{781-873}$ or GST alone was incubated with 10 µg of bait protein (His_6-Csm1 or His_6-Csm$^{69-181}$) in 40µL binding buffer (20mM HEPES pH 7.5, 300mM NaCl, 5% glycerol, 1mM DTT, 0.1% NP-40) for 90 minutes at 4°C. Ten percent of the purification was removed to be analyzed as Input and the remaining fraction bound to glutathione sepharose beads for 2 hours at 4°C. The beads were washed 3 times with 0.5mL binding buffer and eluted with 25 µL elution buffer (25 mM glutathione in 2x LDS sample buffer) and boiled. The eluted proteins were analyzed by SDS-PAGE and visualized by Coomassie staining.

4.5.3 Gene silencing assay

Yeast strains were grown and normalized to an equal density and serial diluted 10-fold to plate on CSM complete and CSM-URA plates. Plates were incubated at 30°C for at least 3 days before imaging.

4.5.4 Quantitative mass spectrometry analysis of intracellular sumoylation

Quantitative MS analysis used to measure changes in sumoylated protein abundance between two strains was previously described [60]. Each mutant strain was grown in synthetic media containing either light or heavy stable isotope-labeled lysine and arginine. Cell pellets of the two yeast strains to be compared were combined and used to purify sumoylated proteins under

denaturing conditions for quantitative MS analysis. MS data was searched using SEQUEST on a Sorcerer 2 (Sage-N) system and quantified using XPRESS (Trans-Proteomic Pipeline v4.3). A complete list of sumoylated proteins and their abundance changes are shown in Table 4.3. Each sumoylated protein was quantified based on the median of the abundance ratios of at least three unique peptides per protein.

4.5.5 Crystallography

We obtained crystals of Ulp2$^{821-847}$:Csm1$^{69-181}$ by mixing protein (15 mg/mL) 1:1 in a crystallization buffer containing 100 mM M HEPES pH 7.5 and 20% PEG 3350. We added 25% glycerol for cryoprotection, then flash-froze crystals in liquid nitrogen and collected diffraction data on beamline 14-1 at the Stanford Synchrotron Radiation Lightsource (support statement below). We processed all datasets with the SSRL autoxds script, which uses XDS [129] for data indexing and reduction), AIMLESS [130] for scaling and TRUNCATE [131] for conversion to structure factors. We determined the structure by molecular replacement in PHASER [132] using a previous structure of Csm1 (PDB ID 3N4S) [124]. We manually built Ulp2 residues 821-845 into difference density maps in COOT [133], guided by the structure of Mam1$^{221-290}$:Csm1 (PDB ID 4EMC). We refined the model in phenix.refine [134] using positional, individual B-factor, and TLS refinement. The final model is of high quality, judged by refinement statistics and model geometry (Table 4.1).

SSRL Synchrotron support statement: Use of the Stanford Synchrotron Radiation Lightsource, SLAC National Accelerator Laboratory, is supported by the U.S. Department of Energy, Office of Science, Office of Basic Energy Sciences under Contract No. DE-AC02-76SF00515. The SSRL Structural Molecular Biology Program is supported by the DOE Office of Biological and Environmental Research, and by the National Institutes of Health, National Institute of General Medical Sciences (including P41GM103393). The contents of this publication are solely the responsibility of the authors and do not necessarily represent the official views of NIGMS or NIH.

4.6 Acknowledgements

The authors thank the staff of beamline 14-1 at the Stanford Synchrotron Radiation Laboratory for assistance with data collection (see Materials and Methods for SSRL support statement), A. Bobkov for assistance with isothermal titration calorimetry, and members of the Zhou and Corbett laboratories for helpful discussions and comments. This work was supported by the Ludwig Institute for Cancer Research (to HZ and KDC), NCI training grant T32 CA009523 (to JL), and National Institutes of Health (R01-GM116897 to HZ, R01-GM104141 to KDC).

Chapter 4, in part is in preparation for publication of the material and will appear as Monopolin stabilizes rDNA silencing complexes through direct

recruitment of the SUMO isopeptidase Ulp2. Liang J, Singh N, Carlson CR, Albuquerque CP, Corbett KD, Zhou H. The dissertation author is primary co-author for this paper.

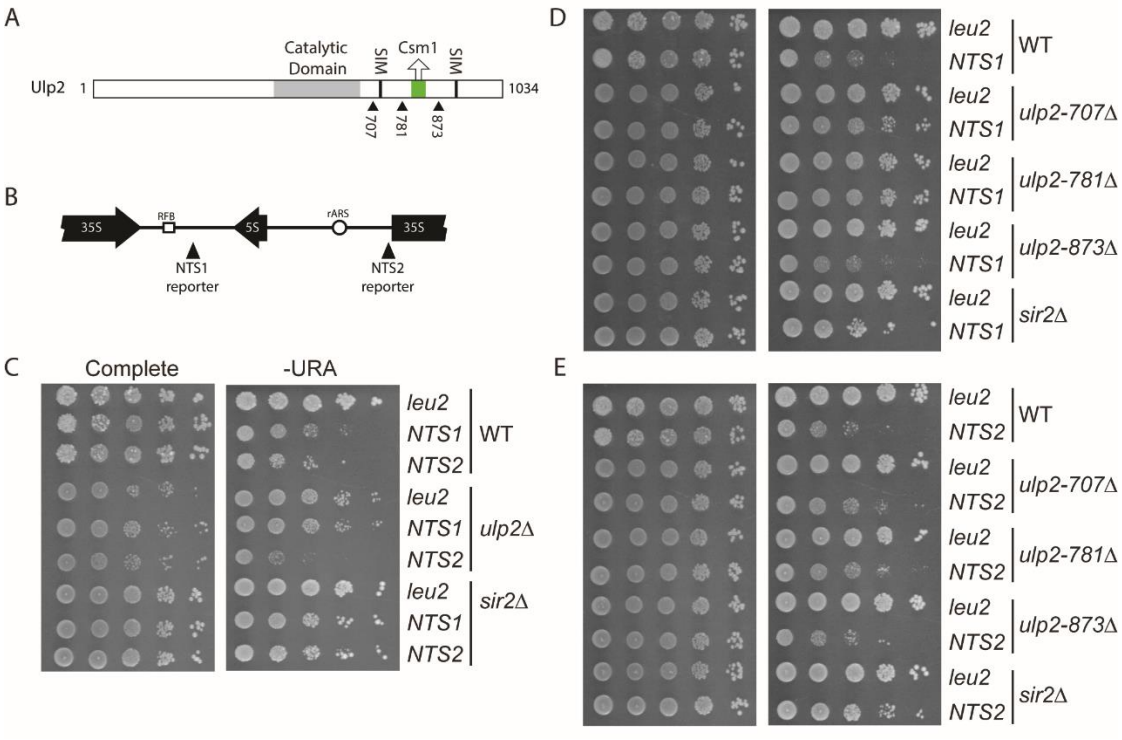

Figure 4.1 Ulp2 C-terminal domain is required for silencing in the rDNA region

A) Domain map of Ulp2, showing the catalytic domain (residues 456-674), two predicted SUMO-interacting motifs (SIMs; 725-728 IQII; 931-934 VNLI), and the locations of three truncations at residues 707, 781 and 873. Shown in red is the minimal region for Csm1 binding (residues 821-847). B) Schematic of a single rDNA repeat in *S. cerevisiae*. The locations of the 35S and 5S rRNA genes, the replication fork block sequence (RFB), and the origin of replication (rARS) are shown. Insertion sites for the mURA3 reporter gene in non-transcribed sequences (NTS) 1 and 2 are indicated. C) Effect on rDNA silencing of the *ulp2*Δ and sir2Δ mutations. (D and E) Effect of *ulp2* C-terminal truncations on rDNA silencing at NTS1 D) and NTS2 E).

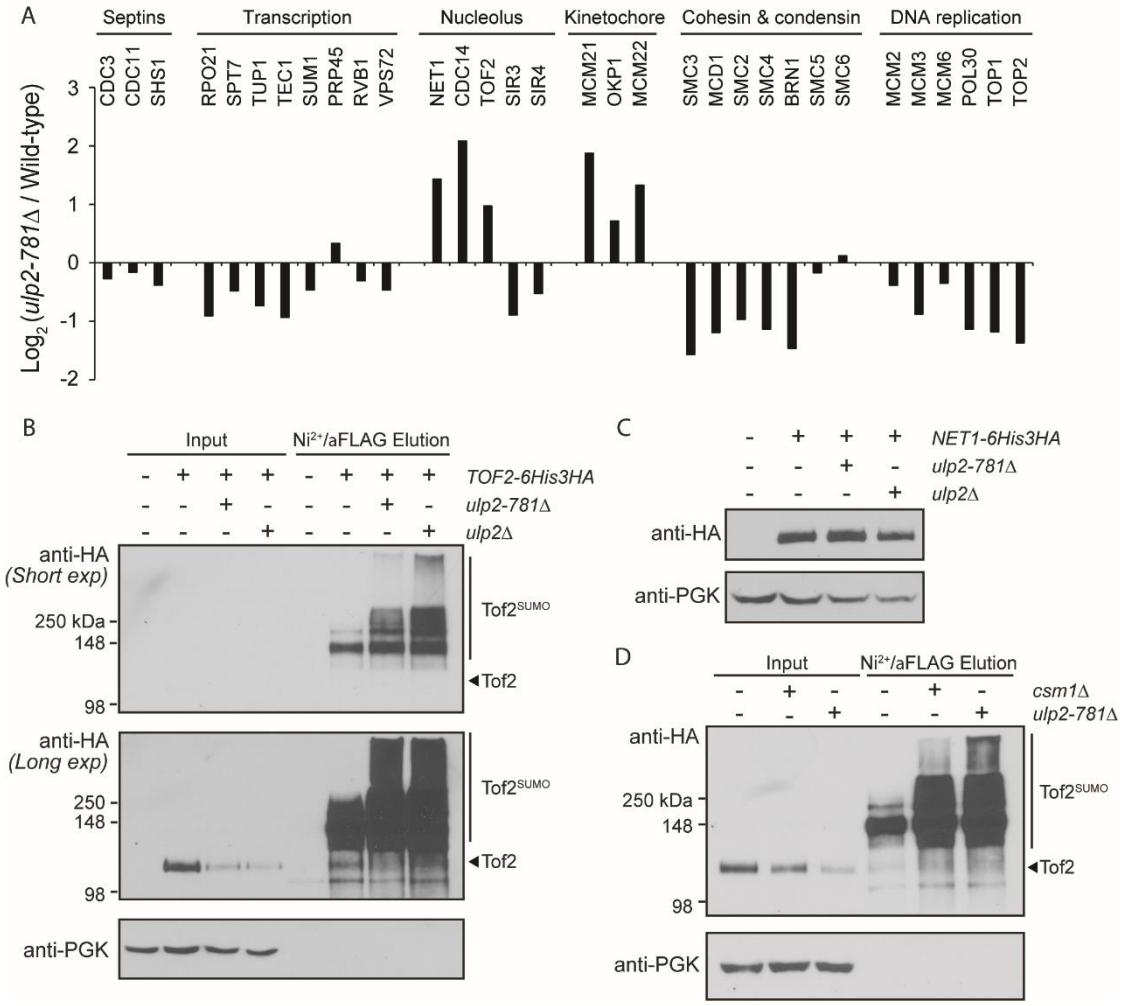

Figure 4.2 The Ulp2 C-terminal domain and Csm1 contribute to Tof2 desumoylation and prevent its abundance loss

A) Quantitative mass spectrometry analysis of *ulp2-781*Δ vs WT reveals a role of Ulp2 C-terminal domain in facilitating desumoylation of a subset of nucleolar and kinetochore proteins. B) The ulp2Δ and *ulp2-781*Δ mutants both cause decreased abundance and increased sumoylation of Tof2. C) Western blot showing that Net1 protein abundance is not affected by the ulp2Δ and *ulp2-781*Δ mutants. D) Western blot showing that the *csm1*Δ and *ulp2-781*Δ mutants have similar effects on Tof2 sumoylation and abundance.

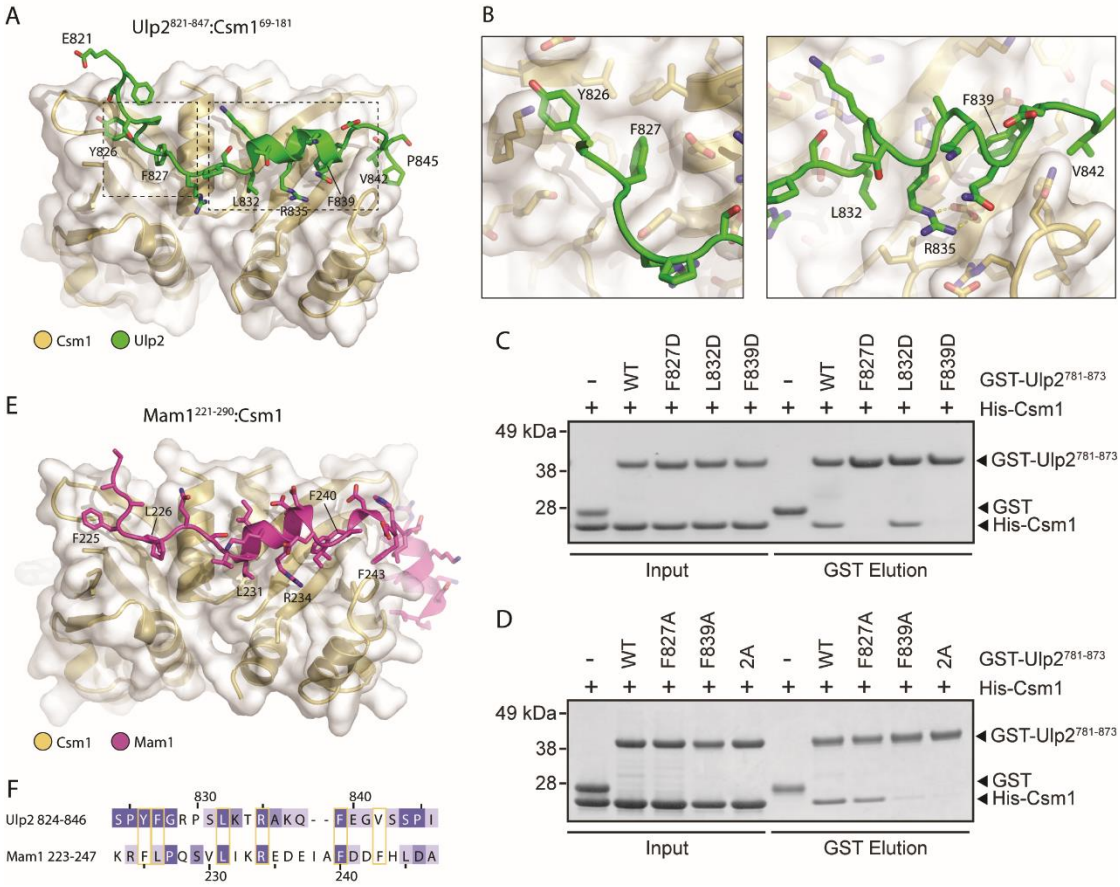

Figure 4.3 Structural basis for Ulp2 binding to Csm1

A) Structure of Ulp2$^{821-847}$ (green) bound to Csm1$^{69-181}$ (yellow, white surface). Biochemical characterization of this complex, and additional views of the structure, in Figure 4.8C-F. B) Detail views of Ulp2 binding to Csm1 (locations indicated by dotted boxes in panel A). C) and D) GST pulldown assays showing effects of mutating Ulp2 residues F827, L832, and F839 on its interaction with Csm1. See Figure 4.7E for isothermal titration calorimetry measurements of Ulp2$^{781-873}$ (WT and F839D) binding Csm1$^{69-190}$. D) Structure of Mam1$^{221-290}$ (magenta) bound to Csm1$^{69-181}$ (yellow, white surface). View is equivalent to panel (A). Shown is a rebuilt version of our original Csm1:Mam1 structure (PDB ID 5KTB), with a register error fixed (see Materials & Methods). E) Structure-based sequence alignment of Ulp2 and Mam1, with equivalent Csm1-binding residues boxed in yellow.

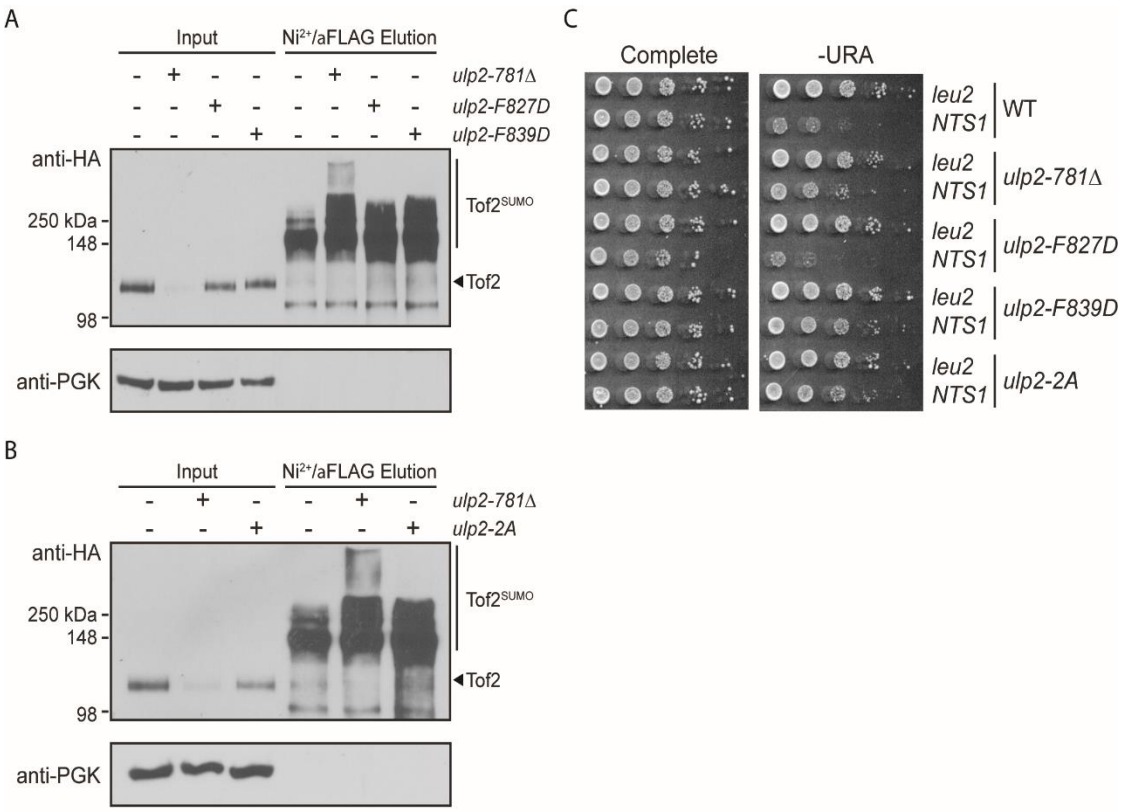

Figure 4.4 Ulp2-Csm1 binding is required for rDNA silencing and maintenance of Tof2 sumoylation

A-B) Western blot of Tof2 after purifying for sumoylated protein in *ulp2* mutants: *ulp2-781Δ, ulp-F827D, ulp2-F839D,* and *ulp2-2A(F827,839A)*. C) Effect of *ulp2* mutants, defective in Csm1 binding, on rDNA silencing at NTS1.

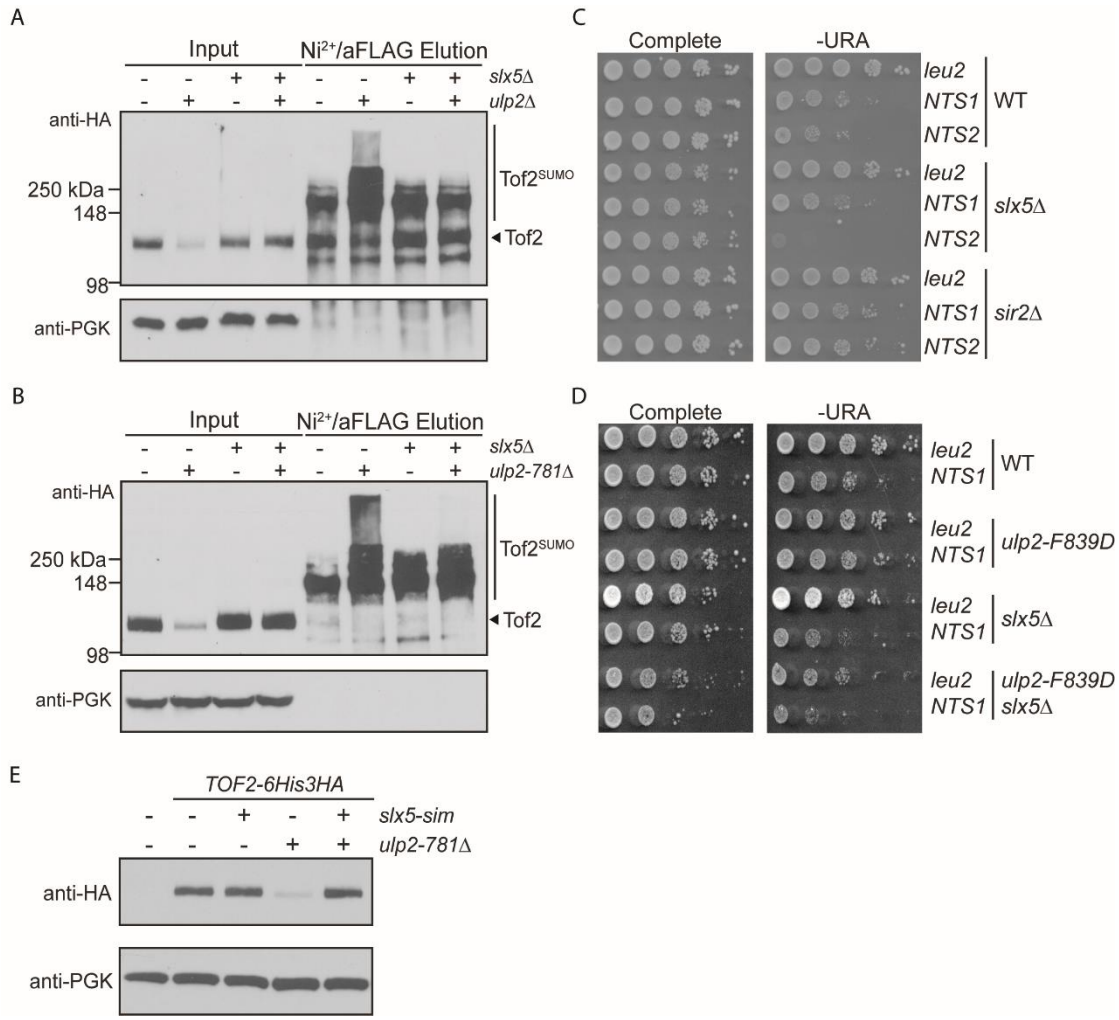

Figure 4.5 Roles of Slx5 in rDNA silencing and the control of Tof2 abundance

A-B) Western blot of Tof2 after purifying for sumoylated protein in *slx5* and *ulp2* mutants show a rescue in protein abundance. C-D) Effect of *slx5*Δ on rDNA silencing at NTS1 in *ulp2* mutants. E) Western blot of Tof2 show that *slx5-sim* mutation rescues the loss of Tof2 protein abundance in the *ulp2-781*Δ mutant strain.

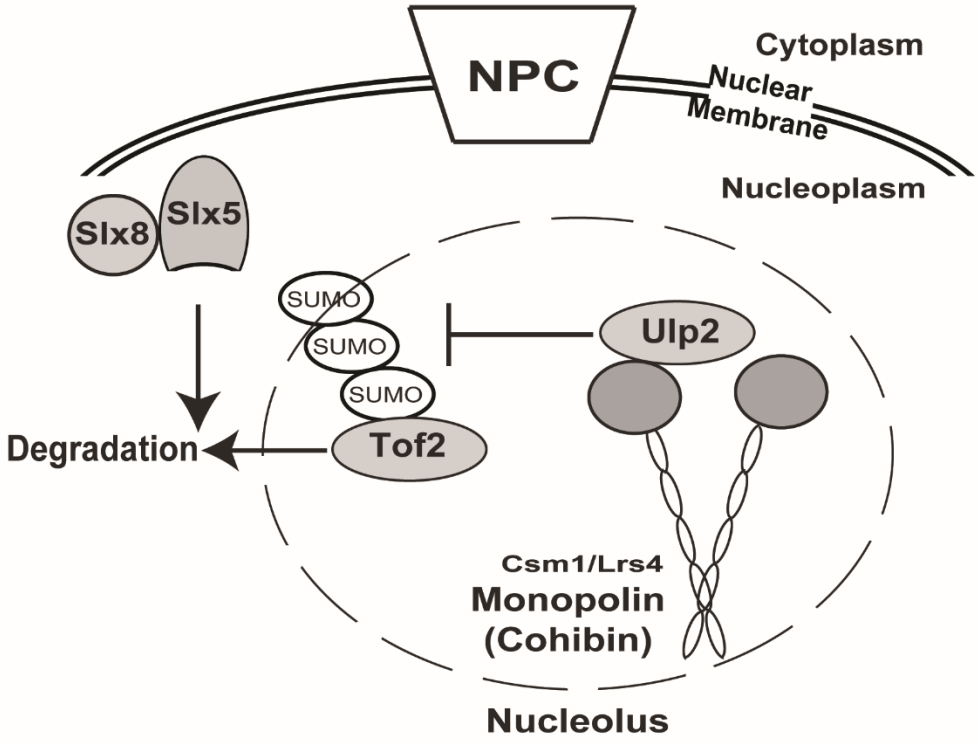

Figure 4.6 Control of rDNA silencing complexes by SUMOylation/deSUMOylation

Illustration depicting Ulp2 localization to the nucleolus through Csm1 interaction. Ulp2 regulates Tof2 sumoylation at the rDNA to prevent Slx5-Slx8 ubiquitin-mediated degradation.

Figure 4.7 Monopolin complex structure and Ulp2 binding

A) Overall structure of the Csm1:Lrs4 monopolin/cohibin subcomplex (Corbett Cell 2010). The complex comprises two dimers of Csm1 (four copies in total) and two copies of Lrs4. B) Detail views of the Csm1 globular C-terminal domain. The two subunits of the dimer are shown in yellow and gray, respectively. The top view is equivalent to the views in Figure 3A and E. Shown in sticks are the four residues in the conserved hydropobic surface that are implicated in Dsn1 and Tof2 binding (Corbett Cell 2010). C) GST pulldown assay showing a direct interaction between Csm1 (full-length or isolated C-terminal domain residues 69-181) and GST-Ulp2$^{781-873}$. The Ulp2-Csm1 interaction is not affected by mutations to the conserved hydrophobic surface on Csm1 that has been implicated in binding Dsn1 and Tof2 (**Figure S3**) [124]. D) GST pulldown assay showing that mutation of the Csm1 conserved hydrophobic surface does not disrupt binding of Ulp2. E) Isothermal titration calorimetry showing binding between Csm1$^{69-190}$ and Ulp2$^{781-873}$, wild-type versus Ulp2 F839D mutant.

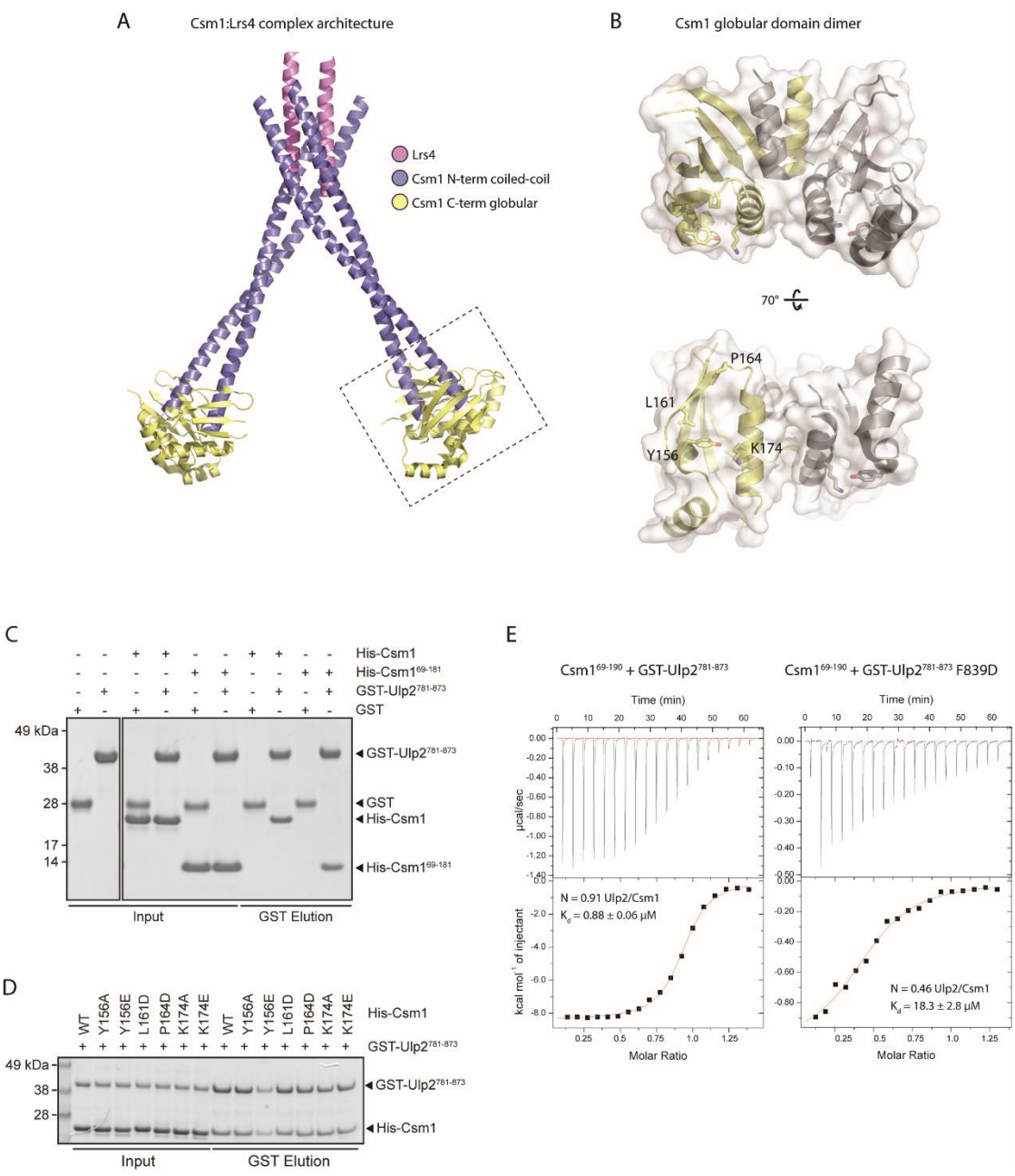
A
Csm1:Lrs4 complex architecture
Lrs4
Csm1 N-term coiled-coil
Csm1 C-term globular
B
Csm1 globular domain dimer
70°
P164
L161
Y156
K174
C
His-Csm1
His-Csm1 69-181
GST-Ulp2 781-873
GST
49 kDa
38
28
17
14
GST-Ulp2 781-873
GST
His-Csm1
His-Csm1 69-181
Input
GST Elution
D
WT
Y156A
Y156E
L161D
P164D
K174A
K174E
His-Csm1
GST-Ulp2 781-873
49 kDa
38
28
Input
GST Elution
E
Csm1 69-190 + GST-Ulp2 781-873
Csm1 69-190 + GST-Ulp2 781-873 F839D
Time (min)
µcal/sec
kcal mol-1 of injectant
N = 0.91 Ulp2/Csm1
Kd = 0.88 ± 0.06 µM
N = 0.46 Ulp2/Csm1
Kd = 18.3 ± 2.8 µM
Molar Ratio

Figure 4.8 Biochemical and structural characterization of the Ulp2:Csm1 complex and crystal packing interactions

(A) Ni^{2+} pulldowns from co-expression tests of His_6-SUMO-Ulp2 fragments with untagged $Csm1^{69-181}$. Lanes are marked “S” (soluble fraction after cell lysis) and “B” (bound to Ni^{2+} resin). All four tested fragments efficiently bind and pull down untagged $Csm1^{69-181}$. (B) Size exclusion chromatography/multi-angle light scattering (SEC-MALS) analysis of the $Ulp2^{781-873}$:$Csm1^{69-181}$ complex. Elution volumes of 158 and 44 kDa standards are shown at top. Calculated molecular weight is shown in red, and agrees closely with a 2:2 stoichiometry for the complex. (C) Two views of crystal packing interactions in the $Ulp2^{821-847}$:$Csm1^{69-181}$ structure. The asymmetric unit comprises one chain each of Csm1 and Ulp2 (orange/green), with a two-fold rotation axis generating the full 2:2 complex (gray/cyan; left panel). In addition, the N-terminus of the Ulp2 fragment (residues ~821-825) contact the conserved hydrophobic patch of a third symmetry-related Csm1 (yellow; right panel). (D) Detail of Ulp2 residues 821-825 interacting with the Csm1 conserved hydrophobic patch. This interaction, anchored by the poorly-conserved Ulp2 residue Phe822, is structurally similar to a crystal packing interaction observed in the Csm1:Mam1 structure [127]. (E) Overall view of the $Ulp2^{821-847}$:$Csm1^{69-181}$ complex structure, without (top) and with (bottom) refined $2F_o$-F_c electron density, contoured at 1.0 I/σ for Ulp2. (F) Stereo detail view of (E).

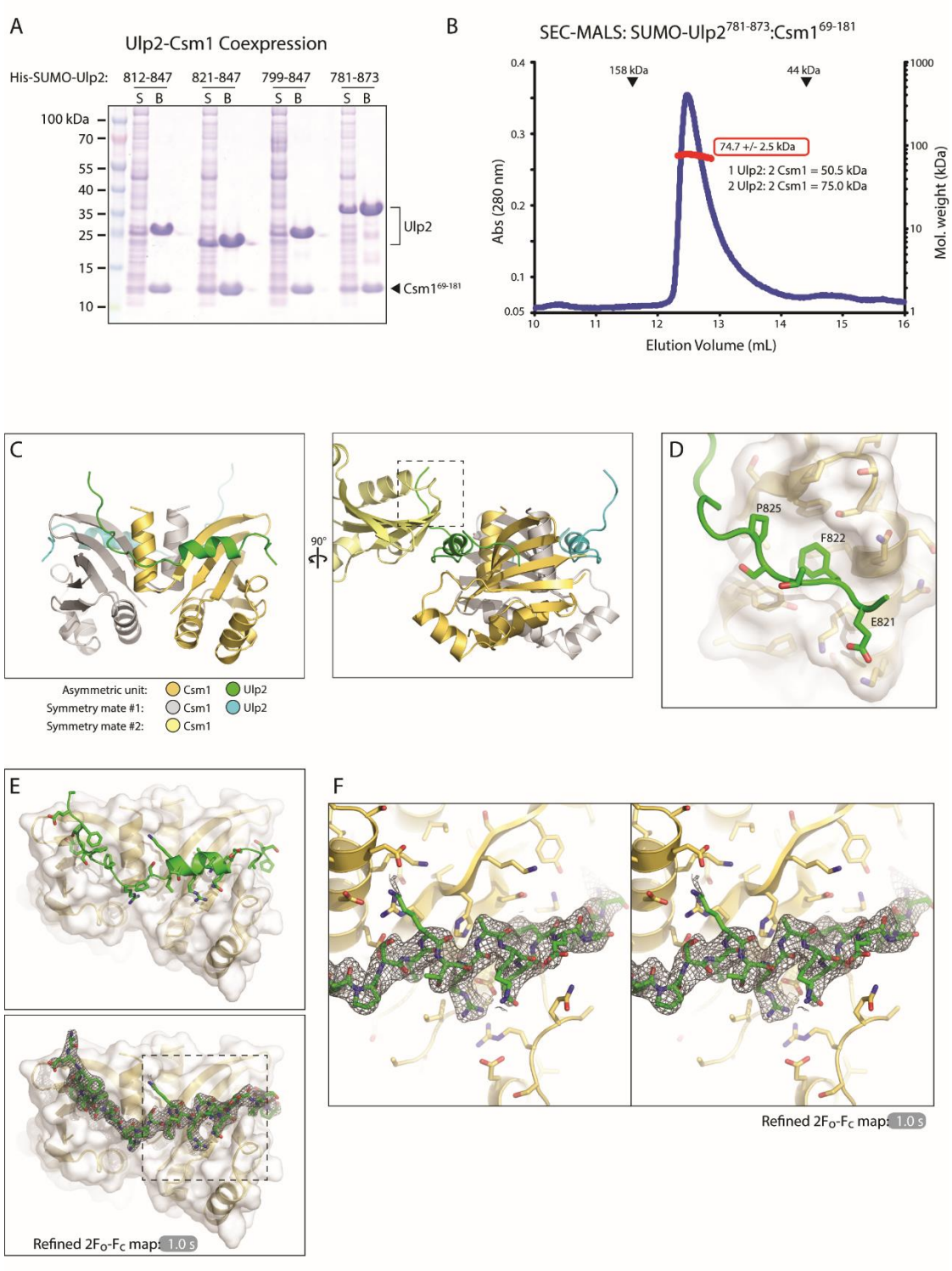
A
Ulp2-Csm1 Coexpression
His-SUMO-Ulp2:
812-847
821-847
799-847
781-873
S B
100 kDa
70
55
40
35
25
15
10
Ulp2
Csm1 69-181
B
SEC-MALS: SUMO-Ulp2 781-873 :Csm1 69-181
158 kDa
44 kDa
74.7 +/- 2.5 kDa
1 Ulp2: 2 Csm1 = 50.5 kDa
2 Ulp2: 2 Csm1 = 75.0 kDa
Abs (280 nm)
Mol. weight (kDa)
Elution Volume (mL)
C
90°
Asymmetric unit: Csm1 Ulp2
Symmetry mate #1: Csm1 Ulp2
Symmetry mate #2: Csm1
D
P825
F822
E821
E
Refined 2Fo-Fc map: 1.0 s
F
Refined 2Fo-Fc map: 1.0 s

Table 4.1 Data collection and refinement statistics

Data collection	***Sc* Csm1:Ulp2**
Resolution (Å)	44.0 – 2.14
Wavelength (Å)	1.1808 Å
Space Group	$P4_32_12$
Unit Cell Dimensions (a, b, c) Å	46.74, 46.74, 124.64
Unit cell Angles (α,β,γ) °	90, 90, 90
I/σ (last shell)	53.9 (2.0)
[1]R_{sym} (last shell)	0.053 (1.318)
[2]R_{meas} (last shell)	0.055 (1.369)
[3]$CC_{1/2}$ (last shell)	0.699
Completeness (last shell) %	98.7 (98.2)
Number of reflections	111900
unique	8129
Multiplicity (last shell)	13.8 (13.4)
Refinement	
Resolution (Å)	44.0 – 2.14
No. of reflections	8102
working	7292
free	810
[4]R_{work} (last shell) (%)	23.45 (31.46)
[4]R_{free} (last shell) (%)	27.82 (34.49)
Structure/Stereochemistry	
No. of atoms	1019
solvent	20
r.m.s.d. bond lengths (Å)	0.003
r.m.s.d. bond angles (°)	0.565
[5]SBGrid Data Bank ID	327
[6]Protein Data Bank ID	TBD

[1]$R_{sym} = \sum\sum_j|I_j - \langle I\rangle|/\sum I_j$, where I_j is the intensity measurement for reflection j and $\langle I\rangle$ is the mean intensity for multiply recorded reflections.

[2]$R_{meas} = \sum_h [\sqrt{(n/(n-1))}\sum_j [I_{hj} - \langle I_h\rangle] / \sum_{hj}\langle I_h\rangle$

where I_{hj} is a single intensity measurement for reflection h, $\langle I_h\rangle$ is the average intensity measurement for multiply recorded reflections, and n is the number of observations of reflection h.

[3]$CC_{1/2}$ is the Pearson correlation coefficient between the average measured intensities of two randomly-assigned half-sets of the measurements of each unique reflection (Karplus & Diederichs (2012) *Science* **336**:1030-1033). $CC_{1/2}$ is considered significant above a value of ~0.15.

[4]$R_{work,\ free} = \sum||F_{obs}| - |F_{calc}||/|F_{obs}|$, where the working and free *R*-factors are calculated using the working and free reflection sets, respectively.

[5]Diffraction data for each structure have been deposited with the SBGrid Data Bank (https://data.sbgrid.org) with the noted accession codes.

[6]Coordinates and structure factors for each structure have been deposited with the Protein Data Bank (http://www.pdb.org) with the noted accession codes.

Table 4.2 Yeast strains used in Chapter 4

All strains are derivatives of W303 and share the same markers as A2587 unless otherwise noted. All strains with HF-SMT3 are isogenic to HZY2101

Strain Number	Relevant Genotype	Reference
HZY2101	MATa *HF-SMT3sml1Δ::TRP1 arg4Δ ura3-52 leu2Δ1 trp1Δ63 his3Δ200 lys2ΔBgl hom3-10 ade2Δ ade8, 2-micron removed.*	(Albuquerque et al., 2013)
HZY4068	MATa *ulp2-781Δ::HIS3 HF-SMT3*	This study
HZY4171	MATa *TOF2-His6-3xHA::His3MX6 HF-SMT3*	This study
JLY881	*MATa TOF2-His6-3xHA::His3MX6 ulp2-781Δ::natMX4 HF-SMT3*	This study
JLY892	MATa *TOF2-His6-3xHA::His3MX6 ulp2Δ::natMX4 HF-SMT3*	This study
HZY3721	MATa *NET1-His6-3xHA::kanMX6 HF-SMT3*	This study
HZY3725	MATa *NET1-His6-3xHA::kanMX6 ulp2Δ::HIS3 HF-SMT3*	This study
HZY1905	MATa *NET1-His6-3xHA::kanMX6 ulp2Δ::HIS3 HF-SMT3*	This study
JLY1013	MATa *TOF2-His6-3xHA::His3MX6 csm1Δ::natMX4 HF-SMT3*	This study
JLY1321	MATa *TOF2-His6-3xHA::His3MX6 ulp2-2A(F827,839A)::kanMX6 HF-SMT3*	This study
JLY1323	MATa *TOF2-His6-3xHA::His3MX6 ulp2-F827D::kanMX6 HF-SMT3*	This study
JLY1326	MATa *TOF2-His6-3xHA::His3MX6 ulp2-F839D::kanMX6 HF-SMT3*	This study
JLY963	MATa *TOF2-His6-3xHA::His3MX6 slx5Δ::URA3 HF-SMT3*	This study
JLY966	MATa *TOF2-His6-3xHA::His3MX6 slx5Δ::URA3 ulp2-781Δ::natMX4 HF-SMT3*	This study
JLY1277	MATa *TOF2-His6-3xHA::His3MX6 KanMX6::pSLX5-slx5-SIM HF-SMT3*	This study
JLY1294	MATa *TOF2-His6-3xHA::His3MX6 KanMX6::pSLX5-slx5-SIM ulp2-781Δ::natMX4 HF-SMT3*	This study
DMY2798 (JLY786)	MATa *leu2::mURA3*	(Huang et al., 2006)
DMY2804 (JLY787)	MATa *RDN1-NTS2::mURA3*	(Huang et al., 2006)
DMY2800 (JLY788)	MATa *RDN1-NTS1::mURA3*	(Huang et al., 2006)
JLY810	MATa *leu2::mURA3 ulp2Δ::natMX4*	This study
JLY812	MATa *RDN1-NTS2::mURA3 ulp2Δ::natMX4*	This study
JLY814	MATa *RDN1-NTS1::mURA3 ulp2Δ::natMX4*	This study
JLY816	MATa *leu2::mURA3 ulp2-707Δ::natMX4*	This study
JLY819	MATa *RDN1-NTS2::mURA3 ulp2-707Δ::natMX4*	This study
JLY822	MATa *RDN1-NTS1::mURA3 ulp2-707Δ::natMX4*	This study
JLY826	MATa *leu2::mURA3 ulp2-781Δ::natMX4*	This study
JLY828	MATa *RDN1-NTS2::mURA3 ulp2-781Δ::natMX4*	This study
JLY830	MATa *RDN1-NTS1::mURA3 ulp2-781Δ::natMX4*	This study
JLY832	MATa *leu2::mURA3 ulp2-873Δ::natMX4*	This study
JLY834	MATa *RDN1-NTS2::mURA3 ulp2-873Δ::natMX4*	This study
JLY836	MATa *RDN1-NTS1::mURA3 ulp2-873Δ::natMX4*	This study

Table 4.2 Yeast strains used in Chapter 4, continued

Strain Number	Relevant Genotype	Reference
JLY838	MATa *leu2::mURA3 sir2Δ::natMX4*	This study
JLY840	MATa *RDN1-NTS2::mURA3 sir2Δ::natMX4*	This study
JLY842	MATa *RDN1-NTS1::mURA3 sir2Δ::natMX4*	This study
JLY1333	MATa *leu2::mURA3 ulp2-F827D::kanMX6*	This study
JLY1335	MATa *leu2::mURA3 ulp2-F839D::kanMX6*	This study
JLY1337	MATa *leu2::mURA3 ulp2-2A(F827,839A)::kanMX6*	This study
JLY1339	MATa *RDN1-NTS1::mURA3 ulp2-F827D::kanMX6*	This study
JLY1341	MATa *RDN1-NTS1::mURA3 ulp2-F839D::kanMX6*	This study
JLY1344	MATa *RDN1-NTS1::mURA3 ulp2-2A(F827,839A)::kanMX6*	This study
JLY1075	MATa *leu2::mURA3 slx5Δ::HIS3 RAD5+, 2um removed*	This study
JLY1070	MATa *RDN1-NTS2::mURA3 slx5Δ::HIS3 RAD5+, 2um removed*	This study
JLY1045	MATα *RDN1-NTS1::mURA3 slx5Δ::HIS3 RAD5+, 2um removed*	This study
JLY1147	MATa *leu2::mURA3 slx5Δ::HIS3 ulp2-781Δ::natMX4 RAD5+, 2um removed*	This study
JLY1076	MATα *RDN1-NTS1::mURA3 slx5Δ::HIS3 ulp2-781Δ::natMX4 RAD5+, 2um removed*	This study

Table 4.3 Abundance of sumoylated protein identified and quantified by comparing *ulp2-781Δ* (HZY4068) and wild-type (HZY2101) strains

Gene	ORF	Median ratio (HZY4068/HZY2101)	# of peptides found
ABF1	YKL112W	1.075	43
ABP1	YCR088W	0.863	5
AOS1	YPR180W	0.711	11
ASF2	YDL197C	0.797	8
AZF1	YOR113W	0.777	7
BDF1	YLR399C	0.966	9
BDP1	YNL039W	0.451	34
BIR1	YJR089W	0.6635	52
BOP3	YNL042W	0.7345	26
BRF1	YGR246C	0.524	22
BRN1	YBL097W	0.363	33
CBF1	YJR060W	1.226	9
CBF2	YGR140W	1.3735	12
CDC11	YJR076C	0.894	13
CDC14	YFR028C	4.235	13
CDC3	YLR314C	0.829	40
CDC48	YDL126C	0.959	31
CET1	YPL228W	0.432	27
CIN5	YOR028C	1.1325	6
CRZ1	YNL027W	0.795	6
CTI6	YPL181W	0.737	11
CYC8	YBR112C	0.839	6
DIG1	YPL049C	0.488	5
EBP2	YKL172W	0.44	7
ENO2	YHR174W	1.822	5
FOB1	YDR110W	0.53	24
GCN5	YGR252W	0.728	13
GCR2	YNL199C	0.508	11
HIR2	YOR038C	0.4335	4
HMO1	YDR174W	0.4175	12
HMS1	YOR032C	0.5915	4
HPC2	YBR215W	0.571	30
HSP104	YLL026W	1.654	3
HTA2|HTA1	YBL003C|YDR225W	0.6495	6
HTB2|HTB1	YBL002W|YDR224C	0.675	13
IPP1	YBR011C	1.72	9
ISW1	YBR245C	0.731	9
ISW1|ISW2	YBR245C|YOR304W	0.6475	4
MAD1	YGL086W	0.844	14
MCD1	YDL003W	0.438	12
MCM2	YBL023C	0.7665	12
MCM21	YDR318W	3.661	4
MCM22	YJR135C	2.505	3

Table 4.3 Abundance of sumoylated protein identified and quantified by comparing *ulp2-781Δ* (HZY4068) and wild-type (HZY2101) strains, continued

Gene	ORF	Median ratio (HZY4068/HZY2101)	# of peptides found
MCM3	YEL032W	0.5435	8
MCM6	YGL201C	0.785	7
MET4	YNL103W	0.5495	10
MLP1	YKR095W	0.7665	82
MLP2	YIL149C	0.685	50
MRP8	YKL142W	1.059	14
NET1	YJL076W	2.695	127
NFI1	YOR156C	1.02	6
NGG1	YDR176W	0.808	11
NPL6	YMR091C	0.699	4
NUP2	YLR335W	1.019	33
NUP60	YAR002W	1.299	5
OKP1	YGR179C	1.6395	4
PAF1	YBR279W	0.719	12
PDC1	YLR044C	3.774	15
PGK1	YCR012W	1.1195	40
POB3	YML069W	0.752	19
POL30	YBR088C	0.456	18
PRP45	YAL032C	1.259	27
RAD16	YBR114W	0.661	8
RAP1	YNL216W	0.946	43
REB1	YBR049C	0.751	37
RPA190	YOR341W	0.308	4
RPA43	YOR340C	0.519	13
RPB4	YJL140W	0.649	17
RPC37	YKR025W	0.427	17
RPC53	YDL150W	0.6045	36
RPC82	YPR190C	0.2095	6
RPO21	YDL140C	0.534	25
RPO26	YPR187W	0.587	11
RRP5	YMR229C	0.877	3
RSC1	YGR056W	0.6145	4
RSC2	YLR357W	0.669	28
RSC58	YLR033W	0.676	16
RSC8	YFR037C	0.779	32
RVB1	YDR190C	0.809	13
SGF73	YGL066W	0.723	7
SHS1	YDL225W	0.768	21
SIR3	YLR442C	0.539	4
SIR4	YDR227W	0.6965	74
SIZ1	YDR409W	0.6485	22
SKO1	YNL167C	1.017	20
SLI15	YBR156C	0.6265	14
SMC2	YFR031C	0.512	7

Table 4.3 Abundance of sumoylated protein identified and quantified by comparing *ulp2-781Δ* (HZY4068) and wild-type (HZY2101) strains, continued

Gene	ORF	Median ratio (HZY4068/HZY2101)	# of peptides found
SMC3	YJL074C	0.337	7
SMC4	YLR086W	0.456	23
SMC5	YOL034W	0.89	15
SMC6	YLR383W	1.085	6
SNF5	YBR289W	0.56	3
SPC24	YMR117C	0.876	9
SPN1	YPR133C	0.532	11
SPP41	YDR464W	1.0545	70
SPT15	YER148W	0.718	8
SPT5	YML010W	0.556	39
SPT7	YBR081C	0.718	25
STB3	YDR169C	0.9255	22
STE12	YHR084W	0.5835	6
STH1	YIL126W	0.635	7
SUB2	YDL084W	1.7535	4
SUM1	YDR310C	0.7265	38
SWC3	YAL011W	0.734	9
SWI3	YJL176C	0.601	15
SWI4	YER111C	0.66	5
TAF12	YDR145W	0.737	3
TAL1	YLR354C	4.7845	14
TEC1	YBR083W	0.524	15
TFC3	YAL001C	0.7035	6
TFC6	YDR362C	0.63	8
TFC7	YOR110W	0.584	13
TFG1	YGR186W	0.518	35
TKL1	YPR074C	4.758	3
TOA1	YOR194C	0.5715	6
TOF2	YKR010C	1.9595	42
TOP1	YOL006C	0.441	10
TOP2	YNL088W	0.387	12
TUP1	YCR084C	0.601	53
TYE7	YOR344C	0.381	11
UAF30	YOR295W	0.746	9
UBA2	YDR390C	1.0605	24
UBC9	YDL064W	0.968	15
UPC2	YDR213W	0.668	4
VID21	YDR359C	0.734	10
VPS72	YDR485C	0.726	23
WTM1	YOR230W	0.545	18
YMR111C	YMR111C	1.073	44

CHAPTER 5

Discussion

5.1 Conclusion and future directions

These studies here illustrate the vast and complex roles of different post-translational modifications and their regulation of the genome. The findings will help further the understanding of how PTMs regulate the functions of different proteins and their contribution to cellular homeostasis.

In chapter 2 we describe a role for the Mec1/Tel1-dependent phosphorylation of Sae2. We find that a phosphorylation-defective mutant of Sae2, *sae2-2AQ*, can impair its DNA repair and checkpoint functions resulting in genome instability. Since the *sae2-2AQ* mutant abrogates checkpoint inactivation it would suggest that it can also prevent adaptation, a phenomenon that occurs in yeast where cells can cope with irreparable DNA lesions, such as in a *sae2Δ* mutant. The interaction between phosphorylated Sae2 with FHA-domain containing proteins gives new insight into how the DNA damage checkpoint can couple with DNA repair to maintain genome integrity. The interaction between phosphorylated Sae2 and either Rad53 or Dun1 suggests that it could be localizing either kinase to the sites of DNA lesions to target additional substrates. It would be interesting to look into the combination of FHA mutants of Rad53, Dun1, and Xrs2 to see if they have an effect on Sae2 functions like DNA end resection and resolving inverted *Alu* repeats [34].

In chapter 3 we determine the substrates of Ulp1 and Ulp2 and implicate Ulp1 as a suppressor of GCRs. Ulp2 substrates are distinct and assemble into large protein complexes found localized to rDNA, centromeres, and origins of

replication. Ulp1 on the other hand has a broader role in regulating the bulk of intracellular sumoylation. A truncation of the N-terminus of Ulp1, that mis-localizes it from the nuclear periphery, reduces sumoylation of Ulp2 substrates including the MCM complex. Sumoylation of several MCM subunits including Mcm3 are also dependent on the SUMO E3 ligase Mms21. Given that the MCM complex is a critical component of the DNA replication fork and its sumoylation is decreased in both *ulp1* and *mms21-CH* mutants, suggests that sumoylation of MCM plays a role in genome maintenance.

The results in chapter 4 describe how a SUMO isopeptidase, Ulp2, can interact with a perinuclear complex, Csm1-Lrs4, to promote stabilization of rDNA silencing complexes. Since Csm1, as part of the monopolin complex, recruits to kinetochores at both mitotic anaphase and meiotic prophase, it would be intriguing to see whether these *ulp2* mutants also affect chromosome segregation. Since we discovered that increased Tof2 sumoylation leads to a loss of its protein abundance, we should explore whether this function is recurring for other Ulp2 substrates like the COMA complex or other kinetochore subcomplexes. While Tof2 and Net1 both show elevated sumoylation levels in *ulp2* mutants, only Tof2 levels are affected and dependent on the Slx5-Slx8 StUbL. This suggests that Slx5-Slx8 is not broadly regulating sumoylated protein levels, and that it is specific in its substrate selection. Identifying Slx5-Slx8 targets and the mechanism of how the StUbL interacts with its targets

would be considerably important, especially since mutation to *SLX5* and *SLX8* has been shown to cause genome instability [135].

While we studied many different aspects of PTMs like enzyme regulation, substrate identification, and substrate characterization, there remain many layers of complexity. For example, many substrates that are phosphorylated by the DNA damage checkpoint have also been found to be sumoylated or modified by other PTMs. Whether these dynamic modifications work in conjunction to regulate the same substrates remains to be seen. Future studies into the existence of crosstalk across different PTMs will require further analysis.

References

1. Sancar, A., L.A. Lindsey-Boltz, K. Unsal-Kacmaz, and S. Linn, *Molecular mechanisms of mammalian DNA repair and the DNA damage checkpoints.* Annu Rev Biochem, 2004. **73**: p. 39-85.

2. Hoeijmakers, J.H., *Genome maintenance mechanisms for preventing cancer.* Nature, 2001. **411**(6835): p. 366-74.

3. Jeggo, P.A., L.H. Pearl, and A.M. Carr, *DNA repair, genome stability and cancer: a historical perspective.* Nat Rev Cancer, 2016. **16**(1): p. 35-42.

4. Pennaneach, V. and R.D. Kolodner, *Recombination and the Tel1 and Mec1 checkpoints differentially effect genome rearrangements driven by telomere dysfunction in yeast.* Nature genetics, 2004. **36**(6): p. 612-7.

5. Putnam, C.D., K. Pallis, T.K. Hayes, and R.D. Kolodner, *DNA repair pathway selection caused by defects in TEL1, SAE2, and de novo telomere addition generates specific chromosomal rearrangement signatures.* PLoS Genet, 2014. **10**(4): p. e1004277.

6. Myung, K., A. Datta, and R.D. Kolodner, *Suppression of spontaneous chromosomal rearrangements by S phase checkpoint functions in Saccharomyces cerevisiae.* Cell, 2001. **104**(3): p. 397-408.

7. Putnam, C.D., T.K. Hayes, and R.D. Kolodner, *Specific pathways prevent duplication-mediated genome rearrangements.* Nature, 2009. **460**(7258): p. 984-9.

8. Savitsky, K., A. Bar-Shira, S. Gilad, G. Rotman, Y. Ziv, L. Vanagaite, D.A. Tagle, S. Smith, T. Uziel, S. Sfez, M. Ashkenazi, I. Pecker, M. Frydman, R. Harnik, S.R. Patanjali, A. Simmons, G.A. Clines, A. Sartiel, R.A. Gatti, L. Chessa, O. Sanal, M.F. Lavin, N.G. Jaspers, A.M. Taylor, C.F. Arlett, T. Miki, S.M. Weissman, M. Lovett, F.S. Collins, and Y. Shiloh, *A single ataxia telangiectasia gene with a product similar to PI-3 kinase.* Science, 1995. **268**(5218): p. 1749-53.

9. Carney, J.P., R.S. Maser, H. Olivares, E.M. Davis, M. Le Beau, J.R. Yates, 3rd, L. Hays, W.F. Morgan, and J.H. Petrini, *The hMre11/hRad50 protein complex and Nijmegen breakage syndrome: linkage of double-strand break repair to the cellular DNA damage response.* Cell, 1998. **93**(3): p. 477-86.

10. Stewart, G.S., R.S. Maser, T. Stankovic, D.A. Bressan, M.I. Kaplan, N.G. Jaspers, A. Raams, P.J. Byrd, J.H. Petrini, and A.M. Taylor, *The DNA double-strand break repair gene hMRE11 is mutated in individuals with an ataxia-telangiectasia-like disorder.* Cell, 1999. **99**(6): p. 577-87.

11. Murray, A.W., *Creative blocks: cell-cycle checkpoints and feedback controls.* Nature, 1992. **359**(6396): p. 599-604.

12. Hickey, C.M., N.R. Wilson, and M. Hochstrasser, *Function and regulation of SUMO proteases.* Nat Rev Mol Cell Biol, 2012. **13**(12): p. 755-66.

13. Harrison, J.C. and J.E. Haber, *Surviving the breakup: the DNA damage checkpoint.* Annual review of genetics, 2006. **40**: p. 209-35.

14. Gillies, J. and M. Hochstrasser, *A new class of SUMO proteases.* EMBO Rep, 2012. **13**(4): p. 284-5.

15. Shiloh, Y., *ATM and ATR: networking cellular responses to DNA damage.* Current opinion in genetics & development, 2001. **11**(1): p. 71-7.

16. Durocher, D. and S.P. Jackson, *DNA-PK, ATM and ATR as sensors of DNA damage: variations on a theme?* Current opinion in cell biology, 2001. **13**(2): p. 225-31.

17. Johnson, E.S. and A.A. Gupta, *An E3-like factor that promotes SUMO conjugation to the yeast septins.* Cell, 2001. **106**(6): p. 735-44.

18. Zhao, X. and G. Blobel, *A SUMO ligase is part of a nuclear multiprotein complex that affects DNA repair and chromosomal organization.* Proc Natl Acad Sci U S A, 2005. **102**(13): p. 4777-82.

19. Reindle, A., I. Belichenko, G.R. Bylebyl, X.L. Chen, N. Gandhi, and E.S. Johnson, *Multiple domains in Siz SUMO ligases contribute to substrate selectivity.* J Cell Sci, 2006. **119**(Pt 22): p. 4749-57.

20. Alcasabas, A.A., A.J. Osborn, J. Bachant, F. Hu, P.J. Werler, K. Bousset, K. Furuya, J.F. Diffley, A.M. Carr, and S.J. Elledge, *Mrc1 transduces signals of DNA replication stress to activate Rad53.* Nature cell biology, 2001. **3**(11): p. 958-65.

21. Osborn, A.J. and S.J. Elledge, *Mrc1 is a replication fork component whose phosphorylation in response to DNA replication stress activates Rad53.* Genes & development, 2003. **17**(14): p. 1755-67.

22. Tanaka, K. and P. Russell, *Mrc1 channels the DNA replication arrest signal to checkpoint kinase Cds1.* Nature cell biology, 2001. **3**(11): p. 966-72.

23. Lopes, M., C. Cotta-Ramusino, A. Pellicioli, G. Liberi, P. Plevani, M. Muzi-Falconi, C.S. Newlon, and M. Foiani, *The DNA replication checkpoint response stabilizes stalled replication forks.* Nature, 2001. **412**(6846): p. 557-61.

24. Santocanale, C. and J.F. Diffley, *A Mec1- and Rad53-dependent checkpoint controls late-firing origins of DNA replication.* Nature, 1998. **395**(6702): p. 615-8.

25. Weinert, T.A., G.L. Kiser, and L.H. Hartwell, *Mitotic checkpoint genes in budding yeast and the dependence of mitosis on DNA replication and repair.* Genes Dev, 1994. **8**(6): p. 652-65.

26. Zhao, X. and R. Rothstein, *The Dun1 checkpoint kinase phosphorylates and regulates the ribonucleotide reductase inhibitor Sml1.* Proc Natl Acad Sci U S A, 2002. **99**(6): p. 3746-51.

27. Symington, L.S. and J. Gautier, *Double-strand break end resection and repair pathway choice.* Annual review of genetics, 2011. **45**: p. 247-71.

28. Mimitou, E.P. and L.S. Symington, *Sae2, Exo1 and Sgs1 collaborate in DNA double-strand break processing.* Nature, 2008. **455**(7214): p. 770-4.

29. Zhu, Z., W.H. Chung, E.Y. Shim, S.E. Lee, and G. Ira, *Sgs1 helicase and two nucleases Dna2 and Exo1 resect DNA double-strand break ends.* Cell, 2008. **134**(6): p. 981-94.

30. Nakada, D., K. Matsumoto, and K. Sugimoto, *ATM-related Tel1 associates with double-strand breaks through an Xrs2-dependent mechanism.* Genes & development, 2003. **17**(16): p. 1957-62.

31. Zou, L. and S.J. Elledge, *Sensing DNA damage through ATRIP recognition of RPA-ssDNA complexes.* Science, 2003. **300**(5625): p. 1542-8.

32. Brush, G.S., D.M. Morrow, P. Hieter, and T.J. Kelly, *The ATM homologue MEC1 is required for phosphorylation of replication protein A in yeast.* Proceedings of the National Academy of Sciences of the United States of America, 1996. **93**(26): p. 15075-80.

33. Gatei, M., D. Young, K.M. Cerosaletti, A. Desai-Mehta, K. Spring, S. Kozlov, M.F. Lavin, R.A. Gatti, P. Concannon, and K. Khanna, *ATM-dependent phosphorylation of nibrin in response to radiation exposure.* Nature genetics, 2000. **25**(1): p. 115-9.

34. Baroni, E., V. Viscardi, H. Cartagena-Lirola, G. Lucchini, and M.P. Longhese, *The functions of budding yeast Sae2 in the DNA damage response require Mec1- and Tel1-dependent phosphorylation.* Molecular and cellular biology, 2004. **24**(10): p. 4151-65.

35. Craven, R.J., P.W. Greenwell, M. Dominska, and T.D. Petes, *Regulation of genome stability by TEL1 and MEC1, yeast homologs of the mammalian ATM and ATR genes.* Genetics, 2002. **161**(2): p. 493-507.

36. Vaze, M.B., A. Pellicioli, S.E. Lee, G. Ira, G. Liberi, A. Arbel-Eden, M. Foiani, and J.E. Haber, *Recovery from checkpoint-mediated arrest after*

repair of a double-strand break requires Srs2 helicase. Molecular cell, 2002. **10**(2): p. 373-85.

37. Zou, L., D. Liu, and S.J. Elledge, *Replication protein A-mediated recruitment and activation of Rad17 complexes.* Proceedings of the National Academy of Sciences of the United States of America, 2003. **100**(24): p. 13827-32.

38. Majka, J., A. Niedziela-Majka, and P.M. Burgers, *The checkpoint clamp activates Mec1 kinase during initiation of the DNA damage checkpoint.* Molecular cell, 2006. **24**(6): p. 891-901.

39. Lee, J.H. and T.T. Paull, *Direct activation of the ATM protein kinase by the Mre11/Rad50/Nbs1 complex.* Science, 2004. **304**(5667): p. 93-6.

40. Gareau, J.R. and C.D. Lima, *The SUMO pathway: emerging mechanisms that shape specificity, conjugation and recognition.* Nat Rev Mol Cell Biol, 2010. **11**(12): p. 861-71.

41. Takahashi, Y., T. Kahyo, E.A. Toh, H. Yasuda, and Y. Kikuchi, *Yeast Ull1/Siz1 is a novel SUMO1/Smt3 ligase for septin components and functions as an adaptor between conjugating enzyme and substrates.* J Biol Chem, 2001. **276**(52): p. 48973-7.

42. Cheng, C.H., Y.H. Lo, S.S. Liang, S.C. Ti, F.M. Lin, C.H. Yeh, H.Y. Huang, and T.F. Wang, *SUMO modifications control assembly of synaptonemal complex and polycomplex in meiosis of Saccharomyces cerevisiae.* Genes Dev, 2006. **20**(15): p. 2067-81.

43. Kroetz, M.B., D. Su, and M. Hochstrasser, *Essential role of nuclear localization for yeast Ulp2 SUMO protease function.* Mol Biol Cell, 2009. **20**(8): p. 2196-206.

44. Li, S.J. and M. Hochstrasser, *A new protease required for cell-cycle progression in yeast.* Nature, 1999. **398**(6724): p. 246-51.

45. Li, S.J. and M. Hochstrasser, *The yeast ULP2 (SMT4) gene encodes a novel protease specific for the ubiquitin-like Smt3 protein.* Mol Cell Biol, 2000. **20**(7): p. 2367-77.

46. Li, S.J. and M. Hochstrasser, *The Ulp1 SUMO isopeptidase: distinct domains required for viability, nuclear envelope localization, and substrate specificity.* J Cell Biol, 2003. **160**(7): p. 1069-81.

47. Matunis, M.J., E. Coutavas, and G. Blobel, *A novel ubiquitin-like modification modulates the partitioning of the Ran-GTPase-activating protein RanGAP1 between the cytosol and the nuclear pore complex.* J Cell Biol, 1996. **135**(6 Pt 1): p. 1457-70.

48. Shiio, Y. and R.N. Eisenman, *Histone sumoylation is associated with transcriptional repression.* Proc Natl Acad Sci U S A, 2003. **100**(23): p. 13225-30.

49. Nathan, D., K. Ingvarsdottir, D.E. Sterner, G.R. Bylebyl, M. Dokmanovic, J.A. Dorsey, K.A. Whelan, M. Krsmanovic, W.S. Lane, P.B. Meluh, E.S. Johnson, and S.L. Berger, *Histone sumoylation is a negative regulator in Saccharomyces cerevisiae and shows dynamic interplay with positive-acting histone modifications.* Genes Dev, 2006. **20**(8): p. 966-76.

50. Hardeland, U., R. Steinacher, J. Jiricny, and P. Schar, *Modification of the human thymine-DNA glycosylase by ubiquitin-like proteins facilitates enzymatic turnover.* EMBO J, 2002. **21**(6): p. 1456-64.

51. Song, J., L.K. Durrin, T.A. Wilkinson, T.G. Krontiris, and Y. Chen, *Identification of a SUMO-binding motif that recognizes SUMO-modified proteins.* Proc Natl Acad Sci U S A, 2004. **101**(40): p. 14373-8.

52. Cremona, C.A., P. Sarangi, Y. Yang, L.E. Hang, S. Rahman, and X. Zhao, *Extensive DNA damage-induced sumoylation contributes to replication and repair and acts in addition to the mec1 checkpoint.* Mol Cell, 2012. **45**(3): p. 422-32.

53. Psakhye, I. and S. Jentsch, *Protein group modification and synergy in the SUMO pathway as exemplified in DNA repair.* Cell, 2012. **151**(4): p. 807-20.

54. Galanty, Y., R. Belotserkovskaya, J. Coates, S. Polo, K.M. Miller, and S.P. Jackson, *Mammalian SUMO E3-ligases PIAS1 and PIAS4 promote responses to DNA double-strand breaks.* Nature, 2009. **462**(7275): p. 935-9.

55. Zhou, W., J.J. Ryan, and H. Zhou, *Global analyses of sumoylated proteins in Saccharomyces cerevisiae. Induction of protein sumoylation by cellular stresses.* J Biol Chem, 2004. **279**(31): p. 32262-8.

56. Manza, L.L., S.G. Codreanu, S.L. Stamer, D.L. Smith, K.S. Wells, R.L. Roberts, and D.C. Liebler, *Global shifts in protein sumoylation in response to electrophile and oxidative stress.* Chem Res Toxicol, 2004. **17**(12): p. 1706-15.

57. Hoege, C., B. Pfander, G.L. Moldovan, G. Pyrowolakis, and S. Jentsch, *RAD6-dependent DNA repair is linked to modification of PCNA by ubiquitin and SUMO.* Nature, 2002. **419**(6903): p. 135-41.

58. Stelter, P. and H.D. Ulrich, *Control of spontaneous and damage-induced mutagenesis by SUMO and ubiquitin conjugation.* Nature, 2003. **425**(6954): p. 188-91.

59. Pfander, B., G.L. Moldovan, M. Sacher, C. Hoege, and S. Jentsch, *SUMO-modified PCNA recruits Srs2 to prevent recombination during S phase.* Nature, 2005. **436**(7049): p. 428-33.

60. Albuquerque, C.P., G. Wang, N.S. Lee, R.D. Kolodner, C.D. Putnam, and H. Zhou, *Distinct SUMO ligases cooperate with Esc2 and Slx5 to suppress duplication-mediated genome rearrangements.* PLoS Genet, 2013. **9**(8): p. e1003670.

61. Motegi, A., K. Kuntz, A. Majeed, S. Smith, and K. Myung, *Regulation of gross chromosomal rearrangements by ubiquitin and SUMO ligases in Saccharomyces cerevisiae.* Mol Cell Biol, 2006. **26**(4): p. 1424-33.

62. Kats, E.S., J.M. Enserink, S. Martinez, and R.D. Kolodner, *The Saccharomyces cerevisiae Rad6 postreplication repair and Siz1/Srs2 homologous recombination-inhibiting pathways process DNA damage that arises in asf1 mutants.* Mol Cell Biol, 2009. **29**(19): p. 5226-37.

63. Clerici, M., D. Mantiero, G. Lucchini, and M.P. Longhese, *The Saccharomyces cerevisiae Sae2 protein negatively regulates DNA damage checkpoint signalling.* EMBO reports, 2006. **7**(2): p. 212-8.

64. Lee, K., Y. Zhang, and S.E. Lee, *Saccharomyces cerevisiae ATM orthologue suppresses break-induced chromosome translocations.* Nature, 2008. **454**(7203): p. 543-6.

65. Li, S., N.S. Ting, L. Zheng, P.L. Chen, Y. Ziv, Y. Shiloh, E.Y. Lee, and W.H. Lee, *Functional link of BRCA1 and ataxia telangiectasia gene product in DNA damage response.* Nature, 2000. **406**(6792): p. 210-5.

66. Peterson, S.E., Y. Li, F. Wu-Baer, B.T. Chait, R. Baer, H. Yan, M.E. Gottesman, and J. Gautier, *Activation of DSB processing requires phosphorylation of CtIP by ATR.* Molecular cell, 2013. **49**(4): p. 657-67.

67. Wang, H., L.Z. Shi, C.C. Wong, X. Han, P.Y. Hwang, L.N. Truong, Q. Zhu, Z. Shao, D.J. Chen, M.W. Berns, J.R. Yates, 3rd, L. Chen, and X. Wu, *The interaction of CtIP and Nbs1 connects CDK and ATM to regulate HR-mediated double-strand break repair.* PLoS genetics, 2013. **9**(2): p. e1003277.

68. Huertas, P., F. Cortes-Ledesma, A.A. Sartori, A. Aguilera, and S.P. Jackson, *CDK targets Sae2 to control DNA-end resection and homologous recombination.* Nature, 2008. **455**(7213): p. 689-92.

69. Fu, Q., J. Chow, K.A. Bernstein, N. Makharashvili, S. Arora, C.F. Lee, M.D. Person, R. Rothstein, and T.T. Paull, *Phosphorylation-regulated transitions in an oligomeric state control the activity of the Sae2 DNA repair enzyme.* Molecular and cellular biology, 2014. **34**(5): p. 778-93.

70. Williams, R.S., G.E. Dodson, O. Limbo, Y. Yamada, J.S. Williams, G. Guenther, S. Classen, J.N. Glover, H. Iwasaki, P. Russell, and J.A.

Tainer, *Nbs1 flexibly tethers Ctp1 and Mre11-Rad50 to coordinate DNA double-strand break processing and repair.* Cell, 2009. **139**(1): p. 87-99.

71. Vance, J.R. and T.E. Wilson, *Yeast Tdp1 and Rad1-Rad10 function as redundant pathways for repairing Top1 replicative damage.* Proceedings of the National Academy of Sciences of the United States of America, 2002. **99**(21): p. 13669-74.

72. Vialard, J.E., C.S. Gilbert, C.M. Green, and N.F. Lowndes, *The budding yeast Rad9 checkpoint protein is subjected to Mec1/Tel1-dependent hyperphosphorylation and interacts with Rad53 after DNA damage.* The EMBO journal, 1998. **17**(19): p. 5679-88.

73. Sun, Z., J. Hsiao, D.S. Fay, and D.F. Stern, *Rad53 FHA domain associated with phosphorylated Rad9 in the DNA damage checkpoint.* Science, 1998. **281**(5374): p. 272-4.

74. Tong, A.H., M. Evangelista, A.B. Parsons, H. Xu, G.D. Bader, N. Page, M. Robinson, S. Raghibizadeh, C.W. Hogue, H. Bussey, B. Andrews, M. Tyers, and C. Boone, *Systematic genetic analysis with ordered arrays of yeast deletion mutants.* Science, 2001. **294**(5550): p. 2364-8.

75. Mimitou, E.P. and L.S. Symington, *Ku prevents Exo1 and Sgs1-dependent resection of DNA ends in the absence of a functional MRX complex or Sae2.* The EMBO journal, 2010. **29**(19): p. 3358-69.

76. Putnam, C.D. and R.D. Kolodner, *Determination of gross chromosomal rearrangement rates.* Cold Spring Harbor protocols, 2010. **2010**(9): p. pdb prot5492.

77. Putnam, C.D., K. Pallis, T.K. Hayes, and R.D. Kolodner, *DNA repair pathway selection caused by defects in TEL1, SAE2, and de novo telomere addition generates specific chromosomal rearrangement signatures.* PLoS genetics, 2014. **10**(4): p. e1004277.

78. Durocher, D., J. Henckel, A.R. Fersht, and S.P. Jackson, *The FHA domain is a modular phosphopeptide recognition motif.* Molecular cell, 1999. **4**(3): p. 387-94.

79. Durocher, D., I.A. Taylor, D. Sarbassova, L.F. Haire, S.L. Westcott, S.P. Jackson, S.J. Smerdon, and M.B. Yaffe, *The molecular basis of FHA domain:phosphopeptide binding specificity and implications for phospho-dependent signaling mechanisms.* Molecular cell, 2000. **6**(5): p. 1169-82.

80. Yu, X. and J. Chen, *DNA damage-induced cell cycle checkpoint control requires CtIP, a phosphorylation-dependent binding partner of BRCA1 C-terminal domains.* Molecular and cellular biology, 2004. **24**(21): p. 9478-86.

81. Cartagena-Lirola, H., I. Guerini, V. Viscardi, G. Lucchini, and M.P. Longhese, *Budding Yeast Sae2 is an In Vivo Target of the Mec1 and Tel1 Checkpoint Kinases During Meiosis.* Cell cycle, 2006. **5**(14): p. 1549-59.

82. Dodson, G.E., O. Limbo, D. Nieto, and P. Russell, *Phosphorylation-regulated binding of Ctp1 to Nbs1 is critical for repair of DNA double-strand breaks.* Cell cycle, 2010. **9**(8): p. 1516-22.

83. Chen, S.H., M.B. Smolka, and H. Zhou, *Mechanism of Dun1 activation by Rad53 phosphorylation in Saccharomyces cerevisiae.* The Journal of biological chemistry, 2007. **282**(2): p. 986-95.

84. Smolka, M.B., S.H. Chen, P.S. Maddox, J.M. Enserink, C.P. Albuquerque, X.X. Wei, A. Desai, R.D. Kolodner, and H. Zhou, *An FHA domain-mediated protein interaction network of Rad53 reveals its role in polarized cell growth.* The Journal of cell biology, 2006. **175**(5): p. 743-53.

85. Bashkirov, V.I., E.V. Bashkirova, E. Haghnazari, and W.D. Heyer, *Direct kinase-to-kinase signaling mediated by the FHA phosphoprotein recognition domain of the Dun1 DNA damage checkpoint kinase.* Molecular and cellular biology, 2003. **23**(4): p. 1441-52.

86. Palmbos, P.L., D. Wu, J.M. Daley, and T.E. Wilson, *Recruitment of Saccharomyces cerevisiae Dnl4-Lif1 complex to a double-strand break requires interactions with Yku80 and the Xrs2 FHA domain.* Genetics, 2008. **180**(4): p. 1809-19.

87. Longtine, M.S., A. McKenzie, 3rd, D.J. Demarini, N.G. Shah, A. Wach, A. Brachat, P. Philippsen, and J.R. Pringle, *Additional modules for versatile and economical PCR-based gene deletion and modification in Saccharomyces cerevisiae.* Yeast, 1998. **14**(10): p. 953-61.

88. Deng, C., J.A. Brown, D. You, and J.M. Brown, *Multiple endonucleases function to repair covalent topoisomerase I complexes in Saccharomyces cerevisiae.* Genetics, 2005. **170**(2): p. 591-600.

89. Chen, S.H., C.P. Albuquerque, J. Liang, R.T. Suhandynata, and H. Zhou, *A proteome-wide analysis of kinase-substrate network in the DNA damage response.* The Journal of biological chemistry, 2010. **285**(17): p. 12803-12.

90. Ong, S.E., B. Blagoev, I. Kratchmarova, D.B. Kristensen, H. Steen, A. Pandey, and M. Mann, *Stable isotope labeling by amino acids in cell culture, SILAC, as a simple and accurate approach to expression proteomics.* Molecular & cellular proteomics : MCP, 2002. **1**(5): p. 376-86.

91. Albuquerque, C.P., M.B. Smolka, S.H. Payne, V. Bafna, J. Eng, and H. Zhou, *A multidimensional chromatography technology for in-depth phosphoproteome analysis.* Molecular & cellular proteomics : MCP, 2008. **7**(7): p. 1389-96.

92. Panse, V.G., B. Kuster, T. Gerstberger, and E. Hurt, *Unconventional tethering of Ulp1 to the transport channel of the nuclear pore complex by karyopherins.* Nat Cell Biol, 2003. **5**(1): p. 21-7.

93. Johnson, E.S., *Protein modification by SUMO.* Annu Rev Biochem, 2004. **73**: p. 355-82.

94. Zhao, X., C.Y. Wu, and G. Blobel, *Mlp-dependent anchorage and stabilization of a desumoylating enzyme is required to prevent clonal lethality.* J Cell Biol, 2004. **167**(4): p. 605-11.

95. Palancade, B., X. Liu, M. Garcia-Rubio, A. Aguilera, X. Zhao, and V. Doye, *Nucleoporins prevent DNA damage accumulation by modulating*

Ulp1-dependent sumoylation processes. Mol Biol Cell, 2007. **18**(8): p. 2912-23.

96. Lewis, A., R. Felberbaum, and M. Hochstrasser, *A nuclear envelope protein linking nuclear pore basket assembly, SUMO protease regulation, and mRNA surveillance.* J Cell Biol, 2007. **178**(5): p. 813-27.

97. Bell, S.D. and M.R. Botchan, *The minichromosome maintenance replicative helicase.* Cold Spring Harb Perspect Biol, 2013. **5**(11): p. a012807.

98. Chen, X.L., A. Reindle, and E.S. Johnson, *Misregulation of 2 microm circle copy number in a SUMO pathway mutant.* Mol Cell Biol, 2005. **25**(10): p. 4311-20.

99. Bylebyl, G.R., I. Belichenko, and E.S. Johnson, *The SUMO isopeptidase Ulp2 prevents accumulation of SUMO chains in yeast.* J Biol Chem, 2003. **278**(45): p. 44113-20.

100. Meluh, P.B. and D. Koshland, *Evidence that the MIF2 gene of Saccharomyces cerevisiae encodes a centromere protein with homology to the mammalian centromere protein CENP-C.* Mol Biol Cell, 1995. **6**(7): p. 793-807.

101. Mukhopadhyay, D., A. Arnaoutov, and M. Dasso, *The SUMO protease SENP6 is essential for inner kinetochore assembly.* J Cell Biol, 2010. **188**(5): p. 681-92.

102. Pelisch, F., R. Sonneville, E. Pourkarimi, A. Agostinho, J.J. Blow, A. Gartner, and R.T. Hay, *Dynamic SUMO modification regulates mitotic chromosome assembly and cell cycle progression in Caenorhabditis elegans.* Nat Commun, 2014. **5**: p. 5485.

103. Shou, W., J.H. Seol, A. Shevchenko, C. Baskerville, D. Moazed, Z.W. Chen, J. Jang, A. Shevchenko, H. Charbonneau, and R.J. Deshaies, *Exit from mitosis is triggered by Tem1-dependent release of the protein phosphatase Cdc14 from nucleolar RENT complex.* Cell, 1999. **97**(2): p. 233-44.

104. Maine, G.T., P. Sinha, and B.K. Tye, *Mutants of S. cerevisiae defective in the maintenance of minichromosomes.* Genetics, 1984. **106**(3): p. 365-85.

105. Hornung, P., P. Troc, F. Malvezzi, M. Maier, Z. Demianova, T. Zimniak, G. Litos, F. Lampert, A. Schleiffer, M. Brunner, K. Mechtler, F. Herzog, T.C. Marlovits, and S. Westermann, *A cooperative mechanism drives budding yeast kinetochore assembly downstream of CENP-A.* J Cell Biol, 2014. **206**(4): p. 509-24.

106. Matson, D.R., P.B. Demirel, P.T. Stukenberg, and D.J. Burke, *A conserved role for COMA/CENP-H/I/N kinetochore proteins in the spindle checkpoint.* Genes Dev, 2012. **26**(6): p. 542-7.

107. Ortiz, J., O. Stemmann, S. Rank, and J. Lechner, *A putative protein complex consisting of Ctf19, Mcm21, and Okp1 represents a missing link in the budding yeast kinetochore.* Genes Dev, 1999. **13**(9): p. 1140-55.

108. Boos, D., J. Frigola, and J.F. Diffley, *Activation of the replicative DNA helicase: breaking up is hard to do.* Curr Opin Cell Biol, 2012. **24**(3): p. 423-30.

109. O'Donnell, M., L. Langston, and B. Stillman, *Principles and concepts of DNA replication in bacteria, archaea, and eukarya.* Cold Spring Harb Perspect Biol, 2013. **5**(7).

110. Takahashi, Y., S. Dulev, X. Liu, N.J. Hiller, X. Zhao, and A. Strunnikov, *Cooperation of sumoylated chromosomal proteins in rDNA maintenance.* PLoS Genet, 2008. **4**(10): p. e1000215.

111. Straight, A.F., W. Shou, G.J. Dowd, C.W. Turck, R.J. Deshaies, A.D. Johnson, and D. Moazed, *Net1, a Sir2-associated nucleolar protein required for rDNA silencing and nucleolar integrity.* Cell, 1999. **97**(2): p. 245-56.

112. Nagai, S., K. Dubrana, M. Tsai-Pflugfelder, M.B. Davidson, T.M. Roberts, G.W. Brown, E. Varela, F. Hediger, S.M. Gasser, and N.J. Krogan, *Functional targeting of DNA damage to a nuclear pore-associated*

SUMO-dependent ubiquitin ligase. Science, 2008. **322**(5901): p. 597-602.

113. Frigola, J., D. Remus, A. Mehanna, and J.F. Diffley, *ATPase-dependent quality control of DNA replication origin licensing.* Nature, 2013. **495**(7441): p. 339-43.

114. de Albuquerque, C.P., J. Liang, N.J. Gaut, and H. Zhou, *Molecular Circuitry of the SUMO (Small Ubiquitin-like Modifier) Pathway in Controlling Sumoylation Homeostasis and Suppressing Genome Rearrangements.* J Biol Chem, 2016. **291**(16): p. 8825-35.

115. Prudden, J., S. Pebernard, G. Raffa, D.A. Slavin, J.J. Perry, J.A. Tainer, C.H. McGowan, and M.N. Boddy, *SUMO-targeted ubiquitin ligases in genome stability.* EMBO J, 2007. **26**(18): p. 4089-101.

116. Burgess, R.C., S. Rahman, M. Lisby, R. Rothstein, and X. Zhao, *The Slx5-Slx8 complex affects sumoylation of DNA repair proteins and negatively regulates recombination.* Mol Cell Biol, 2007. **27**(17): p. 6153-62.

117. Mullen, J.R. and S.J. Brill, *Activation of the Slx5-Slx8 ubiquitin ligase by poly-small ubiquitin-like modifier conjugates.* J Biol Chem, 2008. **283**(29): p. 19912-21.

118. Mullen, J.R., M. Das, and S.J. Brill, *Genetic evidence that polysumoylation bypasses the need for a SUMO-targeted Ub ligase.* Genetics, 2011. **187**(1): p. 73-87.

119. Xie, Y., O. Kerscher, M.B. Kroetz, H.F. McConchie, P. Sung, and M. Hochstrasser, *The yeast Hex3.Slx8 heterodimer is a ubiquitin ligase stimulated by substrate sumoylation.* J Biol Chem, 2007. **282**(47): p. 34176-84.

120. Nie, M. and M.N. Boddy, *Pli1(PIAS1) SUMO ligase protected by the nuclear pore-associated SUMO protease Ulp1SENP1/2.* J Biol Chem, 2015. **290**(37): p. 22678-85.

121. Huang, J., I.L. Brito, J. Villen, S.P. Gygi, A. Amon, and D. Moazed, *Inhibition of homologous recombination by a cohesin-associated clamp complex recruited to the rDNA recombination enhancer.* Genes Dev, 2006. **20**(20): p. 2887-901.

122. Huang, J. and D. Moazed, *Association of the RENT complex with nontranscribed and coding regions of rDNA and a regional requirement for the replication fork block protein Fob1 in rDNA silencing.* Genes Dev, 2003. **17**(17): p. 2162-76.

123. Mekhail, K., J. Seebacher, S.P. Gygi, and D. Moazed, *Role for perinuclear chromosome tethering in maintenance of genome stability.* Nature, 2008. **456**(7222): p. 667-70.

124. Corbett, K.D., C.K. Yip, L.S. Ee, T. Walz, A. Amon, and S.C. Harrison, *The monopolin complex crosslinks kinetochore components to regulate chromosome-microtubule attachments.* Cell, 2010. **142**(4): p. 556-67.

125. Srikumar, T., M.C. Lewicki, and B. Raught, *A global S. cerevisiae small ubiquitin-related modifier (SUMO) system interactome.* Mol Syst Biol, 2013. **9**: p. 668.

126. Gillies, J., C.M. Hickey, D. Su, Z. Wu, J. Peng, and M. Hochstrasser, *SUMO Pathway Modulation of Regulatory Protein Binding at the Ribosomal DNA Locus in Saccharomyces cerevisiae.* Genetics, 2016. **202**(4): p. 1377-94.

127. Corbett, K.D. and S.C. Harrison, *Molecular architecture of the yeast monopolin complex.* Cell Rep, 2012. **1**(6): p. 583-9.

128. Reverter, D. and C.D. Lima, *A basis for SUMO protease specificity provided by analysis of human Senp2 and a Senp2-SUMO complex.* Structure, 2004. **12**(8): p. 1519-31.

129. Kabsch, W., *Xds.* Acta Crystallogr D Biol Crystallogr, 2010. **66**(Pt 2): p. 125-32.

130. Evans, P.R. and G.N. Murshudov, *How good are my data and what is the resolution?* Acta Crystallogr D Biol Crystallogr, 2013. **69**(Pt 7): p. 1204-14.

131. Winn, M.D., C.C. Ballard, K.D. Cowtan, E.J. Dodson, P. Emsley, P.R. Evans, R.M. Keegan, E.B. Krissinel, A.G. Leslie, A. McCoy, S.J. McNicholas, G.N. Murshudov, N.S. Pannu, E.A. Potterton, H.R. Powell, R.J. Read, A. Vagin, and K.S. Wilson, *Overview of the CCP4 suite and current developments.* Acta Crystallogr D Biol Crystallogr, 2011. **67**(Pt 4): p. 235-42.

132. McCoy, A.J., R.W. Grosse-Kunstleve, P.D. Adams, M.D. Winn, L.C. Storoni, and R.J. Read, *Phaser crystallographic software.* J Appl Crystallogr, 2007. **40**(Pt 4): p. 658-674.

133. Emsley, P., B. Lohkamp, W.G. Scott, and K. Cowtan, *Features and development of Coot.* Acta Crystallogr D Biol Crystallogr, 2010. **66**(Pt 4): p. 486-501.

134. Afonine, P.V., R.W. Grosse-Kunstleve, N. Echols, J.J. Headd, N.W. Moriarty, M. Mustyakimov, T.C. Terwilliger, A. Urzhumtsev, P.H. Zwart, and P.D. Adams, *Towards automated crystallographic structure refinement with phenix.refine.* Acta Crystallogr D Biol Crystallogr, 2012. **68**(Pt 4): p. 352-67.

135. Zhang, C., T.M. Roberts, J. Yang, R. Desai, and G.W. Brown, *Suppression of genomic instability by SLX5 and SLX8 in Saccharomyces cerevisiae.* DNA Repair (Amst), 2006. **5**(3): p. 336-46.